Fuel Cell Distributed Generation: Power Conditioning, Control and Energy Management

by

Hani Fadali

A thesis
presented to the University of Waterloo
in fulfillment of the
thesis requirement for the degree of
Master of Applied Science
in
Electrical and Computer Engineering

Waterloo, Ontario, Canada, 2008

Author’s Declaration

I hereby declare that I am the sole author of this thesis. This is a true copy of the thesis, including any required final revisions, as accepted by my examiners.

I understand that my thesis may be made electronically available to the public.

Abstract

Distributed generation is expected to play a significant role in remedying the many shortcomings in today's energy market. In particular, fuel cell power generation will play a big part due to several advantages. Still, it is faced with its own challenges to tap into its potential as a solution to the crisis. The responsibilities of the Power Conditioning Unit (PCU), and thus its design, are therefore complex, yet critical to the fuel cell system's performance and ability to meet the requirements.

To this end, the dc-dc converter, considered the most critical component of the PCU for optimum performance, is closely examined. The selected converter is first modeled to gain insight into its behavior for the purpose of designing suitable compensators. MATLAB is then used to study the results using the frequency domain, and it was observed that the converter offers its own unique challenges in terms of closed-loop performance and stability. These limitations must therefore be carefully accounted for and compensated against when designing the control loops to achieve the desired objectives.

Negative feedback control to ensure robustness is then discussed. The insertion of a second inner loop in Current Mode Control (CMC) offers several key advantages over single-loop Voltage Mode Control (VMC). Furthermore, the insertion of a Current Error Amplifier (CEA) in Average Current Mode Control (ACMC) helps overcome many of the problems present in Peak Current Mode Control (PCMC) whilst allowing much needed design flexibility. It is therefore well suited for this application in an attempt to improve the dynamic behavior and overcoming the shortcomings inherent in the converter. The modulator and controller for ACMC are then modeled separately and combined with the converter's model previously derived to form the complete small-signal model.

A suitable compensation network is selected based on the models and corresponding Bode plots used to assess the system's performance and stability. The resulting Bode

plot for the complete system verifies that the design objectives are clearly met. The complete system was also built in MATLAB/Simulink, and subjected to external disturbances in the form of stepped load changes. The results confirm the system's excellent behavior despite the disturbance, and the effectiveness of the control strategy in conjunction with the derived models.

To meet the demand in many applications for power sources with high energy density and high power density, it is constructive to combine the fuel cell with an Energy Storage System (ESS). The hybrid system results in a synergistic system that brings about numerous potential advantages. Nevertheless, in order to reap these potential benefits and avoid detrimental effects to the components, a suitable configuration and control strategy to regulate the power flow amongst the various sources is of utmost importance. A robust and flexible control strategy that allows direct implementation of the ACMC scheme is devised. The excellent performance and versatility of the proposed system and control strategy are once again verified using simulations.

Finally, experimental tests are also conducted to validate the results presented in the dissertation. A scalable and modular test station is built that allows an efficient and effective design and testing process of the research. The results show good correspondence and performance of the models and control design derived throughout the thesis.

Acknowledgments

First and foremost I would like to thank *Allah* for giving me the drive, ability and patience to seek the completion of this dissertation. I would also like to thank my parents and brothers for their continued and loving support throughout my years at university.

I would like to express my sincere gratitude to my supervisor, Dr. Ehab El-Saadany, for the opportunity, his encouragement, patience and faith in my abilities through my undergraduate years and extended graduate studies. I also thank my colleagues and professors in the Power Distribution System Group for the many open forums for discussion and exchange of knowledge. My thanks go out as well to Dr. Michael Fowler and the students in the chemical engineering department, especially Matt Stevens, for their assistance in the laboratory while performing the experimental research.

Finally, I would like to thank Mr. David Mewdell and Smith + Andersen for their interest, support and investing their time and money in me. My appreciation goes out to NSERC as well for their financial assistance.

To my Family.

Table of Contents

List of Figures

List of Tables

List of Acronyms

AC	Alternating Current
ACMC	Average Current Mode Control
AFC	Alkaline Fuel Cell
CCM	Continuous Conduction Mode
CEA	Current Error Amplifier
CHP	Combined Heat and Power
CMC	Current Mode Control
dB	Decibel
DC	Direct Current
DCM	Discontinuous Conduction Mode
ESR	Equivalent Series Resistance
ESS	Energy Storage System
LHP	Left-Hand Plane
LHV	Lower Heating Value
MCFC	Molten Carbonate Fuel Cell
NMP	Non-Minimal Phase
OCV	Open-Circuit Voltage
OEM	Original Equipment Manufacturer
PAFC	Phosphoric Acid Fuel Cell
PCMC	Peak Current Mode Control
PCU	Power Conditioning Unit
PD	Proportional-plus-Derivative
PEMFC	Proton Exchange Membrane Fuel Cell
PID	Proportional-plus-Integral-plus-Derivative
PWM	Pulse-Width Modulation
RHP	Right-Hand Plane
SOC	State Of Charge
SOFC	Solid Oxide Fuel Cell
VEA	Voltage Error Amplifier
VMC	Voltage Mode Control
VRLA	Valve Regulated Lead Acid

Chapter 1
Introduction

1.1 Background

Environmental concern is now driving the use of renewable and clean energy. The electric energy demands are ever increasing, yet with limited transmission lines, many obstacles for new capacity and steady progress in power deregulation and utility restructuring have all contributed to distributed generation becoming ever more popular. Fuel cell power generation is expected to play a big part due to several advantages, such as reusability of exhaust heat, high efficiency, low environmental pollution, fuel diversity and modularity.

Fuel cells are generally characterized by the type of electrolyte they use, resulting in five major types of fuel cells in current technology for use in the industry. The Proton Exchange Membrane Fuel Cell (PEMFC) in particular is being rapidly developed as the main power source in many applications due to its high energy density, low operating temperature, and rigid yet simple structure. Nevertheless, the fuel cell has its own challenges in order to meet the demand for high energy efficiency and availability.

The fuel cell's far from ideal operating characteristics as a conventional power source necessitate the use of a suitable Power Conditioning Unit (PCU) to process its output power. The challenge for the PCU is to maximize the fuel cell's overall performance, power output, quality and efficiency from a low-voltage, high-current, slow-responding source. Unless efficient means can be found to transfer the energy from the fuel cell to

where it is requested, its potential will be untapped.

1.2 Distributed Generation

Distributed generation represents a small-scale electric power source connected directly to the utility's distribution network, and provides electric power at a site closer to the customers, rather than through lengthy transmission lines spanning from central power stations. The capacity scale of distributed generators range from several kilowatts to the 50 megawatts range. With the deregulation and liberalization in the market, the number and capacity of small to medium scale distributed generators is expected to increase significantly in the near future [1,2].

Many factors have affected the ability to supply energy economically and reliably, thereby sparking a change in the way the market had traditionally operated. Money is the common denominator of the problems as is commonly the case, with the associated high cost of fuel, as well as labor, equipment, land and borrowing money to maintain and upgrade the electric utility supply. Environmental and regulatory action has also contributed, resulting in delay of construction permits and expensive air quality treatment required to meet the standards. The aforementioned has also led to the lack of maintaining and construction of nuclear stations. All the above is further complicated by the basic fact that electric energy cannot be stored, and the installed capacity must meet the demand at all times, thereby requiring that the capacity be sized large enough to meet the peak demand that is only requested for a few hours of the day, for a few months of the year.

Distributed generation can provide alternative solutions to the energy crisis that are more cost-effective, environmentally friendly, and with higher power quality and reliability than conventional solutions. Its services include standby generation, peak shaving, base-

load generation, or cogeneration. For businesses, distributed generation can reduce peak demand charges, overall energy use and emissions, and ensure good power quality and reliability. For large utilities and power producers, distributed generation can augment overall system reliability, avoid large investments in transmission lines upgrades and the associated transmission losses, closely match capacity increases to demand growth, and supply demand more efficiently in remote areas.

Various technologies are available for distributed generation, such as internal combustion engines/generators, micro/mini-turbines and of course fuel cells amongst others. A brief overview of some conventional technologies is shown in Table 1.1 for comparison purposes [3].

Table 1.1: Comparison of fuel cell with various conventional distributed generation technologies.

	Diesel Engine	**Micro-Turbine**	**Mini-Turbine**	**Fuel Cell**
Size (MW)	0.05 – 6	0.03 – 0.5	0.5 – 10	0.001- 3
OEM ($/kWh)	0.005 – 0.015	0.004 – 0.010	0.003 – 0.008	0.002 – 0.015
Electric Efficiency (%) (LHV)[1]	33 – 43	18 – 32	21 – 40	40 – 60
Usable CHP Temp. (Degrees C)	80 – 90	200 – 350	250 – 600	60 – 350
Overall Efficiency (%)[2]	80 – 85	80 – 85	80 – 90	80 - 85
Availability (%)	90 – 93	90 – 98	90 – 98	> 95
Footprint (Sq m/kW)	0.023	0.023	0.028	0.084

[1] Electric Efficiency Lower Heating Value (LHV): net electric output at LHV

[2] Overall Efficiency: the sum of the electric and thermal outputs assuming Combined Heat and Power (CHP)

1.3 Fuel Cells

Steady progress in market deregulation and new legislations in terms of environmental constraints and greenhouse gas emissions have created a significant opportunity for distributed generation. Rising public awareness for ecological protection and continuously increasing energy consumption, coupled with the shortage of power generation due to constraints imposed on new construction have further resulted in a steady rise in interest in renewable and clean power generation. Fuel cell technologies are expected to play a significant role in overcoming the many challenges faced by the power market to satisfy the ever-increasing energy needs [4,5,6].

Fuel cells offer numerous advantages over conventional power plants to help them achieve that goal and widespread adoption, such as:

- High efficiency, even at part-load
- Few moving parts resulting in quiet operation, higher reliability, lower maintenance and longer operating life
- Fuel diversity
- Zero or low emission of greenhouse gases
- Combined Heat and Power (CHP) capability, without the need for additional systems (i.e., low temperature fuel cells can provide district heating while high temperature fuel cells can provide high-quality industrial steam)
- Flexible, modular structure
- Increased energy security by reducing reliance on large central power plants and oil imports

Fuel cells also provide several advantages over renewable technologies, such as wind turbines and photovoltaic power generation. These include the ability to be placed at any site in a distribution system without geographic limitations to provide optimal benefit, and they are not intermittent in nature.

1.3.1 Various Types of Fuel Cell Technologies

Several different types of fuel cells exist, each using a different chemistry. The technologies are generally characterized by the type of electrolyte they use, which also determines their operating temperature. Aqueous electrolytes are limited to temperatures below 200°C due to their high water vapor pressure and/or rapid degradation at high temperatures [7]. The operating temperature further affects the type of fuel that can be used. Low-temperature fuel cells with aqueous electrolytes are mostly restricted to the use of hydrogen as the fuel. In high-temperature fuel cells, other hydrocarbons may be used due to the inherently faster electrode kinetics.

There are five major types of fuel cells being commercially developed. Among these five, Alkaline Fuel Cells (AFC) are the oldest design and have been used in the NASA space program since the 1960s [8]. Nevertheless, it is very expensive and susceptible to contamination, thus requiring hydrogen and oxygen in their purest form as even the smallest amounts of dirt would destroy the cell. They are well suited to closed environments containing their own supplies of hydrogen and oxygen, such as space travel and submarine engines. Proton Exchange Membrane Fuel Cells (PEMFC) have good power density and response time, and are considered the most promising technology, thus being developed for use in various applications. Phosphoric Acid Fuel Cells (PAFC) are very tolerant to impurities in the fuel steam and very similar to the PEMFC in terms of construction. However, due to poor ionic conduction, it is comparatively larger and weighty resulting in increased cost [8]. The phosphoric acid also effloresces irreversibly (i.e., becomes powdery) when the temperature sinks below 42°C and the cell becomes unusable. Still, its high operating temperature makes it well suited for co-generation. Solid Oxide Fuel Cells (SOFC) also operate at high temperature and use a ceramic material as electrolyte, resulting in a complete solid-state design and can operate without a reformer. The high temperature however also affects the reliability of the system. Finally, Molten Carbonate Fuel Cells (MCFC) operate at slightly lower temperature than the SOFC, which in turn reduces the need for exotic materials and thus also the price. Their high quality heat also makes them well suited for CHP applications. A

summary of the various fuel cell technologies is shown in Table 1.2.

Table 1.2: Summary of various fuel cell technologies

Type	Electrolyte	Charge Carrier	Operating Temperature	Fuel	Efficiency (System)	Power Range/ Application
PEMFC	Solid Polymer (e.g. Nafion)	H+	~ 80°C	Pure H2 (tolerates CO2)	35 – 45%	Automotive, CHP (5 – 250 kW), portable
AFC	Aqueous Potassium Hydroxide	OH-	~ 100°C	Pure H2	35 – 65%	< 5 kW, niche markets (military, space)
PAFC	Phosphoric Acid	H+	~ 200°C	Pure H2 (tolerates CO2, ~1% CO)	40 – 45%	CHP (200 kW)
SOFC	Solid Oxide Electrolyte	O2-	~ 1000°C	H2, CO, CH4, hydrocarbons (tolerates CO2)	50 – 60%	2 kW – MW range, CHP and stand-alone
MCFC	Lithium & Potassium Carbonate	CO_3^{2-}	~ 650°C	H2, CO, CH4, hydrocarbons (tolerates CO2)	50 – 60%	2 kW – MW range, CHP and stand-alone

The PEMFC is chosen due to its high power density, which is an order of magnitude higher than other types of fuel cells with the exception of the AFC [1,9]. This is partially a result of the intense research and development in this fuel cell technology over the last decade. It also has a lower operating temperature, allowing for fast start-up and has a simple and composite structure, resulting in relatively high durability. Finally, compared to the other fuel cell technologies, the PEMFC has the ability to rapidly adjust to power demand changes.

1.3.2 Basic Operation of Proton Exchange Membrane Fuel Cell

A fuel cell is an electrochemical device that continuously converts chemical energy into electric energy with some heat, as long as the fuel and oxidant are supplied. This process, along with the various components, is illustrated in Figure 1.1 for the PEMFC. Most fuel cells in use today utilize hydrogen and oxygen as chemicals. Gaseous hydrogen is the most popular due to its high reactivity when suitable catalysts are used, its ability to be produced from hydrocarbons and its high energy density for storage. Similarly, the most common oxidant is gaseous oxygen as it is readily and economically available from air and is easily stored.

At the anode (negative electrode), hydrogen is oxidized to provide electrons and hydrogen ions. Hydrogen ions travel from the anode to the cathode via an electrolyte. However, because the electrolyte is a non-electronic conductor, the electrons can only flow from the anode to the cathode (positive electrode) via the external circuit. At the cathode, oxygen reacts with the incoming electrons and the hydrogen ions to produce water. The equations for the reactions are given in (1.1).

Another familiar electrochemical device is the battery. The difference between fuel cells and batteries is that in batteries all the chemicals are stored inside, which means that they eventually vanish and the battery must be thrown away or recharged. On the other hand, a fuel cell will operate continuously as long as it is supplied with fuel. Still, of course, its lifetime is practically limited due to degradation such as corrosion and malfunction of components.

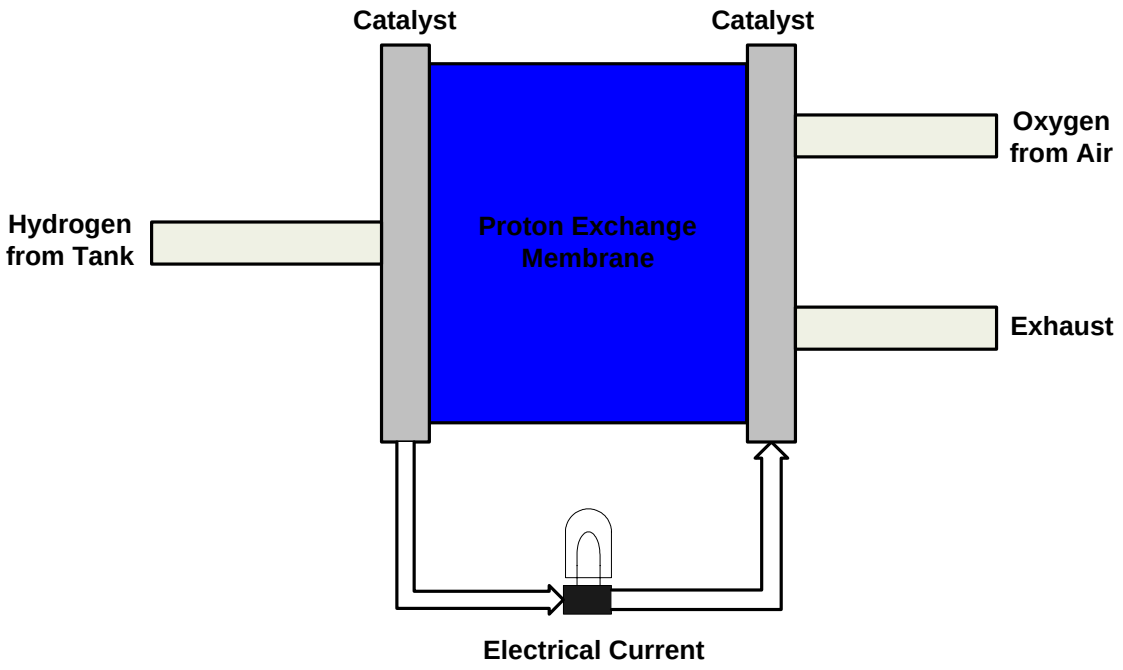

Figure 1.1: Basic PEMFC operation.

$$\begin{aligned} &Anode: && H_2 \rightarrow 2H^+ + 2e^- \\ &Cathode: && 1/2O_2 + 2H^+ + 2e^- \rightarrow H_2O \\ &Overall: && H_2 + 1/2O_2 \rightarrow H_2O \end{aligned} \qquad (1.1)$$

1.3.3 Operating Characteristics

As the fuel cell is operated to supply electrical energy, various mechanisms lead to 'irreversible' losses that further cause its output voltage to fluctuate. There are three main causes for the losses:

1) Activation losses
2) Ohmic losses
3) Concentration losses

These losses cause the cell voltage to be less than the ideal potential, and each are dominant at different current densities. Activation losses are dominant at low currents to overcome electronic barriers in order to transfer electrons to and from the electrodes, and

result in a non-linear drop. As the current increases within the normal range, the ohmic losses become more important due to the resistance to the flow of electrons through the electrodes and also include the resistance to the proton flow through the electrolytes. The curve shows a fairly linear characterization through this range. Finally, concentration losses take over at high currents due to the difficulty associated with supplying enough reactant flow to the cell reaction, causing the cell voltage to decrease rapidly. This operating region should obviously be avoided. These various loss mechanisms should be accounted for when deriving the fuel cell model.

The net system efficiency and power output as a function of current for the 1.2 kilowatt PEMFC used for experimental demonstration is shown in Figure 1.2. The plot represents the fuel cell operating in its normal range, as illustrated by the reasonably linear curves. One can note the tradeoff between output power, where it is desired to maximize the output of the fuel cell, and efficiency, where higher efficiency can be attained at lower output levels. This conflict amongst others will be reviewed in Chapter 4 when developing suitable control strategies that maximize the performance of the system.

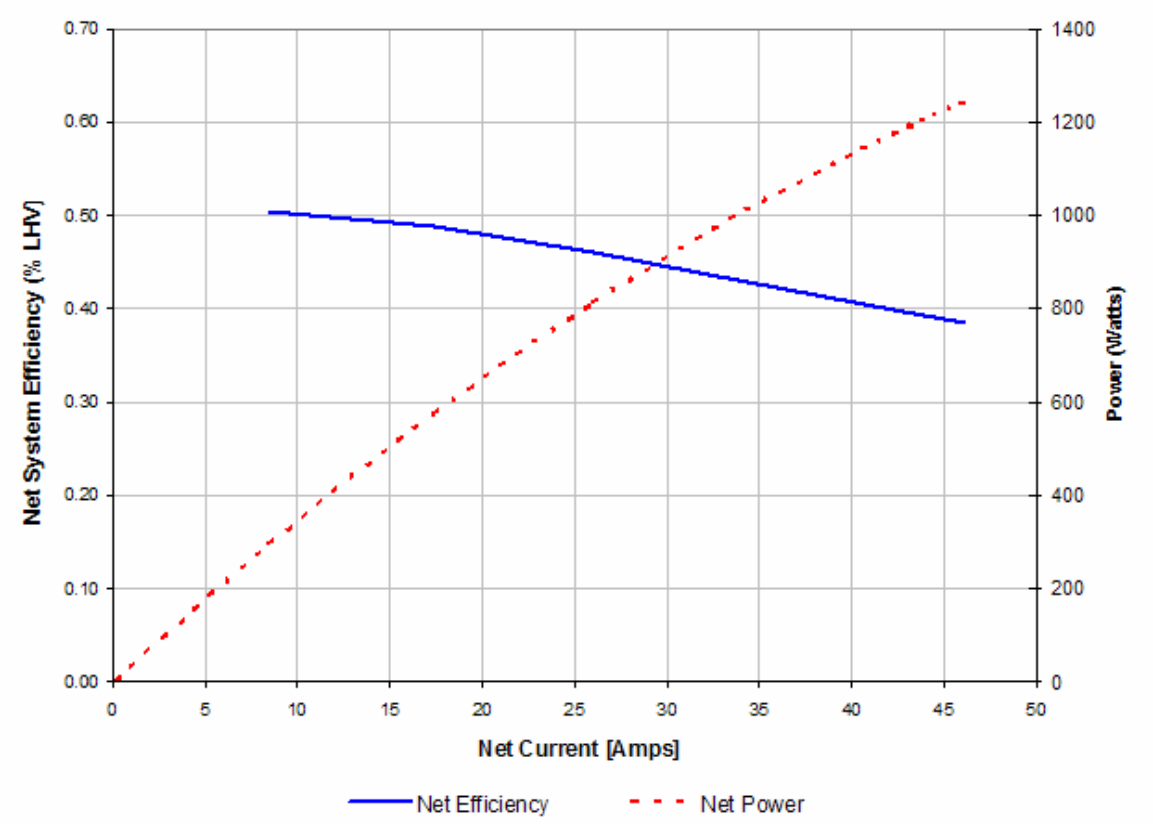

Figure 1.2: Fuel cell system efficiency and power as a function of current for the Ballard Nexa Power Module.

1.3.4 Power Conditioning

A fuel cell generates direct current (dc) power. This power must be controlled in terms of voltage and current to adequately supply the load. In addition, if it is to supply alternating current (ac) loads, dc-ac inversion is required along with frequency control. Nevertheless, the power conditioning at the dc side prior to inversion is the most critical in terms of effectively meeting the fuel cell's requirements and managing its operation to meet the load demand. Once the constraints and design objectives are satisfied in terms of regulation and energy management, the dc power may then be inverted using a simple dc-ac inverter with basic control to synchronize with the grid and manage the output active and reactive powers, whilst still achieving improved performance. Previous papers have attempted to bypass this stage in hope of improving cost and reliability. This causes

the power sharing to be passively determined between the power sources, the bus voltage to not be regulated and instead follow the battery's discharge curve [10,11,12]. Moreover, other work has attempted to control the fuel cell current through the long time constant of the hydrogen delivery system [9,13] or even attempt to actively control the sources using derived inverters such as the Z-source [14,15]. Still, tradeoffs exist and inclusion of the dc conversion stage is necessary for superior performance and flexibility, as will be demonstrated. Additionally, for the given application, the converter fulfills important requirements in association with the fuel cell, as will be described in the following paragraph. Hence, this dissertation will be concerned with the power conditioning at the dc level. Furthermore, a step-up, or boost converter is chosen for the power conversion for better efficiency by reducing the current, and thus the losses, and also since designing fuel cell stacks for higher voltages is less efficient [9].

With this in mind, the PCU is required to have the following characteristics to supplement the fuel cell's operation [3, 4, 9]:

- Output voltage regulation at desired value as dictated by specific application
- Wide input regulation due to fuel cell's significant output voltage dependency on current
- Process power to meet load demand in terms of requested voltage and current
- Protect fuel cell against various disturbances in system, including stepped load changes, which lead to stack lifetime degradation
- Reduce ripple in current and voltage fed back to fuel cell, which also leads to lifetime degradation
- Avoid reversal of current polarity under all circumstances
- High efficiency and reliability
- Stable operation despite external disturbances
- Active and accurate power sharing amongst power sources in case of multiple sources operating in parallel
- Improved system dynamics and output power quality

- Low cost

Although the PCU can be seen as a factor that adds to the cost of the fuel cell power plant and reduces efficiency due to the losses in the solid-state devices, it can also be seen as a way of adding value to the plant by improving the performance, stability, reliability and even the efficiency and cost of the power plant. Still, as fuel cells become more widely used, it is becoming more and more apparent that there is a gap in the power conversion electronics market for the application of fuel cells [16].

1.4 Motivation and Objectives

The deregulation and restructuring of utilities is leading to a massive and rapid industry change with new methods of energy supply. This has opened the door for a wide deployment of distributed generation, in particular fuel cells, to meet the ever-increasing energy demands despite the many constraints and shortcomings in today's market. Nevertheless, the fuel cell is faced with its own constraints and shortcomings, and research must be performed in this area to overcome these obstacles and tap into the fuel cell's potential and its deployment as a solution to the current energy crisis.

In particular, the fuel cell is limited by its far from ideal operation as a power source, which includes its slower dynamics and poor output voltage regulation. It is also sensitive to various disturbances in the system, such as current/voltage ripple and repetitive abrupt load changes. The design of the PCU to compensate for these limitations is therefore a major challenge, yet critical to the fuel cell's overall performance and its applicability, and cannot be overlooked, as is too often the case when performing 'fuel cell research'. Opportunities to add value to the system through the use of the PCU must also be taken advantage of to improve the system and thus justify the

added cost. The PCU is thus chosen as the central topic of this dissertation.

Central to the PCU itself and its success is the dc-dc converter that is connected directly to the fuel cell and is therefore the most sensitive to its behavior, which must in turn ensure its safe operation and extended lifetime as well as its adequate performance and ability to meet the demand requirements. Yet, some papers have bypassed this converter stage altogether and use only a dc-ac inverter in an attempt to improve efficiency and reduce complexity and cost. Still, it is more effective to properly and 'actively' manage the power flow from the various sources at the dc level using a dc-dc converter rather than allowing the power sharing to be determined passively amongst the sources based on their relative impedance characteristics, as will be further discussed in Chapter 4. Attempting to control the power sharing through the hydrogen delivery system or through the dc-ac inverter offers its own challenges and setbacks as well, and superior performance can only be attained through the inclusion of a dc-dc converter.

To this end, a suitable dc-dc converter must first be devised that meets the given constraints for the application. The converter must then be suitably modeled in order to gain insight into its behavior. A wide variety of models exist, many of which are made too complex without any added accuracy, which also hinders the design of the control loops. In this dissertation, a mathematical description is sought that is accurate, yet simple enough to design suitable compensators and provides the opportunity for the use of well-developed control techniques to attain the desired response characteristics. Similarly, a suitable model of the fuel cell that incorporates its dynamics when connected to a switching mode circuit must be used in order to determine the conditions for its interface and analyze the overall performance of the PCU.

A suitable control scheme must then be applied to satisfy the load with the requested dynamics despite changes in the system's parameters. The dc-dc boost converter offers its own challenges in terms of closed-loop performance and stability and thus sophisticated control processes must be developed. Equally important is designing the compensators with the specific application in mind and incorporating the fuel cell's

unique limitations in the process rather than deriving a generic control scheme. The closed-loop control method must still compensate for the system's deficiencies and meet the objectives for robustness and good performance. Minimal research has been performed in the area of deriving suitable models and compensators aimed at the application of fuel cells, and the work presented here bridges the gap between the work performed separately in the two fields.

Opportunities to further improve the system's interface with the load must be investigated in order to efficiently, reliably and cost-effectively satisfy the application's requirements. The combination of the fuel cell with a secondary source of high power density, such as batteries, has shown the potential to provide many benefits and result in a 'synergistic' system where the whole is greater than the sum of its parts. Nonetheless, an effective configuration and control strategy of all power sources is of utmost importance in order to reap these potential benefits and avoid degradation of the components. Intricate control must be implemented that balances the multiple, yet conflicting, design objectives. Moreover, the control scheme should be flexible to not only adhere and overcome the unique constraints of the application at hand, but to also allow extension to various hybrid systems so that it may be widely adopted.

There has been no shortage of control strategies implemented in previous works geared towards hybrid systems, however they tend to be doomed by either their simplicity, typically characterized by state machine and rule-based methods, or their complexity, typically characterized by optimization and model predictive control methods. In both the former and the latter it is difficult to meet and balance all the desired objectives in a flexible manner, and instability issues persist, particularly in the former, where there isn't adequate facility to account for the multiple constraints and compensate for the system's deficiencies. Here, a flexible control strategy is implemented that continuously adjusts the operating parameters in response to variations in the system. Furthermore, it provides the facility to successfully implement a wide variety of control strategies to meet the various objectives as desired.

Finally, all the above must be tested and verified with real components and hardware on top of computer simulations to prove the proposed system's feasibility and effectiveness for real world applications. Moreover, due to the high cost associated with the apparatus, the experimental set-up should be flexible to allow an efficient design and testing process of all the work related to this field, and offers a much-needed facility for academia as well as the industry to bring forth and develop this important research.

In summary, the thesis aims to accomplish the following objectives:

1) Take advantage of the PCU to add value to the fuel cell power plant and tap into its potential to meet the increasing energy demands
2) Devise an effective topology of the PCU to efficiently and reliably meet the load demand with the requested dynamics
3) Devise suitable models of the various components in the PCU to gain insight into their behavior and limitations for the application at-hand
4) Devise suitable compensators by way of the developed models with careful considerations aimed at overcoming the various limitations in the system and satisfying its specific requirements
5) Devise a suitable hybrid control strategy that is flexible and robust in order to maximize the potential benefits of the various sources
6) Build a flexible bench-scale test facility to efficiently test the research
7) Verify the proposed system's feasibility and effectiveness using real components

1.5 Outline

Chapter 2 discusses the requirements for the power conditioning of electronic systems, and thus the need for dc power supplies. In particular, switch-mode power supplies and their operation are discussed to fulfill the requirements for the given application. The chapter then proceeds to derive a suitable model for the power converter that may be used

for control purposes. To this end, the state-space averaging technique is developed and applied for the specific case of the boost dc-dc converter implemented in this work. Important transfer functions are obtained and plotted using MATLAB to gain physical insight into the system's behavior.

Chapter 3 first presents a comparison between the various closed-loop control techniques for dc-dc converters to attain the desired system robustness and performance. The advantages and operating characteristics of current mode control, in particular average current mode control, are highlighted in view of the application at hand. The fundamental control blocks in control theory are also reviewed such that they may be correctly applied to meet the desired properties of the open loop. A thorough analysis of the boost dc-dc converter's behavior is then presented in order to accurately develop the sophisticated control processes necessary to overcome its unique challenges to control design. Models for the control loop are derived and combined with the results for the power stage model from Chapter 2 to obtain a complete system model that may be used to design the compensators. Modeling based on the philosophy of attaining expressions that are accurate and lend insight into dominant system behavior, yet practical and simple enough to design with, is preserved. The complete system is analyzed and simulated using MATLAB once again to observe the ability of the developed control strategy to meet the design objectives for the application at-hand and provide the necessary robustness against external disturbances.

Chapter 4 explores the opportunity to enhance the fuel cell power plant's interface and ability to meet the load characteristics for the given applications. The potential benefits of combining the fuel cell with a secondary power source are discussed. Nevertheless, various factors contribute to the success of such a hybrid system. First, the various potential candidates as energy storage systems to complement the fuel cell are compared to determine their suitability. The configurations of interconnecting the various components in the system are then examined in order to find a topology that maximizes each component's output and provides the flexibility to reap all the potential benefits. Finally, the last piece of the puzzle is an effective control strategy, which is critical to the

overall system's efficiency and reliability. Continuing with the previous design philosophy, a control strategy is sought after that achieves all the desired properties while aiming to maintain an ideal compromise between complexity and performance. A list of control objectives is developed, which leads to a configuration that allows direct application of the closed-loop control method derived in Chapter 3. The performance of the system and versatility of the control strategy are then investigated via simulations using MATLAB/Simulink.

Chapter 5 presents the experimental work to validate the results obtained throughout the dissertation. An overview of the experimental set-up and components is provided in the first section, where it is intended to construct a modular test station that would allow an efficient design process. The results for the conducted tests are then given in the second section.

Appendix A provides the state-space matrices of the dc-dc boost converter's dynamic model developed in Chapter 2.

Appendix B presents simulations results for the hybrid system already presented in Chapter 4. Due to certain component limitations in the experimental setup, the hybrid system is simulated once again with the encountered limitations replicated for comparison and verification purposes.

A flow chart for the dissertation highlighting the progression through the chapters is presented in Figure 1.3.

(a) Chapter 1

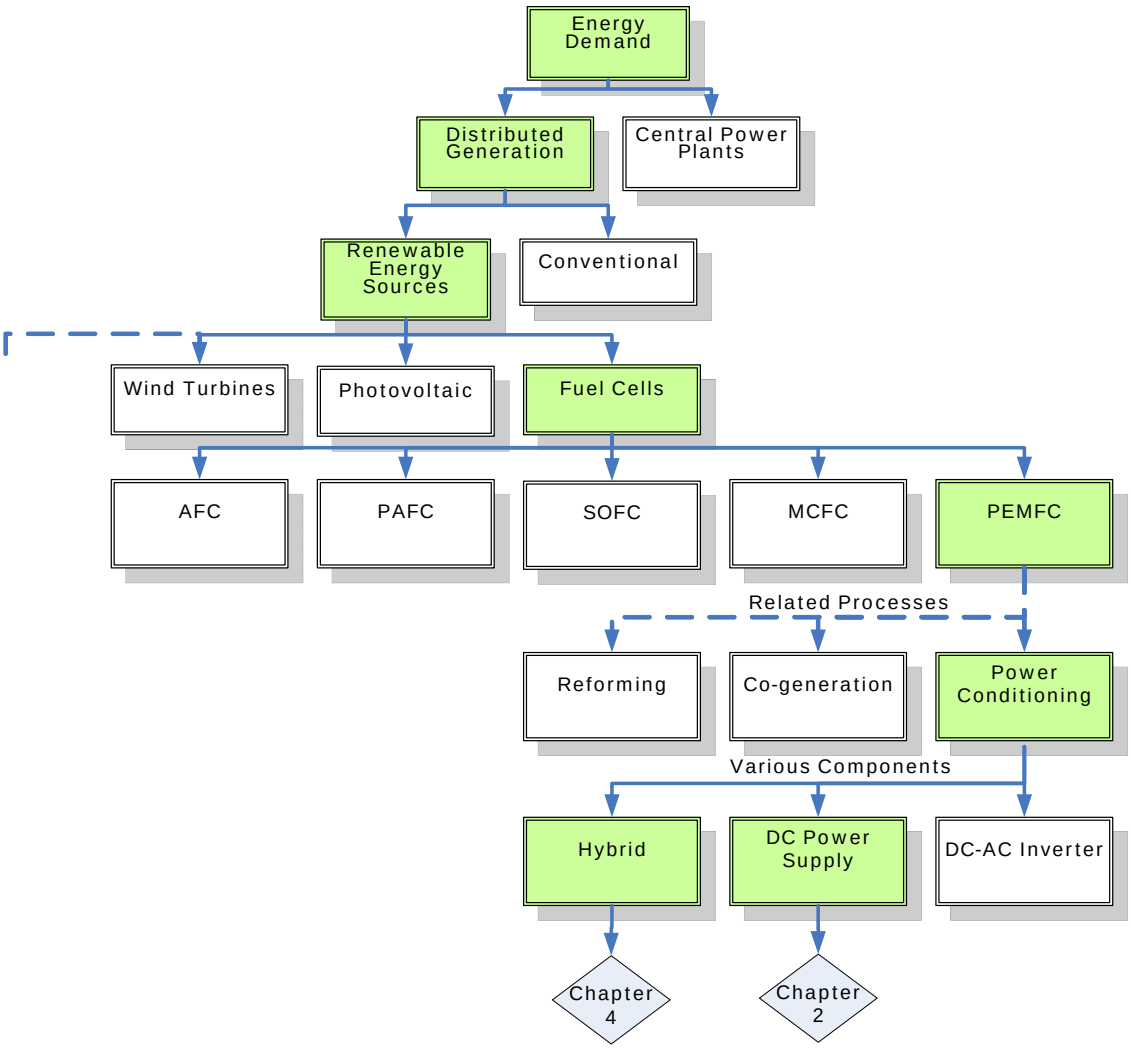
Energy Demand
Distributed Generation
Central Power Plants
Renewable Energy Sources
Conventional
Wind Turbines
Photovoltaic
Fuel Cells
AFC
PAFC
SOFC
MCFC
PEMFC
Related Processes
Reforming
Co-generation
Power Conditioning
Various Components
Hybrid
DC Power Supply
DC-AC Inverter
Chapter 4
Chapter 2

(b) Chapter 2

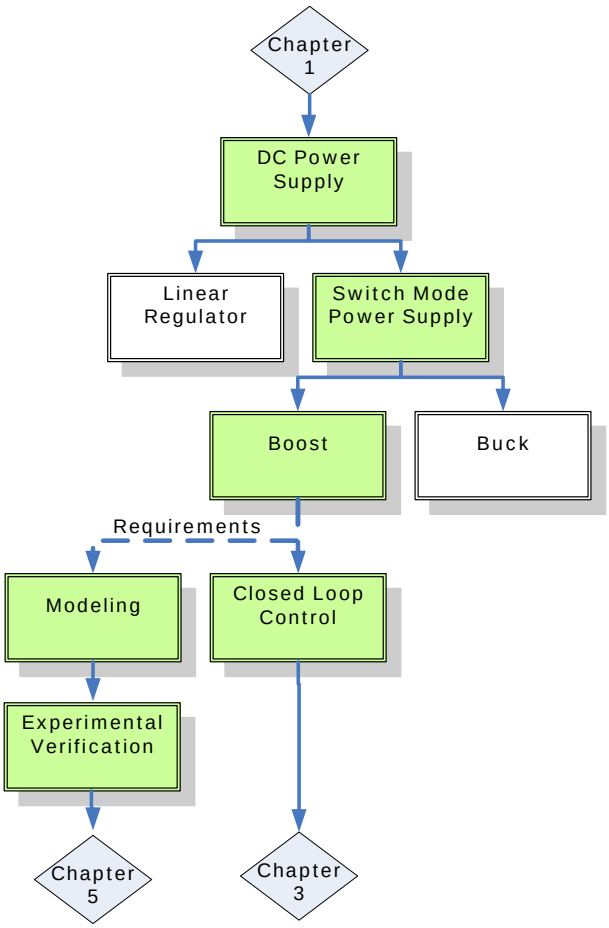
Chapter 1
DC Power Supply
Linear Regulator
Switch Mode Power Supply
Boost
Buck
Requirements
Modeling
Closed Loop Control
Experimental Verification
Chapter 5
Chapter 3

(c) Chapter 3

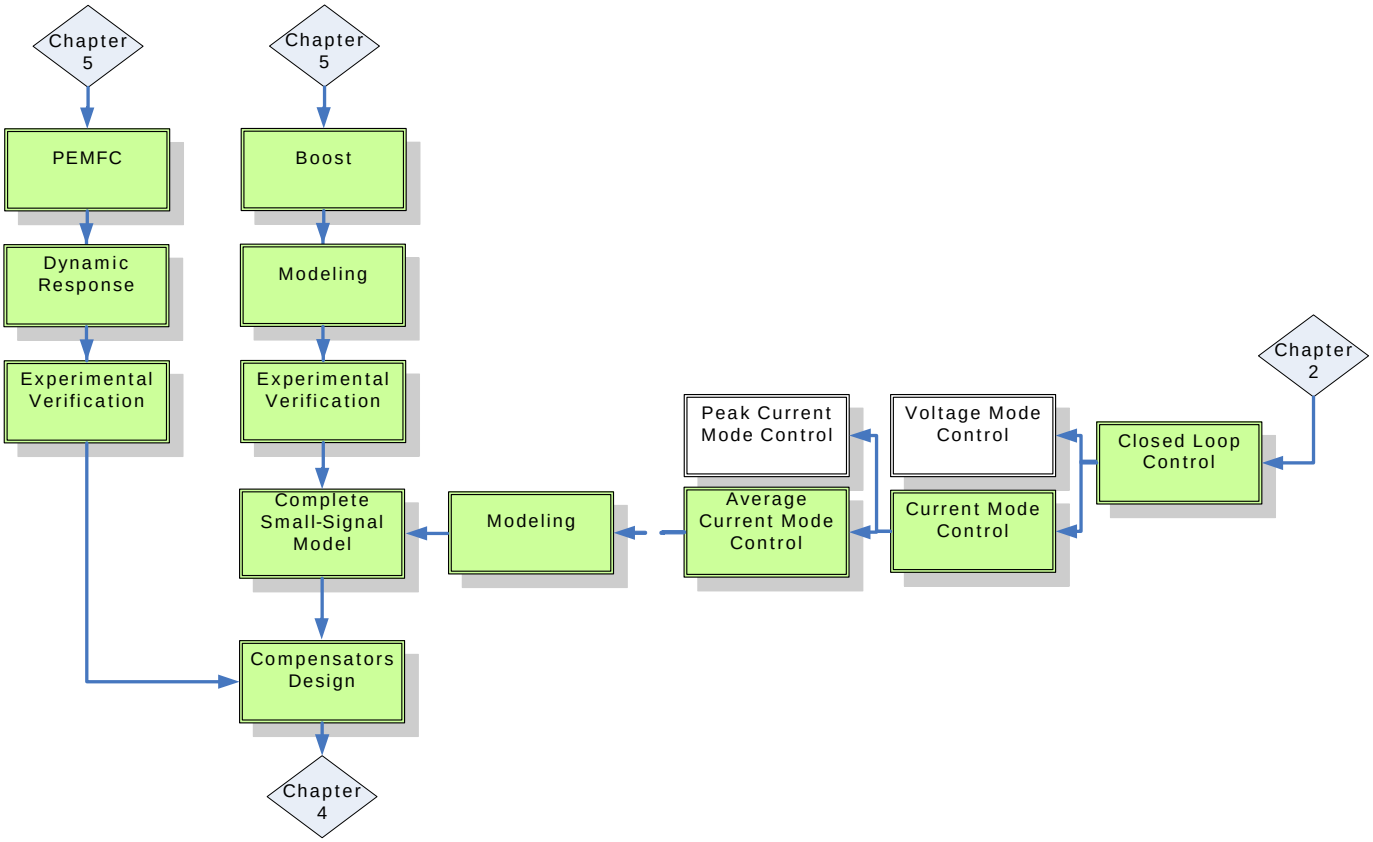

(d) Chapter 4

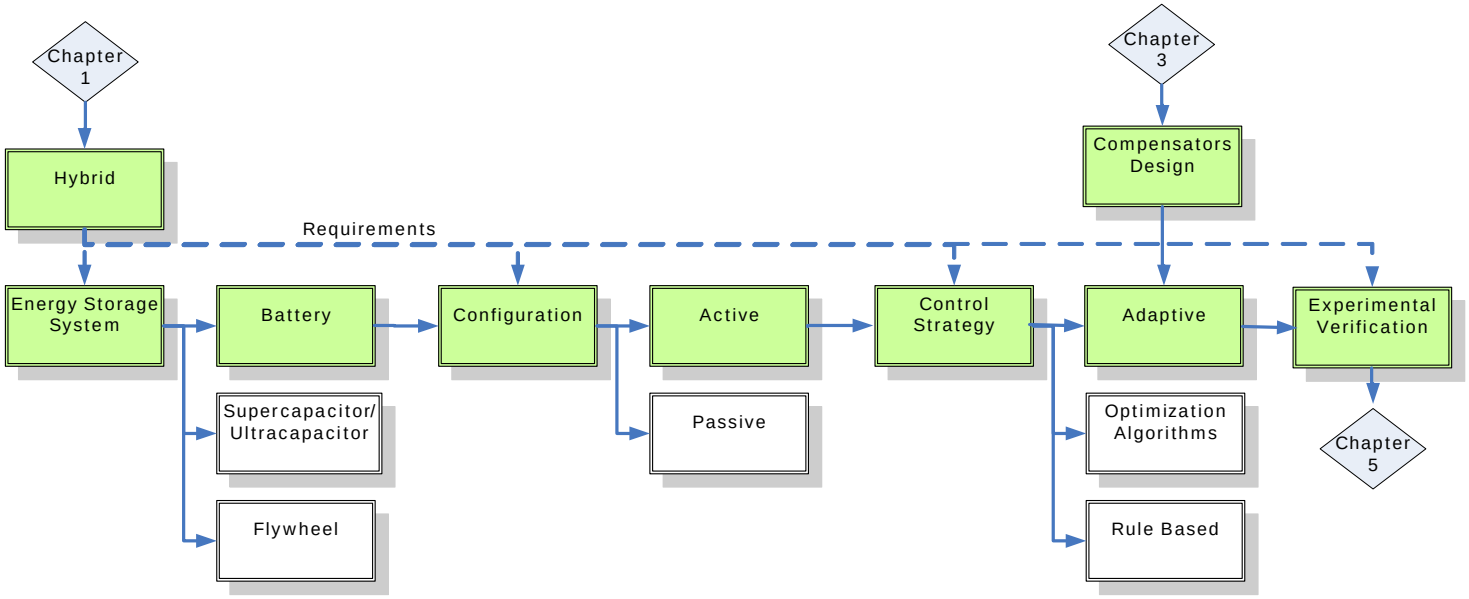

(e) Chapter 5

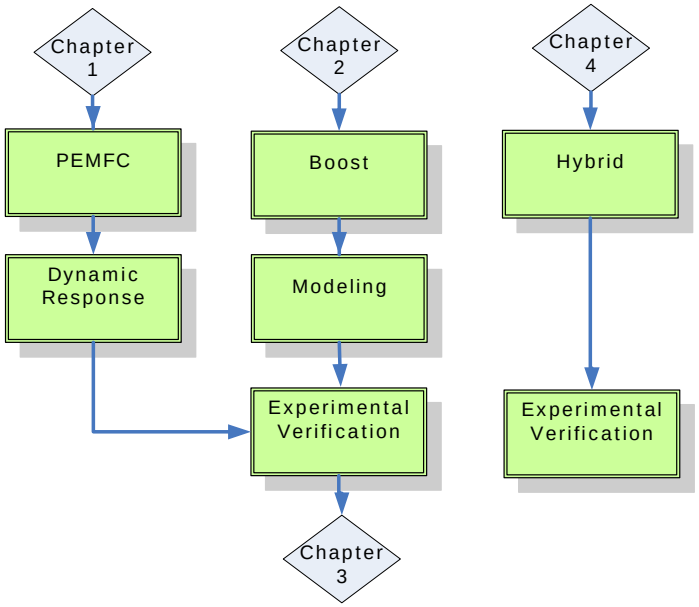

Figure 1.3: Thesis flow chart: (a) Chapter 1 (b) Chapter 2 (c) Chapter 3 (d) Chapter 4 (e) Chapter 5.

Chapter 2
DC-DC Boost Converter

2.1 Introduction

Modern electronic systems require dc power supplies to regulate the output at a given value, reduce ac voltage ripple on the dc output voltage, electrically isolate the output from the input, or achieve multiple outputs that may differ in voltage and currents. In addition, the power supplies are desired to be high-quality, small, light-weight, reliable and efficient. The importance of the latter is two-fold: the cost of the wasted energy and the difficulty in removing the heat generated due to dissipated energy. Linear power regulators, whose principle of operation is based on a voltage or current divider and where the semiconductor devices are operated in their linear (active) region, cannot meet the above objectives in most systems. Furthermore, they are limited to output voltages smaller than the input voltage, and the presence of the transformers and filters brings about a low power density. Thus, their main area of application is at low power levels. At higher power levels, switching regulators are employed that control the *on* and *off* states of power electronic semiconductor switches. Due to the low power loss in both states and not requiring the power devices to operate in their active region, high efficiency can be achieved. Also, due to the ability of the switches to operate at high frequency, the transformers and filters can be made smaller and lighter. Since the corner frequency of the output filter is also increased with increased operating frequency, the converters' dynamic response can also be made faster. For electrical isolation and voltage transformation, the use of a high-frequency transformer instead of a line-frequency transformer also drastically decreases the size and weight of the switching regulators compared to the linear power supplies.

Dc-dc converters are widely used switch-mode power supplies. The input to these converters is typically an unregulated dc voltage that will fluctuate due to changes in the operating conditions. Switch-mode dc-dc converters are used to convert the unregulated dc input into a controlled dc output at a desired voltage level. The average dc output voltage must be controlled to equal a desired level despite variations in input voltage and output load. This is accomplished through the control of the *on* and *off* times of the switches present in the converters. One of the methods of controlling the output voltage is called Pulse-Width Modulation (PWM). It employs switching at a constant frequency and adjusts the *on*-time of the switch to control the output voltage. The duty-cycle, defined as the ratio of the *on*-time to the switching time period, is generated by comparing a signal-level control voltage with a repetitive waveform, typically a sawtooth. This control voltage signal is obtained by amplifying the error between the reference signal and the actual signal, the signal referring to either the voltage or current. The frequency of the repetitive waveform establishes the switching frequency, which is in the few kilohertz to a few hundred kilohertz range. Advantages of PWM switched converters include low component count, constant frequency operation, relatively simple control and commercial availability of integrated circuit controllers. The disadvantages result from its high frequency operation, which leads to increased switching losses and electromagnetic interference due to higher-order harmonics.

2.2 Boost Operation

Dc-dc boost or step-up converter, as the name implies, provides a regulated output voltage that is always greater than the input voltage. The boost converter, along with the buck or step-down converter, form the fundamental converter topologies from which most other converter topologies are derived. The boost converter consists of a dc input voltage source V_s, input capacitor C_i, inductor L, controlled switch S, diode D, output

filter capacitor C_o and output load represented by resistance R_{out}, as shown in Figure 2.1.

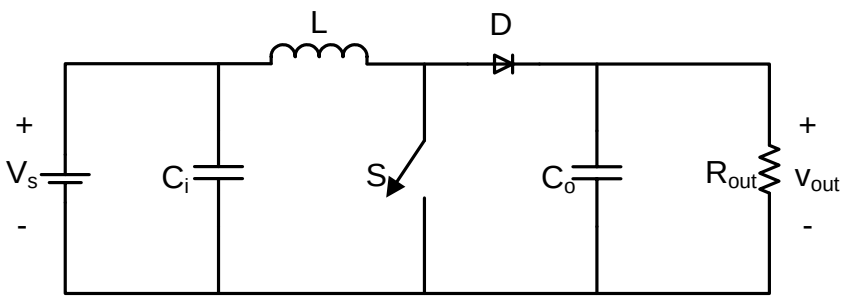

Figure 2.1: Basic dc-dc boost converter topology

When the switch is *on*, the diode is reverse biased, thus isolating the output stage, and the input supplies energy to the inductor while the capacitor discharges into the load. The inductor current ramps up essentially linearly as long as the filter's corner frequency is much lower than the switching frequency. When the switch is *off*, the inductor current commutates the diode, thereby turning it *on* and causing it to conduct, and the output stage receives energy from the inductor as well as from the input. Thus the inductor current ramps down. If it does not reach zero at the end of the switching period when the switch is once again turned *on*, a Continuous Conduction Mode (CCM) of the inductor current exists in which the transistor and diode are alternately *on* and *off*, and operate as a two-position single-pole switch. On the other hand, if the inductor current does reach zero, known as Discontinuous Conduction Mode (DCM), the diode current tries to reverse but cannot, and the diode therefore turns *off*. There is therefore a third interval where both the transistor and diode are *off*. Hence, the diode and switch operate as a three-position single-pole switch. Transition from CCM to DCM occurs when the converter load current falls below some minimum value.

Assuming CCM, the time integral of the inductor voltage over one time-period in steady-state is zero:

$$V_s t_{on} + (V_s - V_{out}) t_{off} = 0 \qquad (2.2)$$

Dividing both sides by T_s and rearranging the terms gives:

$$\frac{V_{out}}{V_s} = \frac{T_s}{t_{off}} = \frac{1}{1-D} \tag{2.3}$$

Assuming a lossless circuit:

$$P_s = P_{out} \tag{2.4}$$

Therefore

$$\frac{I_{out}}{I_s} = (1-D) \tag{2.5}$$

2.3 Power Converter Dynamic Modeling

2.3.1 Introduction

Power converters must be suitably controlled to supply the requested voltages, currents, or frequency ranges for the load with the constrained dynamics despite changes in the output load and input line voltages. This is accomplished through a negative-feedback control system to obtain the necessary robustness. In order to get rid of the guesswork involved in designing the control loop and meet the performance objectives, it is essential to describe the system mathematically with an accurate model in order to obtain physical insight into its behavior. Furthermore, to use linear feedback control methods based on Laplace transform, Bode plots and root locus, the resulting system must be linear. Classical linear systems control theory can then be applied to determine suitable compensation for the power stage in order to attain the desired steady-state and transient

responses.

Middlebrook and Cúk developed a state-space averaging technique that results in a linear model of the power stage for small ac signals linearized around a steady-state dc operating point [17]. State-space modeling provides a general and strong basis for dynamic modeling of various systems such as power converters while maintaining an ideal compromise between accuracy and simplicity, thus justifying its widespread adoption [18,19]. The resulting transfer functions can be used to design the linear control loops and computer simulate the steady-state as well as the dynamic behavior of the power converter. The analysis is first developed in general for any dc-dc switching converter, and then demonstrated in detail for the boost converter at hand, in which parasitic effects of the components are also accounted for.

2.3.2 State-Space Modeling

State-space modeling is based on the fact that any PWM converter is a special class of nonlinear system that is switched between two or more linear circuits according to the associated duty ratio. The transient analysis and control design is therefore complicated by the fact that a number of equations must be solved in sequence. The technique of averaging solves this problem by taking a linearly weighted average of each separate set of equations describing the switched network to form a single set of equations for the states and output. Since the averaging process 'approximates' the behavior of the converter over many cycles, for the approximation to be valid, two main conditions must be satisfied: first the state variables must evolve in an approximately linear manner in all the circuit configurations, and second the switching frequency ripple component of the state variables must be small in comparison with the average component [17]. Both of these conditions are typically satisfied in simple dc-dc converters [19]. The latter condition is equivalent to requiring that the output filter's cutoff frequency be much lower than the switching frequency. The resulting model is accurate at relatively lower frequencies, and becomes better the more the effective low-pass filter's corner frequency

is below the switching frequency.

- State-Space Averaged Model

As previously discussed, there are usually two modes of operation for dc-dc converters: continuous and discontinuous. For a converter operating in CCM, there are two circuit states: one state when the switch is *on* and the other when the switch is *off*, as shown in Figure 2.2. In the case of DCM, an additional circuit state exists. Since CCM is assumed, only a two-switched converter is considered.

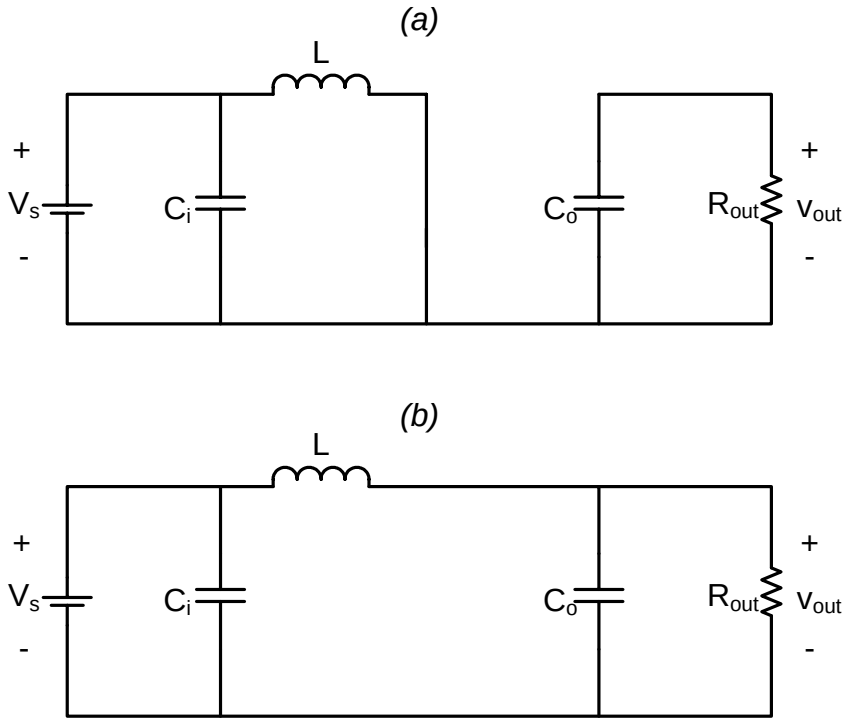

Figure 2.2: Two circuit states for boost converter: (a) switch is *on* (b) switch is *off*.

In each of the two positions of the switch, the system is linear and can be described by state-space equations. The state variables are the inductor currents and capacitor voltages. Therefore, considering ideal switches, the following two sets of state-space equations can be written for each circuit state:

$$\begin{aligned} \dot{x} &= A_1 x + B_1 u \qquad during \;\; d \cdot T_s \\ \dot{x} &= A_2 x + B_2 u \qquad during \;\; (1-d) \cdot T_s \end{aligned} \tag{2.6}$$

where x is the vector of state variables, $\dot{} = d/dt$, u is the vector of input or control independent sources (source voltage, output current, etc…), A_1, B_1 and A_2, B_2 are the respective system matrices and can be derived by applying simple circuit analysis on the two circuits in Figure 2.2. The duty ratio d is the control input that determines the *on* and *off* time of the switch, and thus the fraction of the period each cycle that the system spends in each circuit configuration.

The key is combining the two sets of state-space equations into a single equivalent set over a complete switching period of the form:

$$\dot{x} = A \cdot x + B \cdot u \tag{2.7}$$

where the equivalent matrices A and B are weighted averages of the actual matrices. Since for a given duty ratio d, the system spends $d \cdot T_s$ described by A_1 and B_1, where T_s is the switching period, and the remaining $(1\text{-}d) \cdot T_s$ described by A_2 and B_2, one can write:

$$\begin{aligned} A &= d \cdot A_1 + (1-d) \cdot A_2 \\ B &= d \cdot B_1 + (1-d) \cdot B_2 \end{aligned} \tag{2.8}$$

In the case the output signal required for some transfer function is not one of the state variables, but rather some linear combination of them (e.g., v_{out} in Figure 2.2 if an Equivalent Series Resistance (ESR) for the output capacitor is accounted for), it is necessary to include an output vector y for each of the two-switched networks as well:

$$\begin{aligned} y &= C_1 \cdot x \\ y &= C_2 \cdot x \end{aligned} \tag{2.9}$$

The weighted average of the matrix C is done in the same way as for A and B:

$$C = d \cdot C_1 + (1-d) \cdot C_2 \tag{2.10}$$

allowing to replace (2.9) with (2.11):

$$y = C \cdot x \tag{2.11}$$

Substituting (2.8) and (2.10) into (2.7) and (2.11) gives:

$$\begin{aligned} \dot{x} &= (d \cdot A_1 + d' \cdot A_2) \cdot x + (d \cdot B_1 + d' \cdot B_2) \cdot u \\ y &= (d \cdot C_1 + d' \cdot C_2) \cdot x \end{aligned} \tag{2.12}$$

where $d' = 1 - d$.

To get the average or steady-state dc value of the states, the state equation in (2.12) can be set to zero since the state vector under dc conditions is a constant and its derivative is therefore zero:

$$\left(D \cdot A_1 + D' \cdot A_2\right) \cdot X + \left(D \cdot B_1 + D' \cdot B_2\right) \cdot u_0 = 0 \tag{2.13}$$

where capital letters denote the dc values and subscript '$_0$' denotes the initial value. From (2.13), the state vector for dc conditions is given by:

$$X = -A^{-1} \cdot B \cdot u_0 \tag{2.14}$$

and the dc output voltage is:

$$Y = C \cdot X \tag{2.15}$$

- Perturbed State-Space Averaged Model:

Since the converter output *y* must be regulated through variations in *d* despite perturbations in the converter's inputs *u* due to load and power supply variations, the variables must be decomposed into dc steady-state quantities and small ac perturbations:

$$\begin{aligned} x &= X + \hat{x} \\ u &= u_0 + \hat{u} \\ y &= Y + \hat{y} \\ d &= D + \hat{d} \end{aligned} \tag{2.16}$$

where the lowercase letter represents the variable, the capital letter represents the steady-state value, and the lowercase letter with the hat symbol ('^') represents the small ac perturbation. This procedure now formulates the small-signal ac analysis.

Substituting the perturbations terms of (2.16) into the system of (2.12) and simplifying, we obtain the following perturbed averaged model:

$$\begin{aligned} \dot{\hat{x}} = A \cdot X + B \cdot u_0 + \left[\left(A_1 - A_2 \right) \cdot X + \left(B_1 - B_2 \right) \cdot u_0 \right] \cdot \hat{d} \\ + \left[\left(A_1 - A_2 \right) \cdot \hat{x} + \left(B_1 - B_2 \right) \cdot \hat{u} \right] \cdot \hat{d} \end{aligned} \tag{2.17}$$

$$Y + \hat{y} = C \cdot X + C \cdot \hat{x} + \left(C_1 - C_2 \right) \cdot X \cdot \hat{d} + \left(C_1 - C_2 \right) \cdot \hat{x} \cdot \hat{d}$$

where the following relations were used:

$$\begin{aligned} \hat{d}' &= -\hat{d} \\ \frac{dX}{dt} &= 0 \end{aligned} \tag{2.18}$$

The perturbed state-space description of (2.17) becomes nonlinear due to the presence of the product of two independent quantities, mainly $\hat{x}$ and $\hat{d}$. This is a result of the duty

cycle, which is the control input, not being an element in the input vector *u*.

- Linearized State-Space Averaged Model:

Control of the system with nonlinearities is difficult when performance objectives must be met. Under the assumption of small-signal operation, linearization is done through a Taylor series expansion around the points (*X*, *D*, *Y*, u_0), and nonlinear terms of higher orders are thrown away, i.e., departures from the steady-state values are negligible compared to the steady-state values themselves,

$$\frac{\hat{u}}{u_0} << 1, \qquad \frac{\hat{d}}{D} << 1, \qquad \frac{\hat{x}}{X} << 1 \tag{2.19}$$

and therefore:

$$\hat{x} \cdot \hat{d} \approx 0 \tag{2.20}$$

resulting in a linear approximation of the state-space equations representing the average states subject to a perturbation in *X*, *D*, *Y*, or u_0:

$$\begin{aligned} \dot{\hat{x}} &= A \cdot \hat{x} + B \cdot \hat{u} + \left[\left(A_1 - A_2 \right) \cdot X + \left(B_1 - B_2 \right) \cdot u_0 \right] \cdot \hat{d} \\ \hat{y} &= C \cdot \hat{x} + \left(C_1 - C_2 \right) \cdot X \cdot \hat{d} \end{aligned} \tag{2.21}$$

Equation (2.21) represents the final dynamic small-signal state-space averaged model of any two-state switching dc-dc converter operating in CCM, with the final steady-state dc model given by (2.14) and (2.15).

- Small-Signal Transfer Functions:

Taking the Laplace transform of (2.21) with zero initial conditions and solving for the

duty cycle-to-output transfer function, we obtain the following relation:

$$\frac{Y(s)}{D(s)} = C \cdot \left(s \cdot I - A\right)^{-1} \cdot \left[\left(A_1 - A_2\right) \cdot X + \left(B_1 - B_2\right) \cdot u_0\right] + \left(C_1 - C_2\right) \cdot X \qquad (2.22)$$

This expression is used to analyze the converter's dynamic behavior and design the compensators. Recalling that for a linear system defined by state-space equations in the standard form:

$$\begin{aligned} \dot{x} &= A_s \cdot x + B_s \cdot u \\ y &= C_s \cdot x + E_s \cdot u \end{aligned} \qquad (2.23)$$

Its transfer function from the input-to-output is given by:

$$\frac{Y(s)}{U(s)} = C_s \cdot \left(s \cdot I - A_s\right)^{-1} \cdot B_s + E_s \qquad (2.24)$$

If (2.22) can be put back into the 'standard' state-space form of (2.24), then all the mathematics and design techniques available based on state-space description can be directly used for the system at hand. By comparison of the two equations, this transformation can be done by making the following relations:

$$\begin{aligned} A_s &= A \\ B_s &= \left(A_1 - A_2\right) \cdot X + \left(B_1 - B_2\right) \cdot u_0 \\ C_s &= C \\ E_s &= \left(C_1 - C_2\right) \cdot X \end{aligned} \qquad (2.25)$$

The *A* and *C* matrices remain as previously defined, whereas the *B* matrix has changed and an *E* matrix is introduced and replaces any *E* matrix that may have been previously defined by the circuit analysis performed on the two switched networks, hence the reason it was neglected in the derivations. All the design and analysis tools in MATLAB can

now be applied using the new matrices.

- Boost converter:

The boost topology used for dynamic modeling is the half-bridge converter depicted in Figure 2.3, which includes the components' parasitics in the form of an ESR to model their non-idealities as well as the conduction losses. Note that the load is represented by a current source rather than a resistor, which can now act as a dynamic input in the analysis and represent a disturbance. This boost topology has a low component count and thus relatively high efficiency while still meeting the requirements for the application. Although this converter is bi-directional, only the boost action is used and the buck action must not occur to avoid current reversal into the fuel cell. Thus only the bottom transistor and the top diode operate, which realize a configuration similar to that previously discussed in Figure 2.1. Furthermore, the experimental boost converter consists of additional passive components as shown in Figure 3.12 to attenuate transients and reduce the ripple content. Although these additional components contribute poles and zeros to the loop, their corner frequencies are so far beyond the gain crossover frequency that they offer no threat to the system's stability [20].

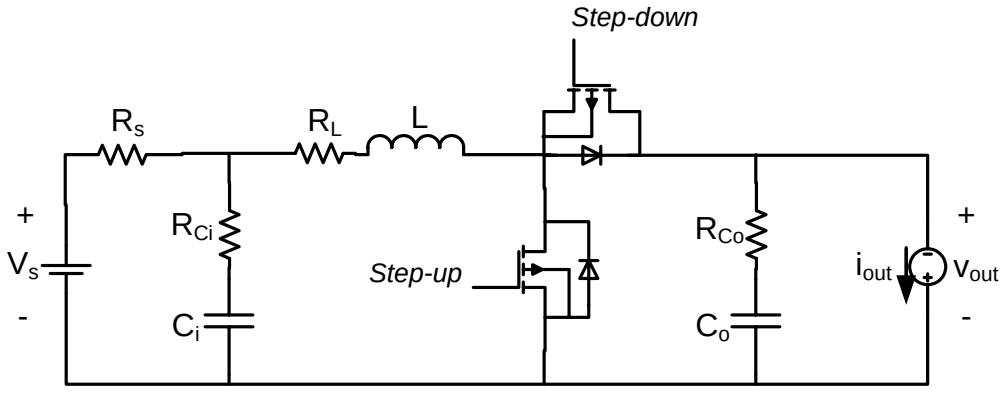

Figure 2.3: Dc-dc converter topology for dynamic modeling.

The values for the converter's components used for the analysis are given in Table 2.1. These parameters are chosen to emulate the experimental set-up. Given that the experimental fuel cell operates nominally at 26 Volts, a duty cycle in the vicinity of 0.5 is

chosen to regulate the dc bus at 48 Volts. These values are used in the derived matrices and transfer functions for the dynamic study of the converter. The two switched circuit models of Figure 2.3 are shown in Figure 2.4.

Table 2.1: Converter's power components for dynamic analysis.

Power Components	Value	ESR
Inductor L	10 μH	2.4 mΩ
Input Capacitor C_i	140 μF	250 mΩ
Output Capacitor C_o	700 μF	5 mΩ
Input Voltage V_s	24 V	15 mΩ

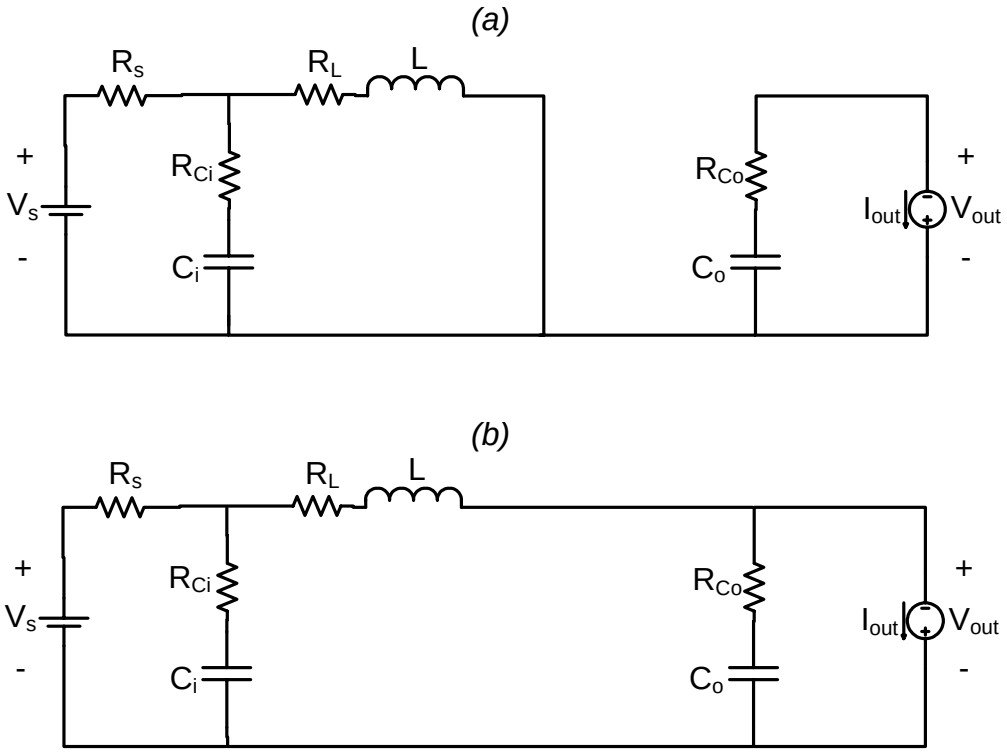

Figure 2.4: Two switched circuit models of bi-directional converter: (a) bottom (boost) switch *on* (b) top (buck) switch *on*.

The matrices A_1, B_1 and C_1 are derived using circuit analysis on Figure 2.4 (a) and the matrices A_2, B_2 and C_2 on Figure 2.4 (b). These matrices are given by (A.3) and (A.5) in Appendix A.

Taking the output voltage V_{out} as the output variable, the transfer function to the duty cycle has the same form as (2.22) and is given by:

$$\frac{V_{out}(s)}{D(s)} = C \cdot (s \cdot I - A)^{-1} \cdot [(A_1 - A_2) \cdot X + (B_1 - B_2) \cdot u_0] + (C_1 - C_2) \cdot X \qquad (2.26)$$

Using MATLAB, the Bode plot for this duty cycle-to-output voltage transfer function was obtained and is shown in Figure 2.5. One can observe the fixed gain and minimal phase shift at low frequency. The dc gain value depends on the input voltage and duty cycle. Beyond the resonant frequency of the output filter, the gain begins to fall with a –40 dB/decade slope and a phase lag of 180° takes place. The complex pole pair also exhibit a quality factor greater than 0.5, resulting in an under-damped and peak in the response. The resulting steep phase lag is undesirable and triggers stability issues, and it can be observed that the transfer function has a negative phase margin and is unstable.

For comparison purposes, the same transfer function is shown in Figure 2.6 for the case of an ideal converter where the parasitics of the components are not taken into account. One can note the difference at high frequencies due to the presence of an additional zero, located in the Left Hand Plane (LHP), caused by the ESR of the output capacitor, and is positioned at high frequency. There is another zero in the Right Hand Plane (RHP) that is characteristic of the boost converter in CCM and exists regardless of whether the components' parasitics are included or not. The effect of the RHP zero can be seen in the additional phase lag it introduces by causing the phase to drop below 180° in both cases. On the other hand the LHP zero adds phase lead and causes the phase to return to 180°, as shown for the non-ideal case. Both zeros contribute to counteract the –40 dB/decade slope and flatten out the gain. Thus, the presence of the RHP introduces additional delay in the system on top to the lag of the complex poles, and greatly limits the performance of

the converter as a stable system and causes many difficulties in designing the compensators. To make matters worse, the RHP zero's frequency depends on the load, and thus varies with operating conditions, as well as component values. This topic will be investigated in more depth in Chapter 3.

Another important transfer function that is required to form the dynamic model of the converter for control purposes is the duty cycle-to-inductor current transfer function. Taking the inductor current as the output, the *A* and *B* matrices remain the same as in (A.3) and (A.5) since they only depend on circuit modeling. However, the *C* matrices, which depend on the chosen output variable, are now given by (A.6). Since C_1 and C_2 are equal, (2.22) can now be simplified as:

$$\frac{I_L(s)}{D(s)} = C \cdot \left(s \cdot I - A\right)^{-1} \cdot \left[\left(A_1 - A_2\right) \cdot X + \left(B_1 - B_2\right) \cdot u_0\right] \tag{2.27}$$

As just witnessed, various transfer functions to describe the converter can be easily obtained with little manipulation, further illustrating the advantages of this modeling techniques and the use of state-space descriptions. The Bode plot for (2.27) is shown in Figure 2.7. Note the RHP zero does not appear in this transfer function, and it is inherently stable. This has important consequences when deciding on suitable control schemes to cope with the RHP zero in the duty cycle-to-output voltage transfer function, as will be further discussed in the following chapter.

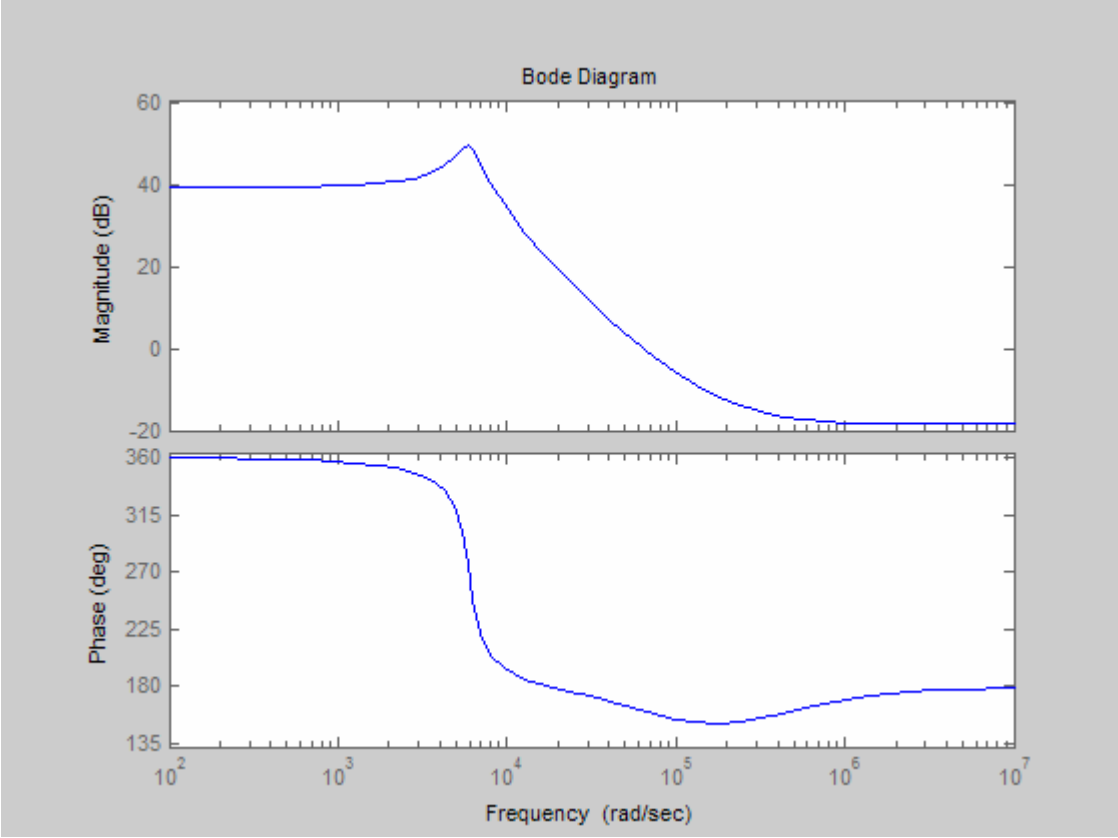

Figure 2.5: Bode plot for duty cycle-to-output voltage transfer function.

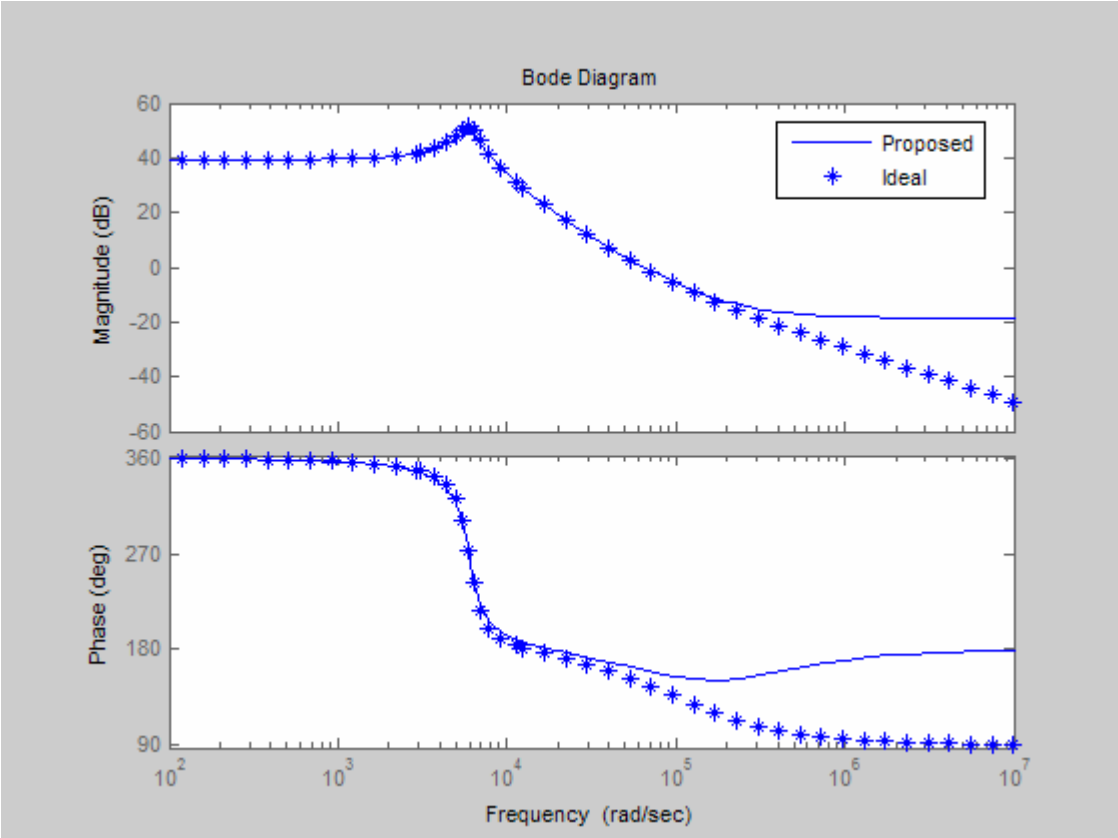

Figure 2.6: Bode plot for duty cycle-to-output voltage transfer function: proposed converter taking into account the components' parasitics versus ideal converter with no parasitics.

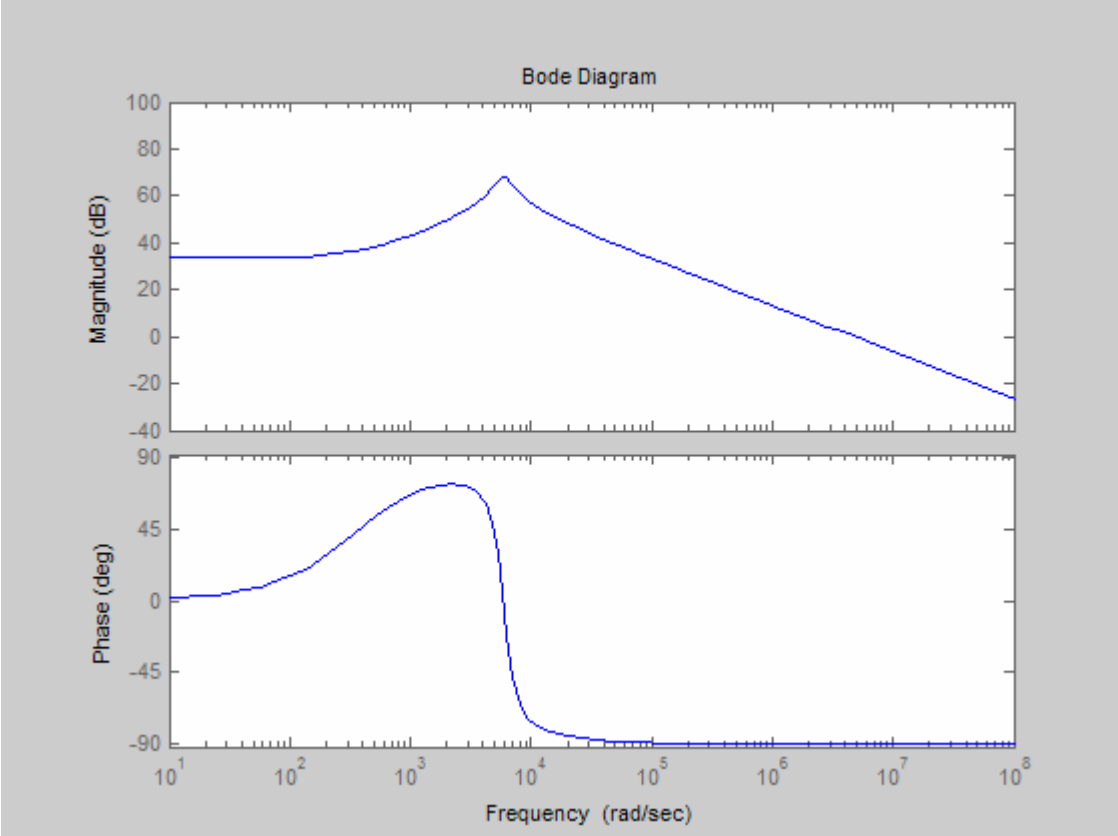

Figure 2.7: Bode plot for duty cycle-to-inductor current transfer function.

2.4 Assessment

A power processing system is required to convert electrical energy from one voltage, current or frequency to another with high efficiency, reliability and in a small light-weight package. Linear regulators cannot meet these objectives at high power levels, and thus switching regulators are considered. For the application at hand, the dc-dc boost converter, one of the fundamental converter topologies from which many other converter topologies are derived, is considered for the purpose of adopting the fuel cell voltage to the bus voltage and effectively managing the power flow to meet the load demand.

Furthermore, in most applications, the output is to be regulated by closing a feedback loop that causes the conversion ratio to be automatically adjusted. In order to study the system transient behavior and design suitable regulators for its feedback loop, dynamic modeling with a mathematical description is necessary so that the designer may gain insight into its behavior. This chapter dealt with the modeling of the power stage subsystem from which state-equations and equivalent transfer functions were obtained. To this objective, the state-space averaging method was chosen, which is well suited for the analysis of nonlinear systems such as switch-mode power supplies, and offers an almost ideal compromise between simplicity and accuracy.

The separate equations describing each switched network are combined by taking their linearly weighted average based on the associated duty ratio, and thus this averaging process ‘approximates’ the behavior of the converter over many cycles. Hence, certain conditions must be satisfied for the approximation to be valid, mainly the state variables must evolve in an approximately linear manner and the output filter’s frequency must be much lower than the switching frequency. Perturbations of the various variables must then be introduced to form the small-signal ac analysis and thus derive the desired transfer functions at a given large-signal operating point. Since the subsystem is

nonlinear, the transfer functions were found through an approximation based on the small-signal assumption so that the widely known linear control techniques may be applied. Once again, the price to pay for the approximations and simplifications is the validity of the result, i.e., the small-signal restriction.

The state-space matrices describing the boost converter for this application were derived and are presented in Appendix A. The resulting Bode plots for two important transfer functions required for the design of the control loops in the following chapter were presented. The ability to easily manipulate the matrices to obtain the various input-output descriptions and the complete system behavior demonstrated the advantage of using a state-space rather than a transfer function description. These plots provided insight into the location of the poles and zeros and their effect on the power stage's response. It was noted that the inclusion of the components' parasitics introduced an additional LHP zero in the converter's transfer function. Moreover, a RHP zero also exists in the duty cycle-to-output voltage transfer function that is inherent to the boost converter's operation. This greatly complicates the design of the compensators, and is thus investigated in more detail in the subsequent chapter when designing the control loops.

Chapter 3
Average Current Mode Control

3.1 Introduction

A dc-dc converter must provide a regulated dc output voltage under varying load, input voltage conditions, as well as converter component values that are changing with time, temperature, and so forth. Hence, negative feedback control to ensure robustness must be applied in order to supply the voltages, currents, or frequency ranges required by the load with the requested dynamics. The two most common closed-loop control methods for PWM dc-dc converters are Voltage Mode Control (VMC) and Current Mode Control (CMC). These two control schemes are shown in Figure 3.1, and are discussed in more detail in subsection 3.1.1.

Among other control methods of dc-dc converters, a hysteretic (or 'bang-bang') control is very simple for hardware implementations. However, the hysteretic control results in variable frequency operation of semiconductor switches. A constant switching frequency is preferred as it allows for easier harmonic filtering and electromagnetic interference shielding as well as better utilization of magnetic components.

There are many different ways to implement CMC, and the two most popular methods, fixed-frequency Peak Current Mode Control (PCMC) and Average Current Mode Control (ACMC), are evaluated. The differences arise from the insertion of a Current Error Amplifier (CEA) into the current loop of ACMC to obtain the average value of the inductor current. This provides the ACMC scheme with several important advantages, as will be discussed in subsection 3.1.2.

Dynamic characteristics of closed-loop dc-dc converters must fulfill certain requirements. To simplify analysis, these requirements are usually translated into desired properties of the open loop. The open loop should provide a sufficient phase margin for stability, high bandwidth for good transient response, and high gain at low frequencies for small steady-state error and disturbance rejection. The boost dc-dc converter offers its own unique challenges to meet the aforementioned objectives, and requires sophisticated control processes to obtain stable operation not only with satisfactory static and dynamic performance, but also provide robustness with low sensitivity against load or line disturbances. Since the converter itself is a part of the control loop, the design of such control processes requires a knowledge of the small-signal characteristics of the converter as derived in Chapter 2 and further completed in section 3.2. The design of such compensation networks will be the topic of section 3.3. Finally, the effectiveness of the control strategy in conjunction with the derived models is validated with simulations in MATLAB.

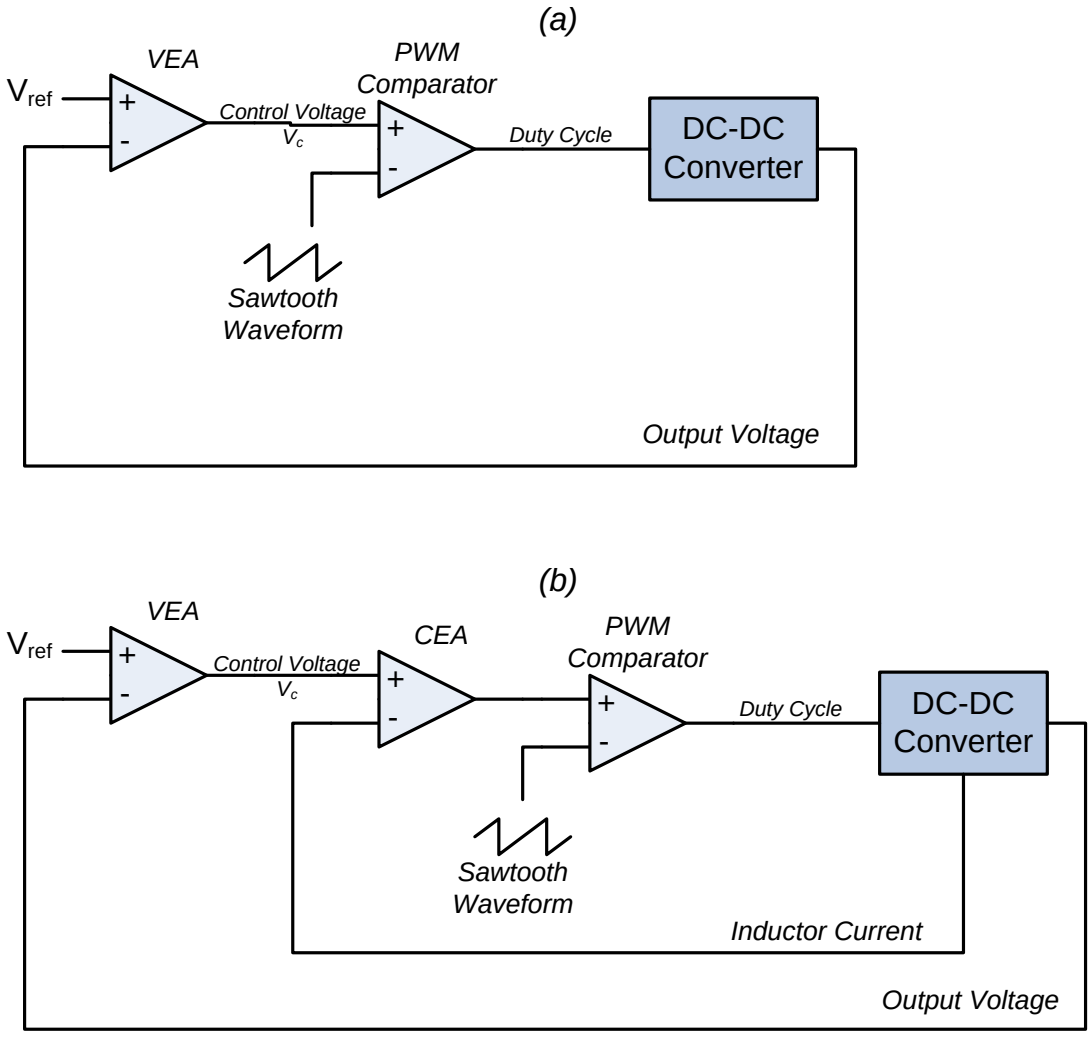

Figure 3.1: Main control schemes for dc-dc converters: a) Voltage Mode Control; b) Current Mode Control

3.1.1 Closed-Loop Control

CMC uses the inductor current in one way or another to control the power converter. It is found in references as early as 1967 [21]. Before that, most control circuits for PWM converters used VMC, or single loop control. In this scheme, the converter output voltage is sensed and subtracted from an external reference voltage in an error amplifier. The error amplifier produces a control voltage that is compared to a constant-amplitude sawtooth waveform. The comparator then produces a PWM signal that is fed to the drivers of the controllable switches in the dc-dc converter to determine their *on*- and *off*-time. The frequency of the PWM signal is the same as the frequency of the sawtooth waveform, and the duty cycle of this PWM signal is proportional to the control voltage. The output voltage is regulated by closing the feedback loop between the output voltage and the duty-ratio signal. The negative feedback summation and the control transfer function are normally implemented using a single op-amp while the PWM modulator is formed by a comparator and ramp generator.

An important advantage of the VMC is its simple hardware implementation and flexibility [18]. However, line regulation, or regulation against variations in the input voltage, is delayed because changes in the input voltage must first manifest themselves in the converter output before they can be corrected. Hence, a feed-forward path is sometimes added to the VMC scheme to enhance line regulation, which directly affects the PWM duty ratio based on the variations in the input voltage. This feature is, however, inherent in the CMC scheme.

In CMC, an additional inner control loop exists that feeds back the inductor current signal as shown in Figure 3.1. CMC is therefore a two-loop system that includes a voltage loop and a current loop. The current loop monitors and maintains the inductor current equal to the reference current. This reference current is the control voltage resulting from the error between the reference voltage and the output voltage of the converter in the outer voltage loop. The net result from the two approaches is ultimately the same; to regulate the output voltage, but the latter approach controls the load current directly, hence the

designation CMC, while the output voltage is controlled only indirectly. This modification of replacing the sawtooth waveform of the VMC scheme by the converter current signal significantly alters the dynamic behavior of the converter, which then takes on some characteristics of a current source. Since the converter current signal is proportional to the input voltage, the inner loop of CMC naturally accomplishes the input voltage feed-forward technique, as previously mentioned.

This direct control over the load current in CMC has further profound effects on the negative feedback loop and offers many advantages. First, since the current is controlled directly, it is possible to limit the output current on a cycle-by-cycle basis, and thus also force different power stages connected in a parallel system for high power applications to share equally, even if there are significant imbalances in circuit component values [22]. CMC also presents a reduced order control-to-output voltage transfer function due to the current source that effectively absorbs the energy storage inductor. This simplifies the design of the outer voltage control loop and allows a simple compensation network to be used. This benefit is of vital importance due to presence of the RHP zero in the converter's transfer functions, which would have been almost impossible to compensate for in a VMC system. Its inherent characteristics such as input and output voltage feed-forward and feedback also improve the power supply performance in many ways, including excellent rejection of input line transients and better dynamic response for disturbances. Since ultimately a change in output voltage is due to a change in load and therefore a change in current, the ability of CMC to address this change directly reduces the delay involved in adjusting the system parameters. In the case of VMC, the output voltage being the only feedback signal causes the output dynamic response to have inherent phase lag of the output voltage with regards to the load current. Lastly, the inner current control loop plays an important role in the application at hand, where it provides the facility to send the reference current to the fuel cell processor synchronously to adjust the fuel flows to match the reactant delivery rate to the usage rate. The main disadvantage of CMC is its complicated hardware and compensation to avoid converter instability. It is also difficult to measure the current accurately and with the required

bandwidth. Current sensing in CMC is further discussed in the following paragraphs.

3.1.2 Current Mode Control Implementations

Many different modulation strategies can be implemented where the peak inductor current is used. The most common approach is to use a constant-frequency clock to turn *on* the power switches, and use the intersection of the current signal with the control voltage signal to turn *off* the power switches. This implementation is commonly referred to as constant-frequency, trailing edge modulation PCMC, or simply PCMC. Another constant-frequency modulation scheme uses a clock signal to turn *off* the switch, and the inductor current to provide the turn-*on* signal. This modulation scheme requires inductor current information during the *off*-time of the power switch, and thus may not be used with certain converter topologies [23]. It is the dual of the previous constant-frequency scheme, and referred to as constant-frequency leading-edge modulation. Other PCMC modulation schemes also exist where the *on*- or *off*-time of the switch is fixed (with a timer), rather than a fixed frequency. These are referred to as constant *on*- or *off*-time control, and many ways can be used to implement these variable-frequency modulation schemes.

Another class of CMC exists where a CEA is inserted into the current loop to obtain the average value of the inductor current, and is thus termed ACMC. The presence of this compensation network is the main difference with PCMC, and the ability to tailor the response of the current loop offers many distinct benefits and remedies to some of the shortcomings in PCMC.

One of the advantages of PCMC is to enable faster current loop dynamics than ACMC [24]. However, its downfalls include its inherent instability for duty cycles greater than 50 percent, resulting in subharmonic oscillation. This is a result of its ‘sampling’ nature, which is therefore limited by the Nyquist frequency, and it can be shown that a pole moves outside the unit circle in the z-plane for duty cycles greater than 0.5 [25]. A

compensating ramp is usually applied to eliminate this instability and provide design flexibility. However, since this ramp is based on the input voltage, which may vary, a fixed ramp providing adequate compensation will overcompensate much of the time, with resulting performance degradation and increased distortion [26]. Hardware must also be provided to estimate the peak current value by sampling the inductor current, input and output quantities. Furthermore, PCMC is extremely susceptible to noise. This is the result of a tradeoff with efficiency, where for converters with relatively high output current (more than a few Amperes), lowering the value of the current-sense resistor helps reduce the power dissipation and increase efficiency. However, it makes the converter increasingly susceptible to noise due to the inability to adequately suppress noise superimposed on the current-sense signal. Other current-sensing techniques exist, such as Hall-effect sensors and current sense transformers, but each potential candidate has its drawbacks and tradeoffs between simplicity, efficiency, accuracy, performance, size and cost. In addition, a peak-to-average current error is inherent in PCMC. While the peak current follows the desired sine wave current program, the average current does not, and this discrepancy becomes much worse at lower current levels. To reduce this peak-to-average current error and its resulting distortion on the input current waveform, a large inductor is required to make the ripple small, which makes the already poor noise immunity much worse.

The aforementioned problems are overcome in ACMC by introducing a high-gain integrating compensation network around the CEA in the current loop. The compensator can be tailored for optimum performance, gain and bandwidth characteristics dictated by the application. The current loop crossover frequency can be made approximately the same as PCMC, but the gain will be much greater at lower frequencies, providing excellent noise immunity and a high degree of accuracy to track the average inductor current, without the expense of poor efficiency. This is a result of the similarities between ACMC and VMC, where it shares its high noise immunity and efficiency, while still combining the stability and performance of PCMC. Nevertheless, using ACMC, the engineer is free to design the current loop compensator to meet the performance and requirements suitable to the specific application, while in PCMC little flexibility is

granted. It also eliminates the need for slope compensation, although a limit exists for the loop gain at the switching frequency to maintain stability. Furthermore, the high gain CEA permits a very small current sense resistor value resulting in low power dissipation as it can make up for the gain lost by using the small resistor, thereby maintaining good noise immunity and accurately programming the output current. In contrast, the current-sense signal in PCMC has a flat gain, causing the system to exhibit a peak-to-average current error as a result of input voltage variations. Finally, ACMC controls the average inductor current, a sought feature in fuel cell hybrid applications where charging and discharging from a controlled current source is needed.

3.2 Modeling Average Current Mode Control

3.2.1 Introduction

Modeling and design of ACMC has been the subject of numerous technical papers. The lack of a single current mode model that is used universally is due to the simple fact that a tradeoff exists between the accuracy and ease of use for the models employed in the design of ACMC circuits. It is desirable to have expressions that lend insight into dominant system behavior, but yet are practical and simple enough to design with. This philosophy is preserved through the derivation of the model in this dissertation.

A PWM dc-dc converter with ACMC consists of three basic functional blocks: the power stage (plant), the modulator, and the controller. The proposed modeling method is based on modeling each component individually, and then combining the results to form a complete model. The power stage was modeled using state-space averaging in Chapter 2. The modulator and controller will be modeled and designed in this chapter. The combined small-signal model generates all the transfer functions required for design purposes. But first, a description of the operating principles of the converter in

conjunction with ACMC is presented to lay the foundation for modeling.

3.2.2 Principles of Operation

The objective of dc-dc conversion is to convert a source voltage to a near-constant output voltage under disturbances at the source voltage and load. In ACMC, this is accomplished through a double-loop system to control the inductor current (inner loop) and output voltage (outer loop). In effect, the outer loop compensates against variations in the output voltage, which in turn are caused by changes in load, while the inner loop compensates against variations in input voltage, which serves as the inherent feed-forward feature in ACMC. A CEA and modulator also exist. As previously stated, the benefit of ACMC is due to the compensation of the CEA with a feedback network, which accomplishes a couple of things: 1) tailor the current-sense signal to exhibit maximum gain at DC, thus allowing the current-sense resistor to be made as small as possible without jeopardizing the noise immunity, and 2) dampen the high frequency noise which is superimposed on the signal. The high dc gain of the CEA allows this control scheme to accurately program the output current without any peak-to-average current error. Thus, the CEA is an essential part of the success of ACMC, which in turn depends on the right choice of compensation network to fulfill these goals. Finally, the output of the CEA is fed to the modulator, where it is compared to a voltage ramp to generate the desired PWM signal to drive the switches. The complete schematic of this process including the boost converter is depicted in Figure 3.2.

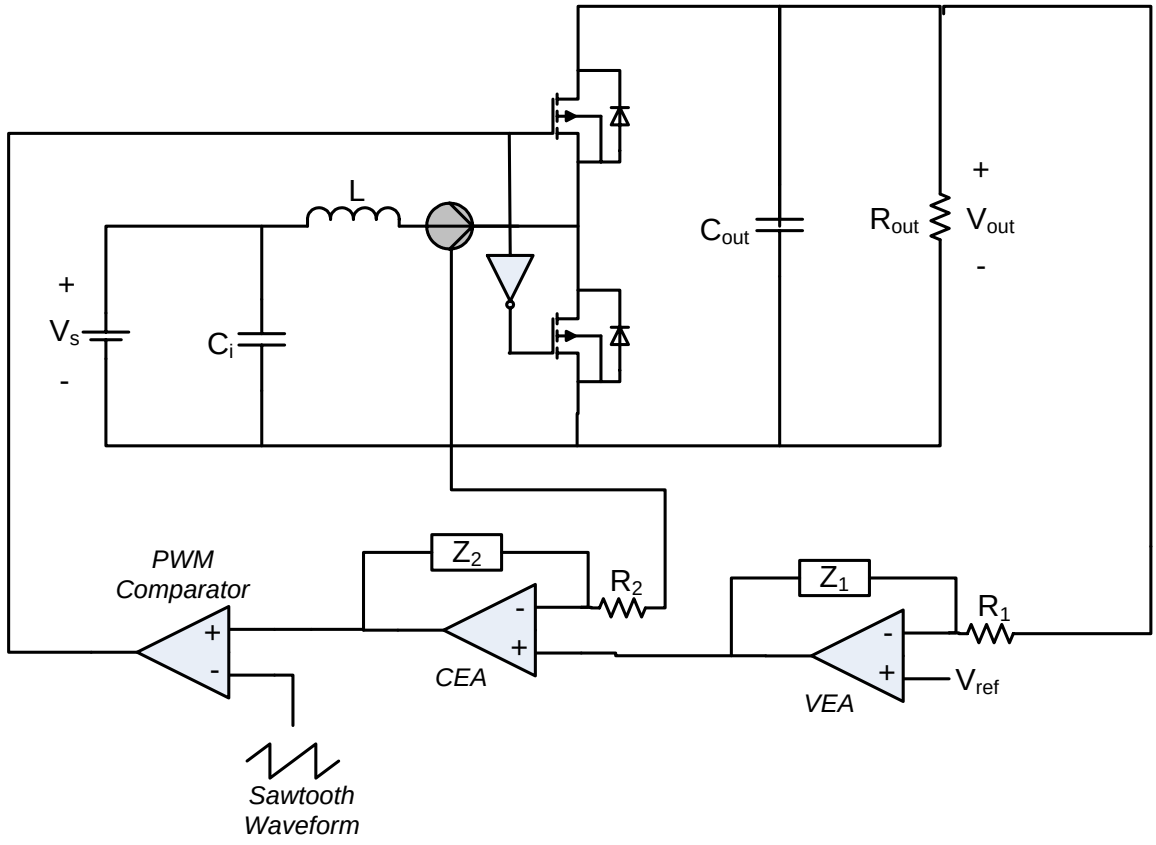

Figure 3.2: Boost converter schematic with ACMC.

The usual implementation of the compensation networks relies on analog operation amplifiers as error amplifiers, and makes use of wide-band sensing of the inductor current to include both the ac and dc components. As shown in Figure 3.2, the voltage waveform representing the inductor current is connected to one input of the CEA that forces the average value of the inductor current to follow the reference current, which is the other input to the CEA. The CEA inverts and amplifies the difference between the inductor current and the reference current signal. The output is then compared with a large amplitude ramp waveform at the converter switching frequency at the inputs to the PWM comparator. These sawtooth waveforms intersect at two points in each cycle, thereby defining the rise and fall instants of the PWM pulse train to the switches. If the reference input to the CEA is the output of a suitably compensated Voltage Error Amplifier (VEA), the average inductor current will be controlled to force the converter output voltage to track the reference voltage.

Comparison of the wide-band inductor current waveform with the PWM ramp waveform results in an inherent fast feed-forward and feedback of the input and output voltage variations, without involving the feedback loops and without direct monitoring. This is due to the fact that the rising and falling slopes of the inductor current waveform are proportional to the input and output voltages, and thus any changes in these slopes results in immediate adjustment of the PWM duty cycle [27].

3.2.3 Modeling Method

The design approach for the modeling of the dc-dc converter is as follows. The power stage is first modeled and analyzed by state-space averaging methods, as was done in Chapter 2. These results are then combined with the model of the control loop and modulator derived in this chapter. Based on the complete averaged model, the controller will be designed. Then simulation programs will be used to test the closed-loop performance.

The differences in particular models arise in the derivation of the gain of the modulator and in the presence of feed-forward and feedback gains from the input and output voltages to the duty cycle. However, although different modulator, feed-forward and feedback gains exist, these different control circuits only account for the phenomena of CMC and do not affect the power stage model previously derived. Since the controlled switch plays a central role in the converter dynamics and the switching action may take the form of a discrete system, the use of sampled-data modeling has also been considered [23,28]. This has been incorporated into the complete model by adding a ‘sampling gain’ term and thus also without affecting the power stage model. The sampling effect was originally derived for PCMC modeling, and was then extended to ACMC in [29].

Although inclusion of the sampling effect has proven to be valuable for improving the accuracy of averaged models for PCMC, its effect in ACMC has been a topic of debate. ACMC more closely resembles VMC in terms of PWM process, where in the latter the

sampling effect had never been considered. Thus it is legitimate to question the benefit of the added complexity of the sampling gain in ACMC. Furthermore, it is shown in [30] that the resulting model is simpler and in fact also more accurate than the previous models that take into account the sampling effect. Even under conditions that may degrade the model accuracy, [30] shows that inclusion of the sampling effect doesn't improve the model accuracy in that case either.

As in the modeling of voltage-controlled converters, the modulator is modeled by a constant gain through a first order approximation, given by (3.28):

$$K_m = \frac{1}{V_m} \tag{3.28}$$

where V_m is the peak-to-peak voltage of the triangular waveform. Equation (3.28) is valid for low ripple conditions, and is an approximation for higher ripple conditions [31].

While a current compensator exists in the current loop, the switching ripple at the output of the compensator is still considerable. The compensator output is thus also a function of the input and output voltages, which in turn affects the duty cycle. The effect of these input and output perturbations can be accounted for by including feed-forward and feedback terms from the input and output, respectively, to properly account for the time varying effects. These terms are given in [31] for a boost converter:

$$\begin{aligned} K_f &= \frac{(2D-1)T_s R_i}{2L} \\ K_r &= \frac{(1-D)^2 T_s R_i}{2L} \end{aligned} \tag{3.29}$$

where K_f and K_r are the feed-forward and feedback terms from the input and output voltages, respectively, D is the duty ratio, T_s is the switching period, R_i is the total current sense gain, and L is the power stage inductance.

3.2.4 Complete Small-Signal Model and Characteristics

The complete small-signal model for ACMC is shown in Figure 3.3, where $G_s(s)$ and $G_p(s)$ represent the current compensator and will be designed in section 3.3, although the results will be given here to complete the small-signal ACMC model.

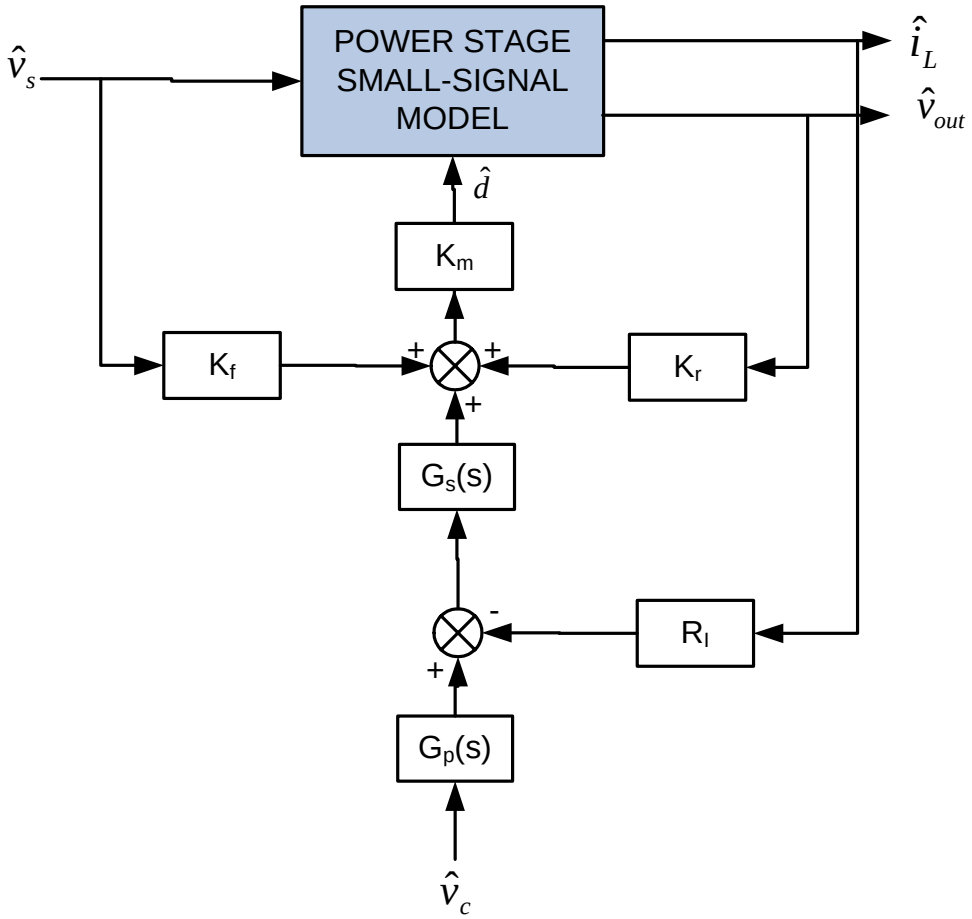

Figure 3.3: Small-signal model of ACMC.

- Current-Loop Gain:

The current-loop gain T_i is defined as the loop gain measured at the output of the duty cycle modulator with the current-loop closed, and is given here by:

$$T_i(s) = R_i K_m G_c G_{dc}(s) \tag{3.30}$$

where $G_{dc}(s)$ is the duty ratio-to-inductor current transfer function, and $G_c(s)$ is the current compensator, as given by (3.31):

$$G_c(s) = G_s(s) * G_p(s)$$

and

$$G_s(s) = \frac{K_c\left(1 + \frac{s}{w_z}\right)}{s} \qquad G_p(s) = \frac{1}{\left(1 + \frac{s}{w_p}\right)} \tag{3.31}$$

where K_c is the dc gain, w_z and w_p represent the zero and pole locations of the compensator, respectively. The Bode plot of the loop gain in (3.30) for the state-space averaged boost converter is shown in Figure 3.4.

- Control-to-output transfer function:

The control-to-output transfer function, similar to the duty cycle-to-output transfer function for the design of the current loop compensator, is the most important small-signal characteristic for the design of the voltage compensator. It represents the partial loop obtained by cutting the VEA out of the closed loop to observe the contribution of the remaining elements to the loop's gain and phase characteristics, thereby allowing the VEA to counteract and compensate for some of the detrimental effects of the loop.

Referring once again to Figure 3.3, the control-to-output transfer function can be derived as:

$$G_{vc}(s) = \frac{\hat{v}_{out}}{\hat{v}_c} = \frac{K_m G_c(s) G_{vd}(s)}{1 + R_i K_m G_s(s) G_{id}(s) - K_r K_m G_{vd}(s)} \tag{3.32}$$

where $\hat{v}_{out}$ is the output voltage, $\hat{v}_c$ is the control reference voltage generated from the voltage loop, R_i is once again the gain of the current-sense network, $G_{vd}(s)$ and $G_{id}(s)$ are the duty cycle-to-output voltage and duty cycle-to-inductor current transfer functions of the power stage, respectively. The Bode plot for (3.32) is shown in Figure 3.5. This transfer function is instrumental in determining the system stability and in designing the compensation for the feedback system.

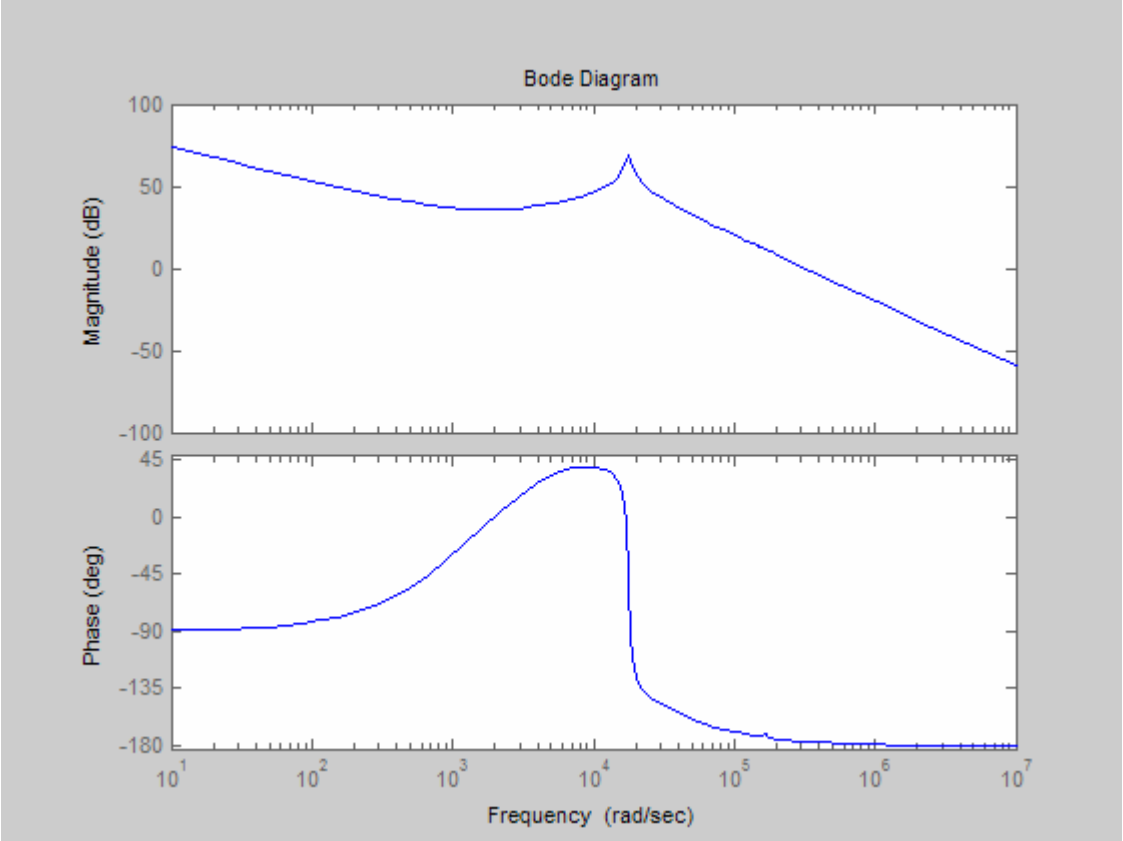

Figure 3.4: Bode plot for current loop-gain and phase

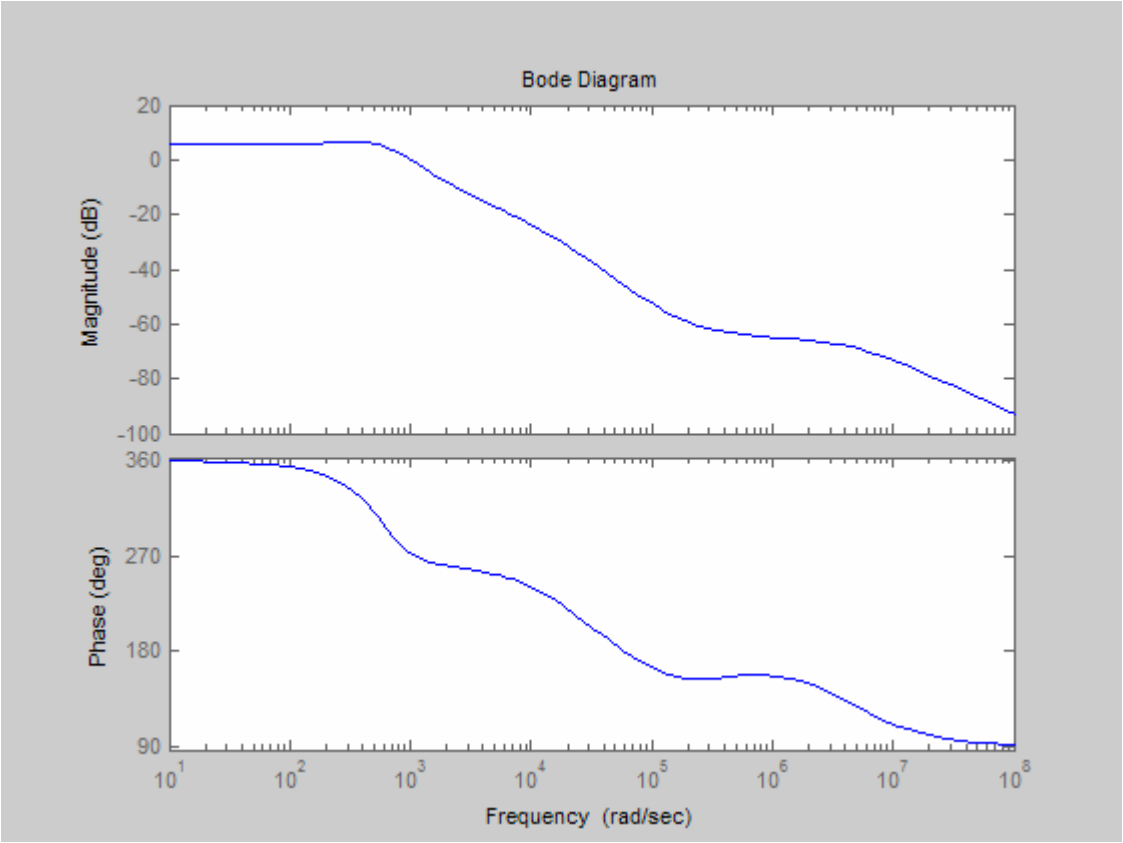

Figure 3.5: Bode plot for control-to-output transfer function

3.3 Feedback Loop Compensation

3.3.1 Introduction

The converter's control system is required to maintain the output voltage constant irrespective of variations in the dc source voltage and the load current. Load changes affect the output voltage transiently and may cause significant deviations from the steady-state level. Furthermore, circuit losses introduce an output voltage dependency on the load current that must be compensated for by the control system.

As previously noted, the main distinguishing feature of ACMC, as compared with PCMC, is that ACMC uses a high gain, wide bandwidth CEA to force the average of one current in the converter, typically the inductor current, to accurately follow the demanded reference current. Numerous benefits can be procured with only a slight increase in complexity, such as good efficiency, large noise margins, no requirement for additional slope compensation, and excellent voltage and current regulation. Nonetheless, the CEA must be properly designed to tap into all these potential benefits, which is one of the tasks tackled in this section.

3.3.2 Compensating Networks

The open-loop dynamic characteristics are shaped by compensating networks of passive components around the error amplifier. Second- or third-order networks consisting of resistors and capacitors are typically used. Using suitable methods to assess system performance and stability, such as Bode plots and root-locus, there are general rules for the design of the open-loop transfer functions, as given below:

- The low-frequency gain should be high enough (several tens of dB) to track

the reference accurately and increase rejection to disturbances of input voltage and load current variations.

- The frequency of 0 dB gain (unity gain) should be placed close to the maximum allowed by the modeling approximations (about one-tenth of the switching frequency).
- To ensure stability, the phase margin, defined as the additional phase shift needed to render the system unstable without any changes in the gain (given by the difference between the open loop system phase at the unity gain frequency and 180°) must be positive, and in general greater than 45°. In the root-locus, no poles should enter the right half of the complex plane.
- To increase stability, at the frequency the phase reaches 180°, the gain should be less than –30 dB (i.e., the gain margin should be greater than 30 dB).

Different types of compensators accomplish different goals, and their selection depends on the converter's characteristics, as given by their transfer functions, and the design objective. The fundamental control blocks in control theory will be briefly discussed in the next paragraph so that one may understand how they may pieced together to properly compensate the system at hand.

The most basic controller is a Proportional controller, which is simply a constant, thus providing a direct proportionality between the input and output. The constant term helps to control the basic response speed of the system; increasing it decreases the rise time and the steady-state error, although this would also increase the overshoot and possibly lead to unstability, and would never eliminate the steady-state error. The next basic controller is an Integral controller, whose main purpose is to eliminate the steady-state error, but typically makes the transient response more ‘sluggish’. On the other hand, Derivative control increases the stability of the system, reduces the overshoot, and generally improves the transient response of the system. Finally, these three control blocks, and thus their attributes, can be combined to form a controller widely known as a Proportional-plus-Integral-plus-Derivative, or PID, controller. An alternative approach to PID control that directly aims to change the open-loop characteristics to meet the design

requirements regarding steady-state error, phase margin and gain margin, is Phase compensation. This dynamic compensation may take many forms, but its building blocks are the Lead and Lag compensators. Phase-lead compensation is similar to a Proportional-plus-Derivative (PD) controller, increasing the phase margin of the system and thus providing additional stability, increasing the system bandwidth and improving the dynamic response. Phase-lag compensation is similar to Integral action, increasing the steady-state accuracy by increasing the low-frequency gain, but decreases the system bandwidth and thus slows down the transient response. These two phase-compensation controllers can also be combined to form a Lead-lag controller in order to take advantage of the phase characteristics of the lead compensator and the magnitude characteristics of the lag compensator.

Referring back to the Bode plot for the duty cycle-to-output voltage transfer function of the converter in Figure 2.5 and the general design objectives enlisted above, several key recommendations can be made:

- The low-frequency gain should be made higher to decrease the steady-state error.
- The phase-margin, which is currently negative, must be drastically increased to at least 45°.
- To further increase the stability, the gain as the phase reaches 180° must be further decreased. The high-frequency gain should also be further decreased to increase the noise immunity.
- The above should be performed without significantly reducing the 0 dB crossover frequency.

An integral, or lag controller, must be incorporated into the CEA network to accomplish the first objective. A phase-lead controller must also be included to satisfy the remaining criteria. Thus an integral-lead controller is chosen, which has a gain as already presented in (3.31), and takes the form shown along with the modulator in Figure 3.6.

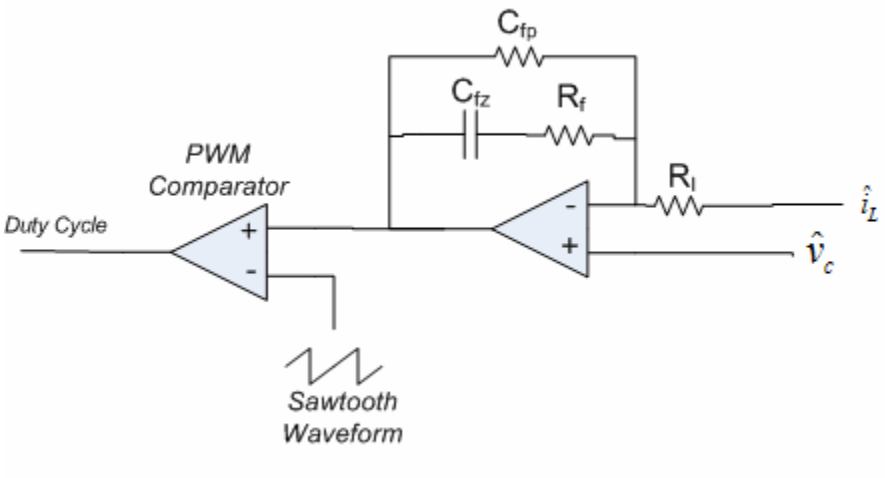

Figure 3.6: Current compensator and modulator.

3.3.3 Designing the Optimum Control Loops

- Current Loop:

Aside from the pole at dc, the current compensator as in (3.31) has three design parameters: dc gain K_c, zero w_z, and pole w_p. The general purpose of the zeros and poles in the CEA is to counteract poles and zeros in the duty cycle-to-output voltage transfer function, respectively, as shown in the root locus plot in Figure 3.7. Since perturbations in the input voltage exist, zero steady-state error is required. Thus the first pole is placed at dc for good output regulation. Furthermore, to counteract the phase lag from the poles of the output filter at low frequency, a zero is introduced to attempt to extend the loop bandwidth, thereby vastly improving the overall transient load response time. This zero, which provides a 'phase bump', should be placed where the greatest phase lag occurs in the duty cycle-to-output transfer function. This phase bump ensures the stability of the current loop and that the phase shift of the integrator is offset at half the switching frequency. Thus, the zero is placed before the power stage filter frequency and at least one decade before half the switching frequency. Finally, the last pole is placed at high frequency to roll off the gain and to counteract the high frequency zero caused by the output capacitor's ESR, thereby eliminating high-frequency noise and also reducing

sensitivity to model uncertainty. To attenuate unwanted switching noise while simultaneously maximizing the bandwidth, the pole should be at least one decade above the zero. The Bode plot for this current loop compensator is shown in Figure 3.8.

As shown in the duty cycle-to-output voltage transfer function Bode plot in Figure 2.5, the output filter poles manifest themselves at a corner frequency of approximately 6,000 rad/s. Thus the compensator zero is placed at 1,000 rad/s to counteract their effect, and to provide the necessary phase bump to improve the phase margin. As also shown in Figure 2.5 and further exposed in Figure 3.7, the high-frequency zero is located at approximately 30,000 rad/s, which is therefore also the chosen range for the location of the high-frequency pole of the compensator. Once the poles and zero have been defined, the dc gain can be determined using the root locus plot of the control-to-output voltage transfer function. This plot is shown in Figure 3.9 along with the approximate pole locations for the chosen gain.

The component values of Figure 3.6 could now be determined by using the equations below. First, a standard value is chosen for C_{fp} as 0.0047 μF. The remaining two unknowns C_{fz} and R_f are then found by solving (3.33):

$$\begin{aligned} K_c &= \frac{1}{R_1(C_{fp} + C_{fz})} \\ w_z &= \frac{1}{R_f C_{fz}} \\ w_p &= \frac{C_{fz} + C_{fp}}{R_f C_{fz} C_{fp}} \end{aligned} \tag{3.33}$$

where R_1 is the input resistor. From the result, the closest standard values for C_{fz} and R_f are selected as 0.10 μF and 10 kΩ respectively. The gain K_c and pole w_p were then recalculated using these new values and found as 955 and 22,277, respectively, whereas the zero w_z remained unchanged. The final current compensator of (3.31) is then:

$$G_c(s) = 955\frac{(1+\frac{s}{1{,}000})}{s(1+\frac{s}{22{,}277})} \tag{3.34}$$

- Voltage Loop:

Once the current loop is designed, the converter with the closed current loop can be treated as the new open loop plant with $G_{vc}(s)$ as its control-to-output transfer function, as given by (3.32) and shown in Figure 3.5. The voltage loop compensator $G_v(s)$ can then be designed based on $G_{vc}(s)$.

Due to the prevailing steady-state error in the control-to-output transfer function, the voltage controller is chosen to have an integral characteristic at low frequency. To further counteract the converter's second order output filter pole characteristic depicted by the severe 180° phase lag and –40 dB/decade gain roll-off, another zero must be added to get any sort of wide bandwidth and adequate stability margin. This zero serves a similar purpose to the zero from the current loop: counteract the gain and especially the phase of the double filter pole. This results in a closed-loop slope of –20 dB/decade above the filter pole. The voltage loop zero's placement is therefore chosen to be the same as that of the current loop zero, although satisfactory results can also be obtained by separating the zeros and placing one on either side of the output filter pole's corner frequency in a similar attempt to minimize the gain effects of the filter's quality factor.

The expression for the voltage compensator is hence given as:

$$G_v(s) = \frac{s+1000}{s} = 1000\left(\frac{1+\frac{s}{1000}}{s}\right) \tag{3.35}$$

The corresponding implementation for the compensator is shown in Figure 3.10. Its

transfer function is given by (3.36), where R_I is once again the input resistor.

$$G_v(s) = \frac{1}{CR_I} \frac{1 + \frac{s}{CR_f}}{s} \tag{3.36}$$

Solving for (3.36) using (3.35), the component values C and R_f are standardized as 0.102 μF and 10 kΩ respectively. The zero's frequency was then recalculated as 980.4 rad/s using the standard component values. The final voltage compensator is thus given by (3.37).

$$G_v(s) = \frac{s + 980.4}{s} \tag{3.37}$$

The Bode plot for the complete system's response including the voltage compensator is shown in Figure 3.11. The response exhibits a gain margin in excess of 45 dB, a phase margin in excess of 80°, while maintaining a bandwidth of 1.7 x 10^3 rads/s. Thus, the design objectives are clearly met with regards to the gain and phase margins, although the bandwidth has decreased by approximately an order of magnitude as a result of the compensators. Still, it will be shown that this smaller bandwidth actually meets the specific requirements for this particular application, as will be discussed in the following paragraphs and confirmed with the simulation results presented in this chapter in conjunction with the experimental results of Chapter 5.

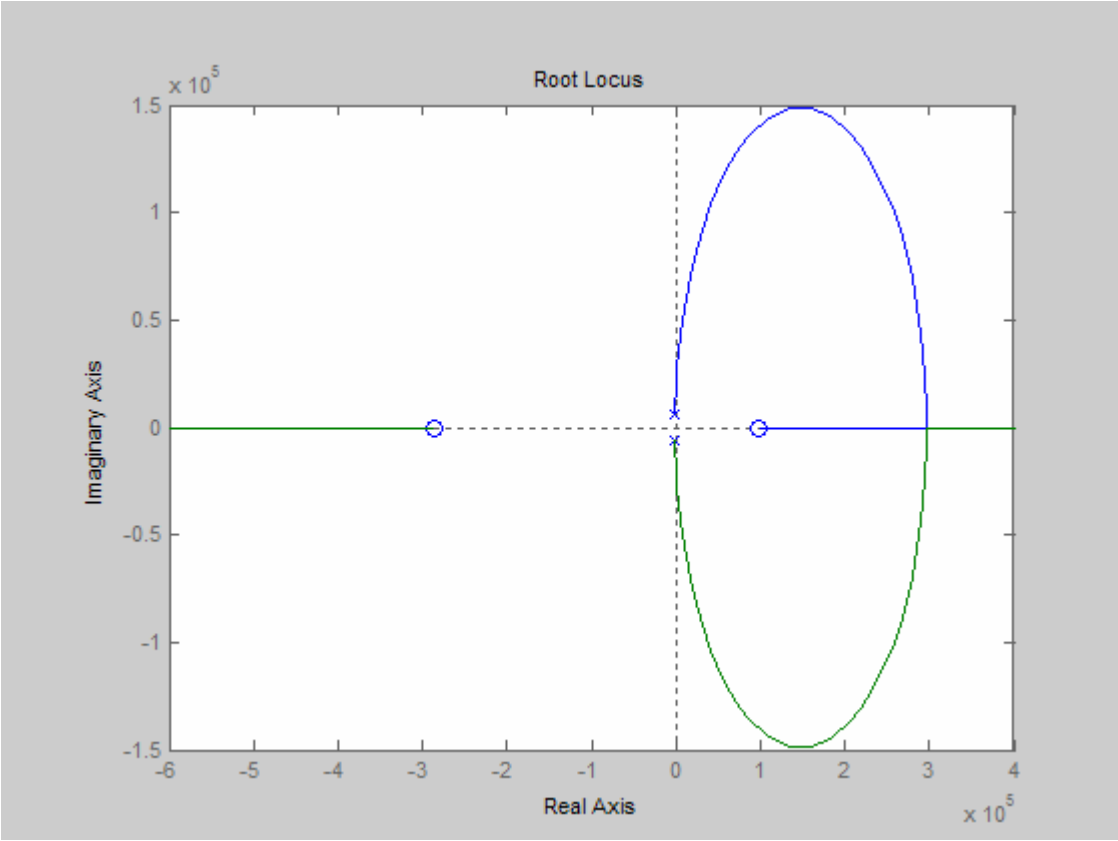

Figure 3.7: Root locus plot for duty cycle-to-output voltage transfer function.

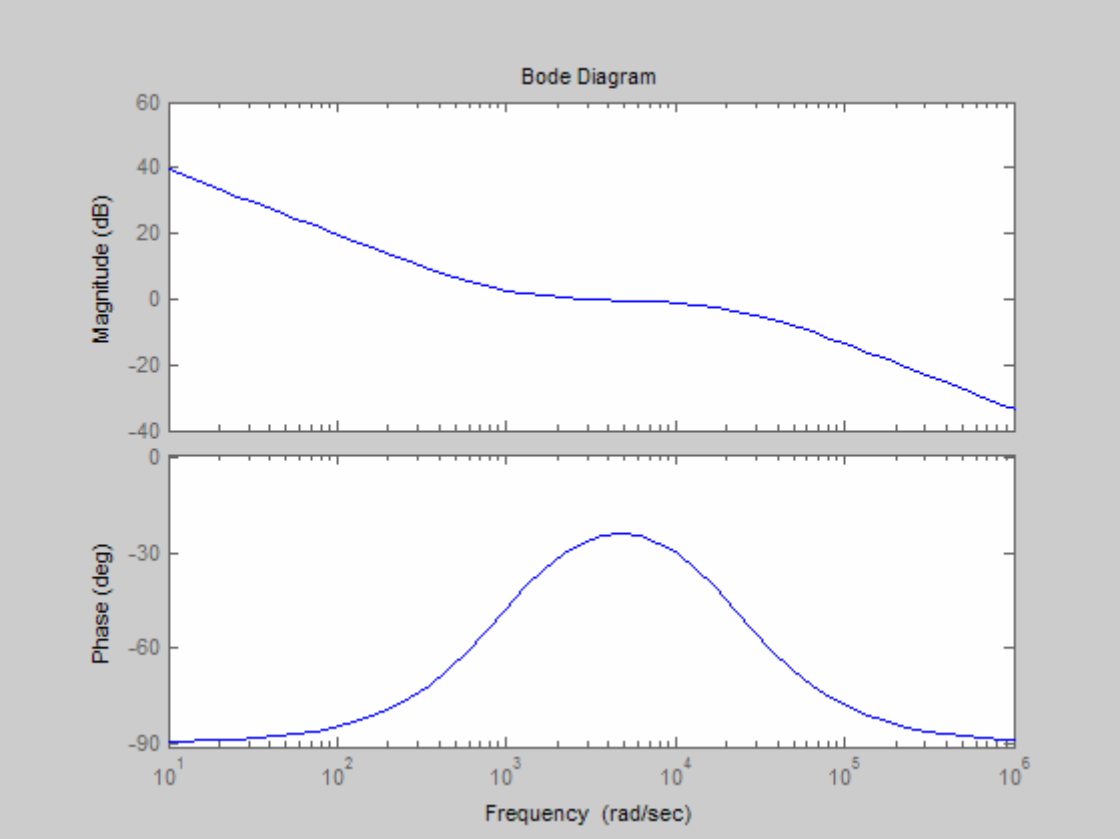

Figure 3.8: Bode plot for current loop compensator: pole at low frequency for steady-state accuracy, zero before filter corner frequency to provide phase 'bump' and improve stability, and pole at high frequency to filter out noise.

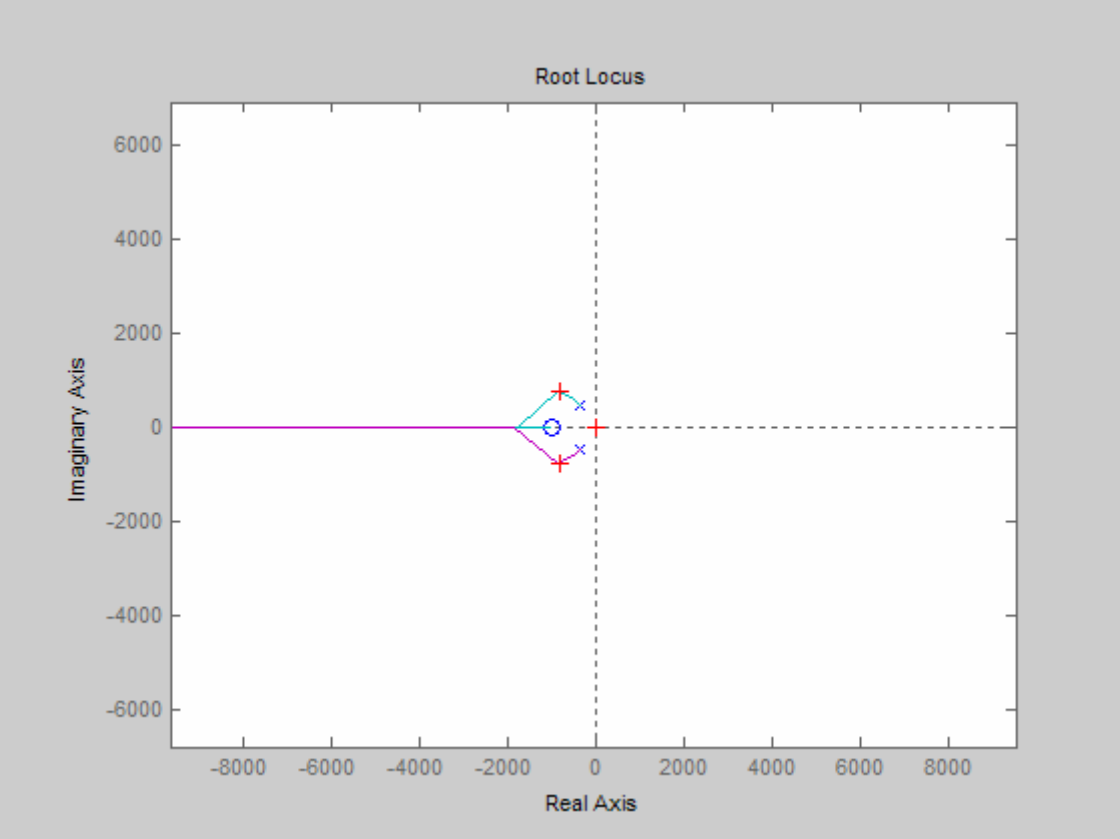

Figure 3.9: Root locus plot for control-to-output voltage transfer function: Dominant pole locations for chosen gain are marked by '+'.

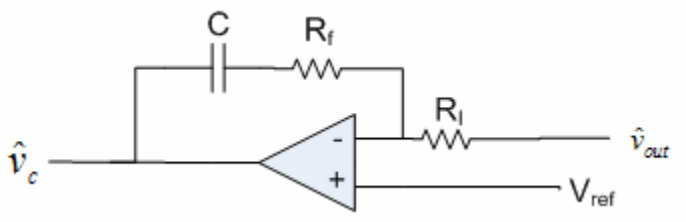

Figure 3.10: Voltage compensator implementation.

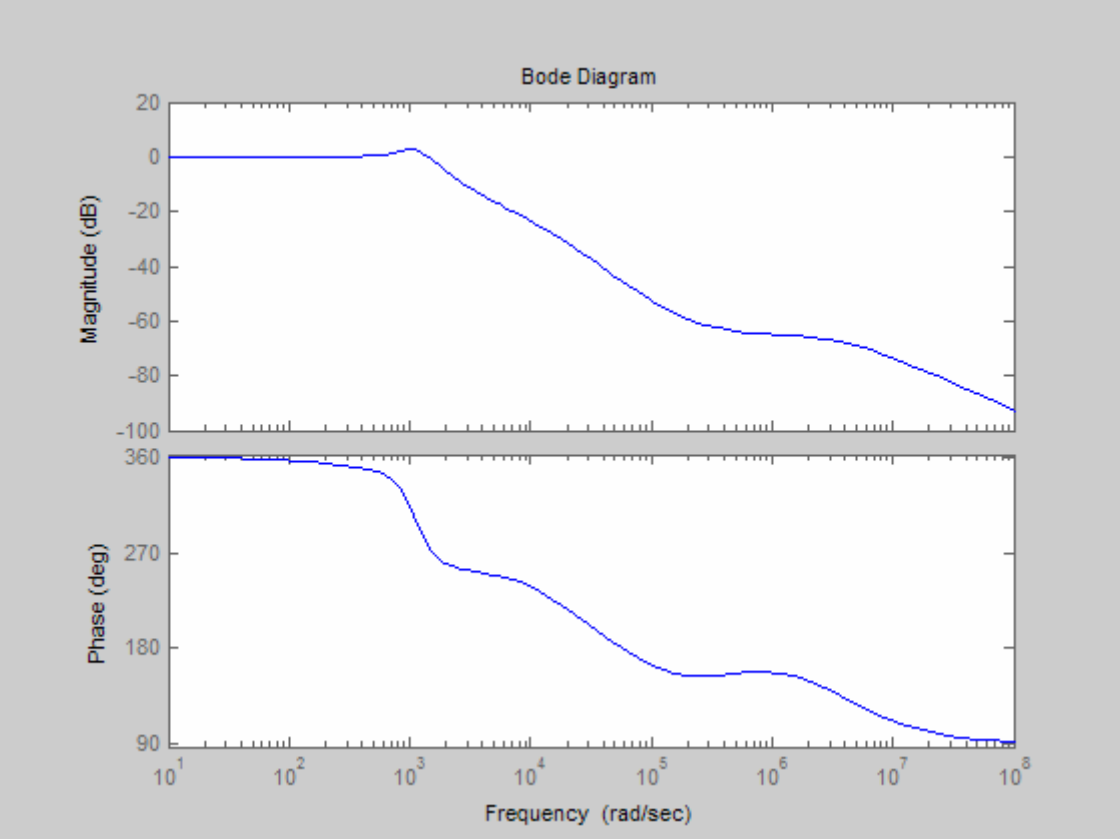

Figure 3.11: Bode plot for input-to-output voltage transfer function.

- A Note on Compensation Design:

As with the design of all compensators, tradeoffs and compromises exist. For the high-frequency pole in the current compensator, as long as it is at least one decade above the zero, it does not significantly alter the current loop gain. In particular, the one design parameter that had the most impact on the overall control loop was the zeros. One key design decision was whether to place the zeros at a higher frequency, thereby increasing the system bandwidth. However, the gain at low frequency and phase margin would have decreased. The net result of increasing the bandwidth and thus the response speed of the system while decreasing the low frequency gain and phase margins would have important implications for the application at-hand. First, a zero closer to the origin as selected provides the required low-frequency gain boost that causes the current loop to rapidly and accurately follow the reference average current set by the outer loop, which homes in on the ACMC characteristics. Furthermore, a slower response helps avoid any harmful effects to the fuel cell due to its slow dynamics, such as voltage degradation and oxygen starvation as previously discussed. Finally, the smaller bandwidth also avoids instabilities due to the presence of a RHP zero in the converter's transfer functions, as will be further discussed. Thus, for the reasons just mentioned, accuracy and stability should take precedence over speed of response, and the zeros' locations were chosen accordingly.

- Compensating for a RHP zero:

A major difficulty in attempting to stabilize a boost power supply operating in CCM is due to the RHP zero, and thus it is worthwhile to spend some time and examine more closely its impact. A RHP zero causes a +20 dB/decade gain just like a LHP zero, but exhibits a –90° phase shift as opposed to +90° as in the case of a LHP zero. This results in a Non-Minimal Phase (NMP) system since the zero introduces more phase lag than the corresponding LHP zero, and the zero acts as a form of 'delay' slowing down the step response, where in contrast the LHP zero increases the response speed. As with any stable system with a RHP zero, the step response will experience 'undershoot', i.e., the

signal at some point will go the ‘wrong way’. To make matters worse, the undershoot gets bigger as the zero moves closer to the origin. In the case of the boost converter, the zero’s frequency decreases as the output current increases. It is therefore important to account for this phenomenon in the design process.

One can understand the physical manifestation of this RHP zero by investigating the converter’s operation in the case of a step change in load current. For a boost converter, in response to a step increase in load, the error amplifier causes the duty-cycle to increase by closing the switch for a longer period. Since the switch is in a parallel path to the output, this causes the output voltage to momentarily decrease. Eventually, after several cycles, the inductor current increases and transfers more energy to the output. This initial decline in the output voltage with increase in duty-cycle is effectively an inversion at higher frequencies, and is opposite to the desired function, and thus results in a delay, or lag, which is revealed as a RHP zero in the converter’s transfer function. At low frequency, the output tracks the input and is in phase. The frequency where the phase transitions from in-phase to out-of-phase is the RHP zero.

A common experiment used to visualize the impact of a RHP zero is aiming to balance a vertical stick on a cart, or on one’s hand for simplicity. In order to move the stick in one direction, one will require to move their hand in the opposite direction to that desired at some point, likely at the start, to ‘tilt’ the stick in the direction of movement and avoid having it fall in the opposite direction.

So how does this RHP zero impact the compensator design? One can start by stating that the zero greatly limits the system’s performance, and no control strategy may divest the system from the delay introduced [20]. Whereas closed-loop poles are highly affected by feedback, feedback has no effect on zeros, except for those that may get canceled out. Since no stable compensator design will cancel a RHP zero, any plant’s NMP zero will remain in the closed-loop system. Furthermore, given its frequency varies with operating conditions, it is of most concern when it is at low frequencies, which limits the available

bandwidth for the converter to operate as a stable regulator.

'Good' performance can only be attained if the gain crossover frequency is placed well below the worst-case lowest frequency of the RHP zero to maintain adequate phase margin at the crossover frequency, thereby improving the stability of the system, and also increasing the gain margin. This results in lower closed-loop bandwidth, but effectively eliminates the RHP zero in the outer loop, which becomes 'buried' within the current loop and the voltage loop only sees a flat gain characteristic with a single pole roll-off at the crossover frequency. Attempting to increase the gain to improve the bandwidth and the system response speed will enlarge the undershoot and may lead to instability. The design of the converter components may also relieve the RHP zero effect. Since the zero moves inversely with inductor current as well as the inductor value, the inductor can be made small to increase the zero frequency and improve the loop response. One does not have to worry about crossing into DCM with ACMC, and thus the inductor can be made as small as possible with the only constraint of maintaining the inductor ripple current limit [26].

3.4 Simulations

The design of the control loops was inspected by means of MATLAB/Simulink. The system built for simulation is shown in Figure 3.12, and its component values are given in Table 3.1. Furthermore, the switching frequency of the converter is 62.5 kilohertz. Although previously ignored when deriving the dynamic model of the converter in Chapter 2, the simulations now include the converter's additional inductors and capacitors used to attenuate transients and reduce the ripple content. More details with regards to the function of these additional components will be given in subsection 4.3.3.

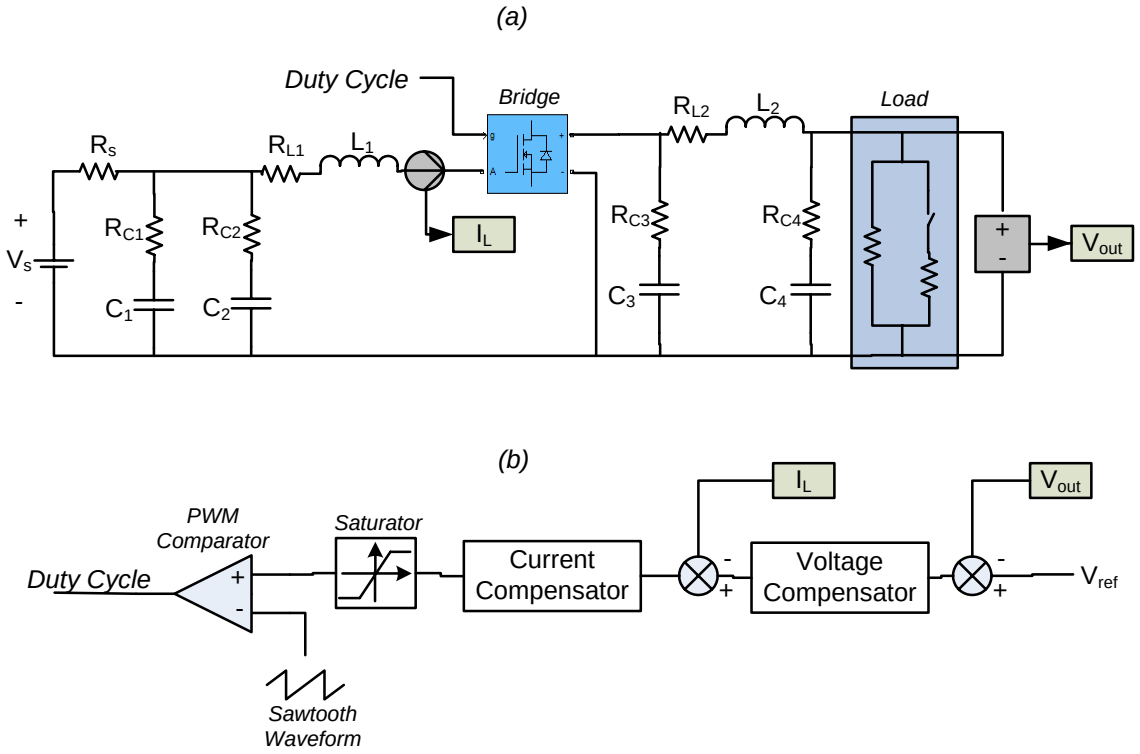

Figure 3.12: Simulated boost converter: (a) topology (b) control loop.

Table 3.1: Converter's power components for simulation.

Power Components	**Value**	**ESR**
Capacitor C_1	100 μF	235 mΩ
Capacitor C_2	40 μF	20 mΩ
Capacitor C_3	700 μF	5 mΩ
Capacitor C_4	10 μF	65 mΩ
Inductor L_1	10 μH	2.4 mΩ
Inductor L_2	3.98 μH	2 mΩ
Input Voltage V_s	24 V	15 mΩ

The converter is now subjected to a step load change to study the performance of the control loops. Its response for a load current step of 25 Amps is shown in Figure 3.13. The simulation results show the converter's ability to accurately track the load demand

and regulate the dc bus voltage at 48 Volts as requested despite the external disturbance. This further verifies the ability of the compensators to effectively deal with the converter's inherent instability issues and deliver a well-behaved response.

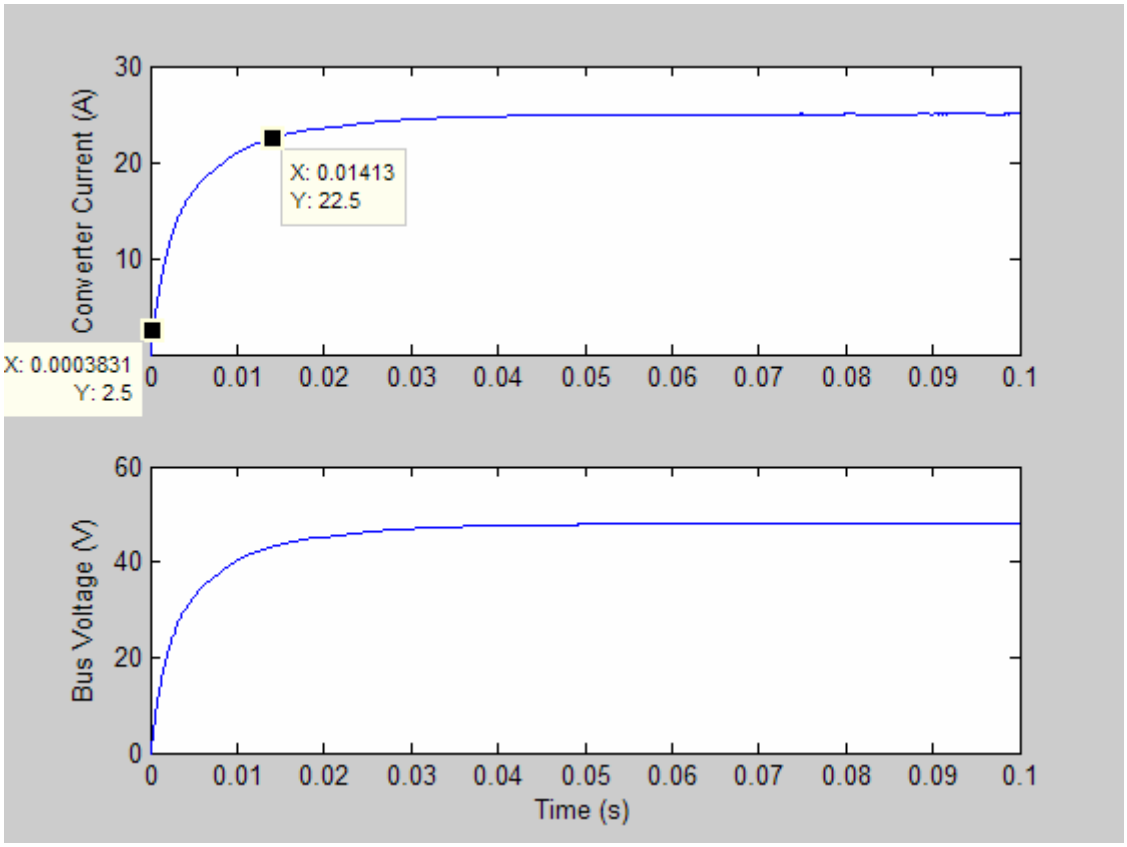

Figure 3.13: Simulated boost converter's response to a load current step: (a) load current supplied by converter (b) bus voltage.

The rise time (i.e., the time to rise from 10 percent to 90 percent of the final value) is also illustrated in Figure 3.13. This measurement is important to ensure sufficient delay has been incorporated into the compensator design to protect the fuel cell against the detrimental effects caused by abrupt load changes. This will be compared with the response of the experimental fuel cell alone to a similar step load change (Chapter 5), where it will be revealed that it is indeed the case, once again highlighting the ability of the control strategy to successfully meet the specific objectives of the application at-hand.

3.5 Assessment

The presence of an additional functional block in CMC using local feedback to create a 'voltage-to-current converter' inside the overall voltage feedback loop offers many advantages over the voltage loop only in VMC. Although the net result of the two approaches is the same, the ability to control the current feeding the output stage directly in CMC has profound effects on the dynamic behavior of the feedback control loop, and offers effective means to deal with the inherent instabilities in the converter. Still, various implementations of CMC exist. While commonly used, the PCMC implementation in switching power supplies, which actually senses and controls the peak inductor current, gives rise to many serious problems, such as a need for slope compensation, poor noise immunity, and peak-to-average current errors that the inherently low current loop-gain cannot correct. The inclusion of a high-gain integrating compensation network in ACMC overcomes the aforementioned problems. The CEA also offers the engineer design flexibility to tailor the compensator for optimum performance, gain and bandwidth characteristics, and is thus well suited for the application at hand to accommodate the fuel cell and converter's unique constraints.

The general tradeoff between accuracy and ease of use has prevented the use of a single ACMC model. Nevertheless, an accurate model that lends insight and better understanding of the system's behavior as the parameters change is vital for the design of an adequate compensator. A small-signal model is derived by modeling each component individually, i.e., the power stage, modulator, and controller, then combining the results to form a complete model suitable for the application of linear systems control theory. It was decided that the sampling gain, which was originally developed for PCMC models then extended to ACMC, is not required due to the added complexity without any increase in accuracy. However, to account for the perturbations in the input and output, feed-forward and feedback terms from the input and output, respectively, are included. Based on the small-signal analysis, design guidelines are proposed. The various control techniques for power converters are also reviewed to form a foundation upon which the

design of the compensators is based.

This task is then tackled to meet the guidelines of good steady-state accuracy, stability margins, bandwidth and noise immunity. To this end, the gain, poles and zeros of the compensators must be appropriately selected, and it was established that the poles and zeros should be placed as to counteract the zeros and poles of the system's transfer functions. As expected, conflicts to achieve the desired goals exist, and a delicate compromise is required for the application at hand that takes into account the presence of a RHP zero, which greatly limits the performance of the system. It was noted that a couple of zeros are necessary to overcome the severe phase lag and gain roll-off caused by the second-order output filter, and poles are required at dc and high-frequency for zero steady-state error and noise reduction, respectively. Furthermore, it was determined that no control strategy may effectively eliminate the delay caused by the presence of this RHP zero. Although placing the gain crossover frequency well below the zero's smallest frequency decreases the bandwidth of the closed-loop, it causes the zero to become 'buried' and disappear in the outer loop. Moreover, the resulting slower response is well suited in the overall implementation due to the slower dynamics of the fuel cell, and alternatives to improve the system's transient response will be further investigated in the following chapter. Simulations in MATLAB confirmed the ability of the control loops to meet the objectives and its effectiveness to stabilize the system despite external disturbances.

Chapter 4
Hybrid Power System

4.1 Introduction

Fuel cells are attractive as efficient, modular, low-pollution means of generating electrical power. However, its challenges still include its poor voltage regulation, lack of storage capability, and its slow dynamics, which are in turn limited by the slow dynamics in the fuel supply system that contains pumps, valves, and reformers. This causes difficulties for the fuel flow to follow step load changes, and leads to fuel starvation and fuel cell lifetime degradation, as previously discussed. To meet the demand in many applications for power sources with high energy density and high power density, it is constructive to combine the high energy density of the fuel cell with a secondary source of high power density, such as batteries or ultracapacitors. These applications are characterized by load profiles with relatively low average power requirements but with an occasional or periodic demand for higher power. While a fuel cell of reasonable size may supply the necessary energy, it cannot (economically) provide the high peak power intermittently demanded. Similarly, while Energy Storage Systems (ESS) may supply the peak power, they are insufficient by themselves to provide the long-term power that the applications require.

Combining the fuel cell with an ESS in a hybrid system allows for much higher peak power while preserving the high energy density to meet the requirements of these applications. There are also many other benefits of hybridizing:

- ESS can provide power to the fuel cell's auxiliary equipment for start-up and also supply load demand while the fuel cell is warming up

- Components can be made to operate in region of higher efficiency since neither one would have to provide the full load and capacity
- Components can be of smaller dimensions, particularly the fuel cell, which is the most expensive component
- ESS can condition power output from fuel cell to provide voltage acceptable to equipment
- Improved reliability and extending lifetime of components
- ESS can be used to supply high transient energy and thus greatly improve system dynamics

Indeed, repetitive stepped loads lead to lifetime degradation of the fuel cell if not supplemented by an ESS. The ESS may now supply the transient power and enable the fuel cell to more slowly adjust to the new power levels or operate under nearly steady-state conditions. The last benefit also leads to improved power quality of the system, since a rapid increase in load demand could not be handled by the fuel cell or would result in a significant drop in its output voltage, which may even cause shutdown of the system. Thus it is clear that the hybrid system brings about 'synergistic' benefits where the whole is greater than the sum of its parts.

4.2 Energy Storage Systems

An auxiliary source to supply or absorb the high transient energy is required to complement the slower output power of the fuel cell. The three potential storage systems considered are the flywheel, supercapacitor or ultracapacitor, and battery. The pros and cons of each are listed below:

- Flywheel:
    - Pros:
        - Very fast response
        - Reduced system complexity
        - Minimal maintenance
        - High efficiency
        - High specific power
    - Cons:
        - Little modularity
        - Low specific energy
        - Less technologically mature

- Supercapacitor/Ultracapacitor:
    - Pros:
        - Very fast response
        - High life cycles
        - Low maintenance
        - High specific power
    - Cons:
        - Low specific energy

- Battery:
    - Pros:
        - Modular
        - Fast time response
        - High specific energy
    - Cons:
        - Reduced life cycles
        - High maintenance

Hybrids containing both supercapacitors/ultracapacitors and batteries are common, and the former's fast response and high number of charge-discharge cycles versus the latter's high specific energy is typically the determining factor for the feasibility of their use in a particular application. Athough the use of supercapacitors or ultracpacitors would better exploit the benefits of the control strategy derived in this chapter as will be further discussed, batteries were chosen for this application as well due to their availability in the laboratory for experimental use.

4.3 Topology

4.3.1 Introduction

The simplest hybrid configuration is formed by connecting the fuel cell and battery directly to a dc bus, as shown in Figure 4.1. In contrast to simply having a single power source by itself, for instance either the fuel cell or battery, such a 'passive' hybrid demonstrates a longer run-time and higher power capability. It also decreases the stress on the fuel cell and accordingly conditions the hybrid source terminal voltage. Nevertheless, there are also a number of disadvantages associated with such a hybrid configuration. First, the battery terminal voltage must match the nominal voltage of the fuel cell in order to not overcharge the battery, thereby greatly limiting much of the system's design flexibility. Second, since the power distribution between the fuel cell and battery is passively determined by the impedance characteristics of each source and is thus determined in a rather fixed way, the hybrid system performance may be unnecessarily limited by one of those two components. For example, the peak power capability of the hybrid may be restricted by the fuel cell when the fuel cell first reaches its safe power limit even while the output power of the battery is still well below its maximum.

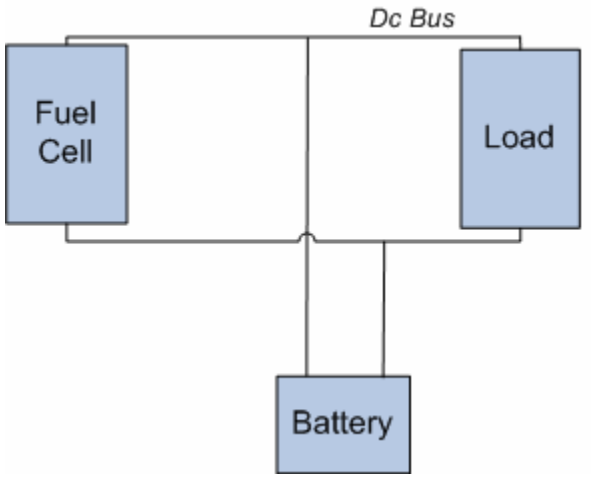

Figure 4.1: Fuel cell connected directly to battery.

These disadvantages can be eliminated by interposing a dc-dc converter between the fuel cell and battery, creating an 'actively' controlled hybrid system. In active hybrids, the power converter is controlled to regulate the power sharing between the fuel cell and battery in order to maximize the advantages of each component. For example, the fuel cell and battery can be controlled to generate the maximum power from each simultaneously, thereby greatly increasing the peak power capability beyond that achievable by a passive hybrid, without much increase to the system weight and volume [32]. Similarly, the active hybrid can be controlled such that the sources operate in their most efficient region, thereby also increasing the system's efficiency. Furthermore, the presence of a power converter at the fuel cell output is essential to obtain bus regulation due to the fuel cell's wide output variation, and more importantly to provide the necessary protection to the fuel cell as discussed. It also allows more flexibility in the system design, as the battery stack terminal voltage no longer must match the fuel cell's nominal voltage.

4.3.2 Active Hybrid Configuration

The position of the separate components results in two possible configurations within the active hybrid configuration, which in turn determine the system's voltage and power

characteristics. In the first, the load is directly connected to the battery while the fuel cell is connected to both the load and the battery through the dc-dc converter, as shown in Figure 4.2. The battery provides additional power when a high peak power is requested by the load or during a step load change while the fuel cell ramps up to the required level. In this configuration, the power flows unidirectionally through the converter stage from the fuel cell to the battery and load. Moreover, the load voltage follows the battery voltage. Although the bus is floating at the battery voltage, controlling the dc-dc converter can change the output current of the fuel cell, and thus the current (and voltage) supplied by the battery.

In the second configuration, the load is connected to the fuel cell rather than the battery, as shown in Figure 4.3. The battery is now charged and discharged through a bidirectional converter where the power must flow in both directions. The load voltage now follows the fuel cell voltage. Similarly, although the bus is floating at the fuel cell terminal voltage, controlling the converter can change the charging and discharging current of the battery, and thus the current (and voltage) of the fuel cell.

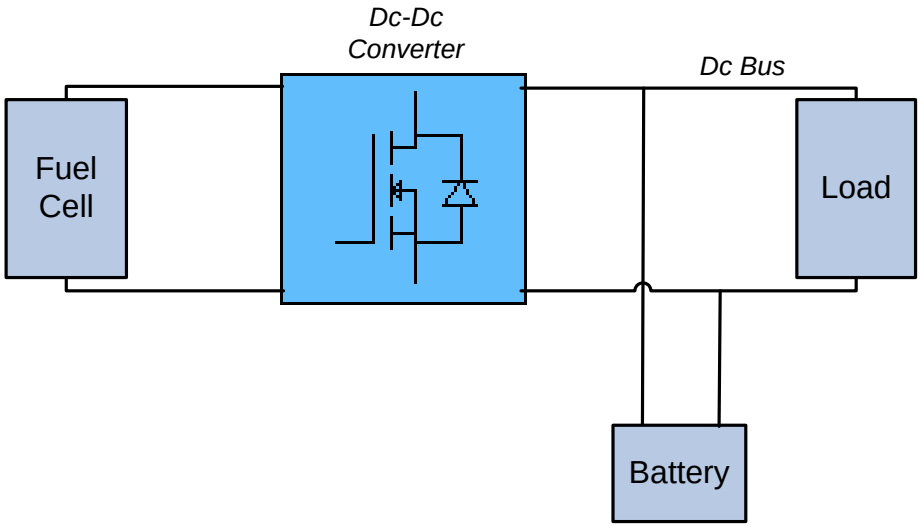

Figure 4.2: Active hybrid configuration 1: load connected to battery.

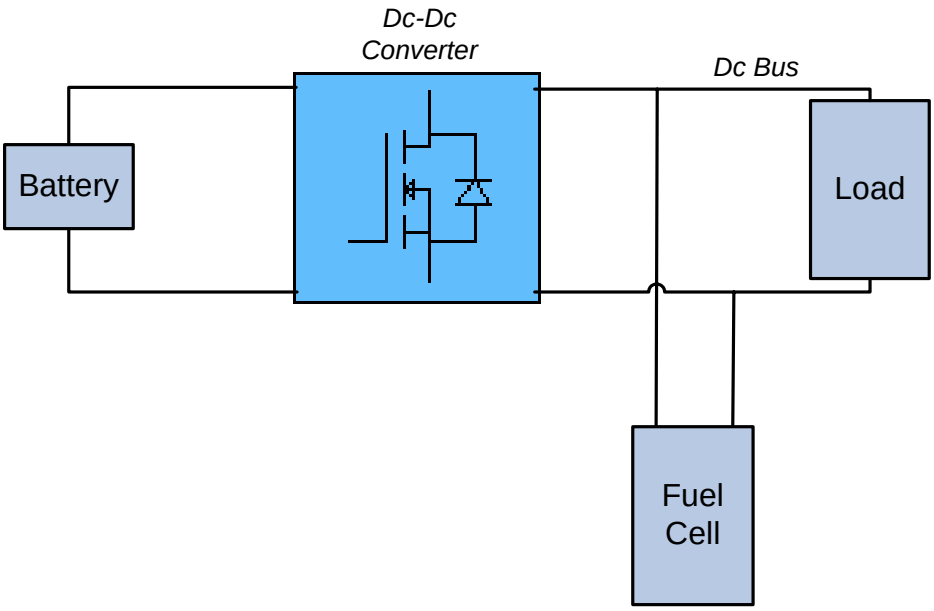

Figure 4.3: Active hybrid configuration 2: load connected to fuel cell.

The chosen configuration of the hybrid power sources depends on the specific application according to the required load voltage and power characteristics. It can be shown that the dynamics in the second topology are slower due to the presence of the converter between the battery and the load, where additional time is required to change the current in the converter's inductor to charge or discharge the battery. A faster response to load changes can be achieved in the first configuration since the battery, rather than the fuel cell, is closer to the load. In addition, the battery offers a 'stiffer' voltage regulation at its output terminals in response to load changes and should therefore be closer to the load. First configuration also allows the fuel cell to be protected from the large pulse power demands of the load by the converter while the battery supplies the load directly. Finally, the first configuration also allows the flow of current unidirectionally through the converter from the fuel cell to the load and battery, which simplifies the converter's design and control. Hence, choosing the first configuration for this application is well justified.

4.3.3 Fuel Cell Dc-Dc Boost Converter

The dc-dc converter adopted in this topology is the boost converter discussed in the previous chapters. It is chosen to adapt the low dc voltage output from the fuel cell to the bus voltage since designing fuel cell stacks for higher voltages is not efficient [9]. The experimental boost converter with all its components is shown in Figure 4.4. At the source input, a simple equivalent electric circuit has been considered for the dynamic modeling of the fuel cell and its various loss mechanisms [33]. Referring back to the fuel cell's operating characteristics discussed in Chapter 1, resistor R_h models the ohmic losses, R_{cl} and C_{cl} model the activation losses, where C_{cl} introduces a delay in the fuel cell's response to abrupt load changes due to the charge layer on the interface of the electrode and electrolyte, and is thus fittingly termed as the 'charge double-layer' phenomenon. The concentration losses are ignored since that operating region with excessive current is avoided. The power stage of the converter consists of switches S_1, S_2 and their associated antiparallel feedback diodes D_1 and D_2. As previously stated, the converter is driven by a PWM generator. Metal Oxide Silicon Field Effect Transistors (MOSFETs) were chosen due to their better voltage drop, translating to higher system efficiency, and the relatively low current requirement. Another diode is present at the fuel cell's output to prevent current from flowing back to the fuel cell stack, which would damage the stack. Input capacitor C_1 serves as an ac short, which along with resistor R_1, are designed for critical damping [34]. Input capacitor C_2 connected across the source terminal minimizes the circulation of high-frequency components through the supply. This filtering is as effective due to the presence of the source's series resistance. Together, capacitors C_1 and C_2 improve the system stability, attenuate transients from being seen at the input and provide the necessary filtering and ripple reduction to meet the requirements of the fuel cell. High-frequency inductor L_1 at the input is also responsible for energy transfer and smoothing. Output capacitors C_3 and C_4 along with inductor L_2 form a large CLC filter to effectively filter the output and limit the ripple in the dc link.

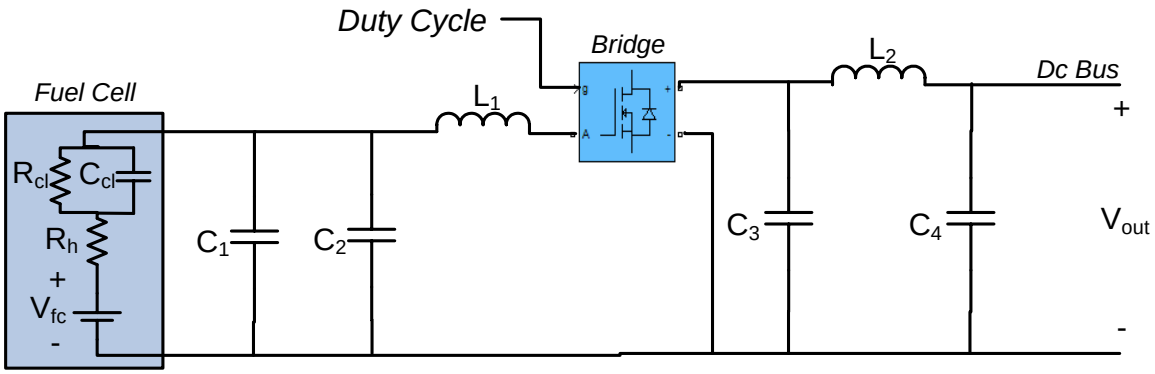

Figure 4.4: Model of experimental boost converter with fuel cell.

4.3.4 Battery Characteristics

Since it is not practical to measure the battery's State of Charge (SOC) directly, an approximate linear relationship between the SOC and Open-Circuit Voltage (OCV) is used when operating within its normal range, as shown in Figure 4.5 for the batteries used in the experimental setup [35,36].

The battery's OCV can be estimated using the equivalent circuit of Figure 4.6, as described by:

$$v_{oc} = v_b - i_b \cdot R_b \tag{4.38}$$

where v_{oc} is the battery's OCV, v_b and i_b are the measured battery terminal voltage and charging current, and R_b is the battery's ESR. Note that for the given model in Figure 4.6, the terminal voltage is replaced by the OCV. This avoids the need to determine the OCV, using a look-up table for instance, whilst still benefiting the control strategy by charging the battery with a smaller current (since in this case $v_b > v_{oc}$), thereby resulting in fuel savings, and in case the battery is discharging, a larger current will be requested from the fuel cell (since $v_b < v_{oc}$), thereby compensating for the increase in load. Thus, this simple resistance model is adequate and used here for control development purposes.

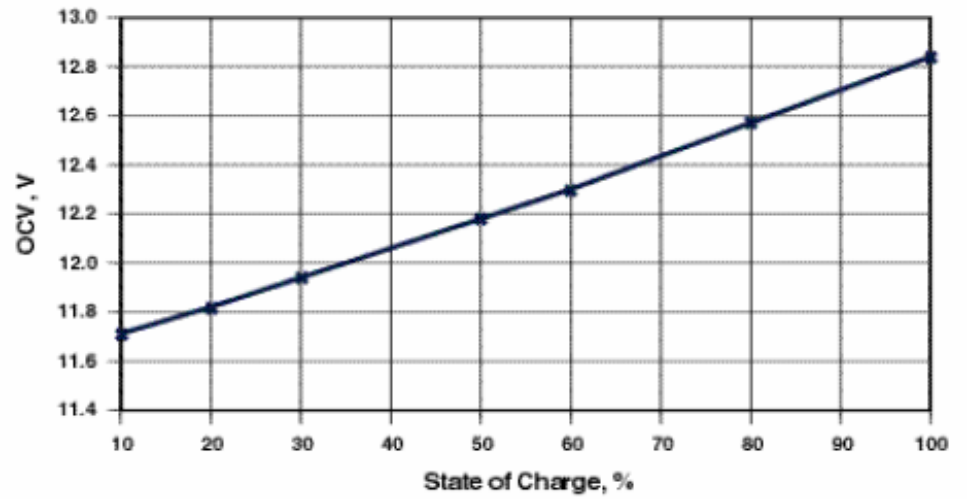

Figure 4.5: Relationship between battery's SOC and OCV for Genesis batteries [37].

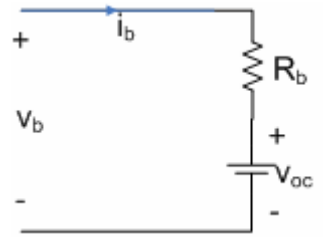

Figure 4.6: Equivalent circuit for approximation of battery's OCV in normal operating range.

4.4 Control Strategy

4.4.1 Introduction

More complex control is required to ensure efficient and robust power transfer from the separate sources without the risks of the components' degraded reliability. To achieve uninterrupted power flow to the load, rather than achieving a single voltage or current

regulation goal, the control system must adjust the power converter to regulate the dc bus and balance the power flow of both sources to satisfy the load requirements and their various constraints.

Many different control strategies can be implemented to meet a set of desired objectives, many of which are conflicting as would be expected, and thus tradeoffs and compromises are necessary. For example, one may attempt to maximize the fuel cell's output power, thereby causing the battery to fully charge, or instead one may attempt to maximize the fuel cell's efficiency, thereby causing the battery to run down to depletion. Similarly, one may decide to charge the battery only at certain suitable times that would result in the highest overall efficiency, as opposed to maintaining the battery's charge at its optimal value that would most effectively meet the load demand and cause the least degradation in its lifetime. Furthermore, there is yet another tradeoff between efficiency and reliability, where it is desirable to turn the fuel cell off during intervals of low power demand to avoid operation in the low efficiency region. However, repetitive switching on and off of the fuel cell also leads to lifetime degradation. It is already clear that the control strategy can be made very complex by implementing optimization algorithms that would aim to achieve the best balance between many design objectives and constraints. The control strategy implemented here attempts to achieve all the desired properties while trying to maintain an ideal compromise between complexity and performance.

4.4.2 Control Objectives

Due to many possible and conflicting indicators of system performance, rather than choosing a single operating region to satisfy a certain performance objective, such as maximum output power or efficiency, the hybrid sources are controlled in an adjustable manner in response to the load, to accomplish the following objectives:

- Dc bus voltage should be regulated
- Battery should provide the peak power demand where the load is greater than the fuel cell's power capacity

- Battery should supply transient power while the fuel cell ramps up to the requested load level to avoid fuel starvation and fuel cell lifetime degradation
- Fuel cell should charge battery to maintain it at a desired SOC whenever the load demand is less than the fuel cell's peak capacity in order to ensure maximum power availability to meet peak demand
- Control battery's charging and discharging currents
- Battery should be disconnected if its SOC is below the minimum value to protect it from over-discharging (this would occur in case of an extremely heavy load or during a prolonged peak power demand), which may cause the battery to subsequently no longer accept a full charge and experience problems holding voltage under load. Overcharging protection should also be integrated by limiting applied voltage
- Battery usage should be minimized to maximize its life and the overall system cost

In effect, the fuel cell acts as the main energy source and is controlled to supply the average power to the load and maintain the ESS at a given SOC, while the battery supplies the peak load demands and transient power while the fuel cell adjusts to the new power levels. In terms of implementation, the latter part regarding the battery's role is achieved by placing the battery closer to the load, as previously discussed, and by integrating adequate delay in the converter's control. The former, which is in regards to the fuel cell, is implemented by allowing the output current of the fuel cell, and thus the output of the converter, to vary as a function of the battery voltage, which in turn will depend on the load demand. As should be anticipated, this configuration allows direct application of the CMC scheme developed in the previous chapter, with the fuel cell current ultimately depending on the battery state.

To protect the fuel cell from fuel starvation due to significant increases in load demand, sufficient delay was incorporated into the design of the compensators to limit its rise. To determine the necessary delay, the experimental fuel cell was tested with stepped load changes and its response was observed to determine the corresponding time constant

(Chapter 5). This avoids the need of implementing additional control blocks to limit the slope of the fuel cell's output current. Still, an upper limit on the fuel cell's output current limit was implemented as dictated by its maximum power capacity.

This continuous adjustable control strategy avoids the instability issues associated with the mode definitions in rule-based and state machine control [32,38,39] when operating at the border of two different modes. There also exists a dead-time operation while the system changes operation mode, such as from battery charging to discharging. Furthermore, rather than attempting to control the dc bus voltage through the currents or powers of the sources, this control method indirectly regulates the bus voltage through control of the power quickly delivered by the ESS and control of the ESS voltage by operating the fuel cell, thereby avoiding the need for mode definitions altogether. Finally, in comparison with the more complex optimization and model predictive control methods [36,40,41,42,43,44,45], its relatively simple structure, ability to account for multiple constraints without the need for computationally intensive algorithms and hardware requirements make it flexible and easily implemented such that it may be widely adopted. As will be demonstrated in the simulated and experimental results, it allows easy extension to control many different types of hybrid systems, including any primary energy source other than a fuel cell, with any other ESS, or even two or more similar sources together in parallel. Simply adjusting the converter's output voltage can also easily control the battery's SOC and its contribution to meet the load demand.

Finally, although the battery offers a stiff voltage regulation and the benefit of regulating the bus voltage through control of the converter as well might be questioned, one should note that the derived control strategy is not aimed at the particular battery and fuel cell hybrid system, but rather to any hybrid system that incorportates the fuel cell. Such a hybrid system of particular interest is that of two fuel cells operating in parallel, as will be simulated to demonstrate the proposed control's flexibility, or even the case of a fuel cell hybrid with an ESS such as ultracapacitors or supercapacitors that do not have a stiff voltage regulation, thereby allowing the control strategy to regulate the dc bus and take

advantage of their quick charge and discharge current.

4.5 Simulations

Ultimately, the only control variable is the converter duty cycle, which would regulate the output current of the fuel cell, and consequently the current (and voltage) of the battery, to meet the load demand and requirements of the sources as per the design objectives. Given the choice of CMC for the application, the two important parameters required for feedback to obtain the duty cycle are the fuel cell current and battery voltage. The controller designed in the previous chapter takes these two system regulation indices as inputs, and continuously outputs the duty cycle for the PWM signal to drive the converter switches. The measured signals are filtered by second-order low-pass filters due to the presence of harmonics and switching ripple generated by the converter. The simulated hybrid system is shown in Figure 4.7 (a), with the control loop shown in Figure 4.7 (b). The specific values for the system are still as given in Table 3.1. In addition, the battery's ESR is 0.004 Ohms, and its OCV is matched to the dc bus at 48 Volts. The case where the converter's output voltage and the battery's OCV are not matched, which in turn alters the power sources' contributions and energy management, will be depicted experimentally in the next chapter and further simulated in Appendix B for comparison purposes.

Simulation results to illustrate the effectiveness of the current hybrid system and its ability to meet the requirements are shown in Figure 4.8. Initially, the system is requested to supply a load current of 10 Amps. At $t = 0.05$ *seconds*, a second similar load in parallel is switched in and the current demand is increased from 10 Amps to 20 Amps. As shown at the top portion of the figure, the bus is regulated at 48 Volts as requested despite the disturbance. One can also note that the battery supplies the load while the fuel cell ramps up to the requested power at the maximum predetermined rate

established by the compensators, thereby avoiding any detrimental effects. After this transient state, the fuel cell once again supplies all the power to the load and charges the battery as required.

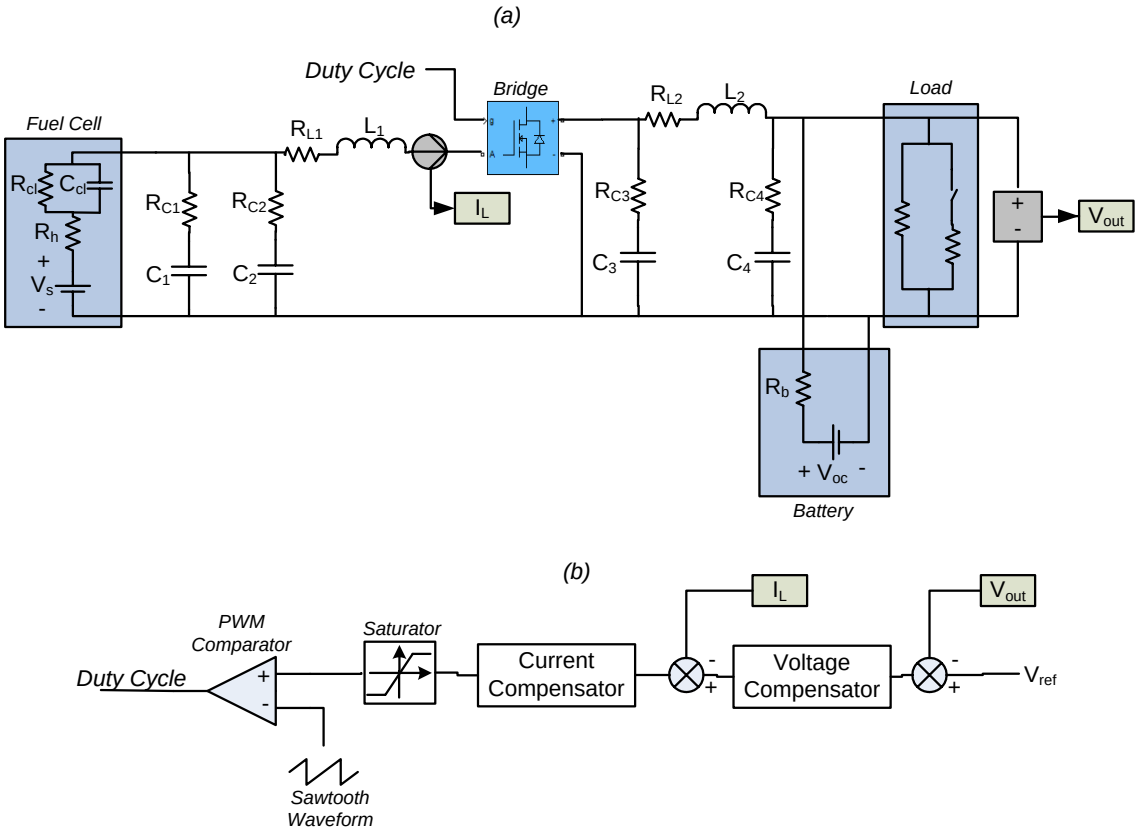

Figure 4.7: Simulated hybrid system: (a) schematic (b) control loop.

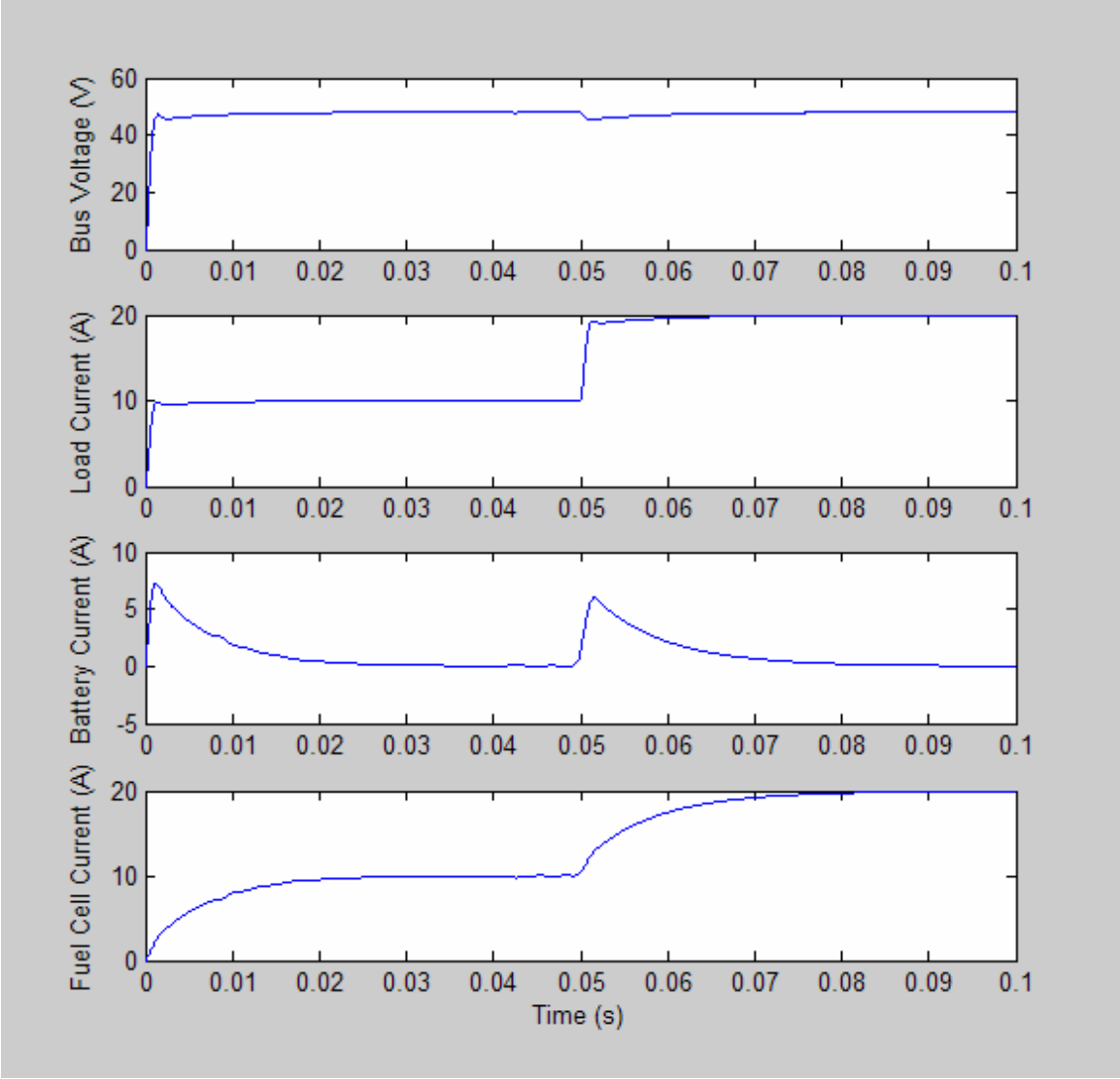

Figure 4.8: Simulated hybrid system's response to step load change: (a) bus voltage (b) load current (c) battery current (d) fuel cell current.

To demonstrate the flexibility of the developed control strategy, it is applied to the case of two fuel cells operating in parallel to supply the load. Although different approaches can be taken to determine how the demand should be shared between the two sources, here it is based solely on the relative capacity of each fuel cell, and the requested source currents are adjusted accordingly based on this relationship. The hybrid system is shown in Figure 4.9, and its response to a step load disturbance is shown in Figure 4.10.

For the simulated hybrid system, one fuel cell is considered twice the size of the other. Referring once again to Figure 4.10, one can note the larger fuel cell accordingly supplies twice as much of the load demand. Furthermore, as expected, the dc bus voltage's response to the disturbances is not as fast as in the case of the previous hybrid system with the battery that has quicker dynamics. Still, the control strategy is effective and robust in maintaining stability and steady state accuracy, thus illustrating its flexibility for use with various power sources, as was intended.

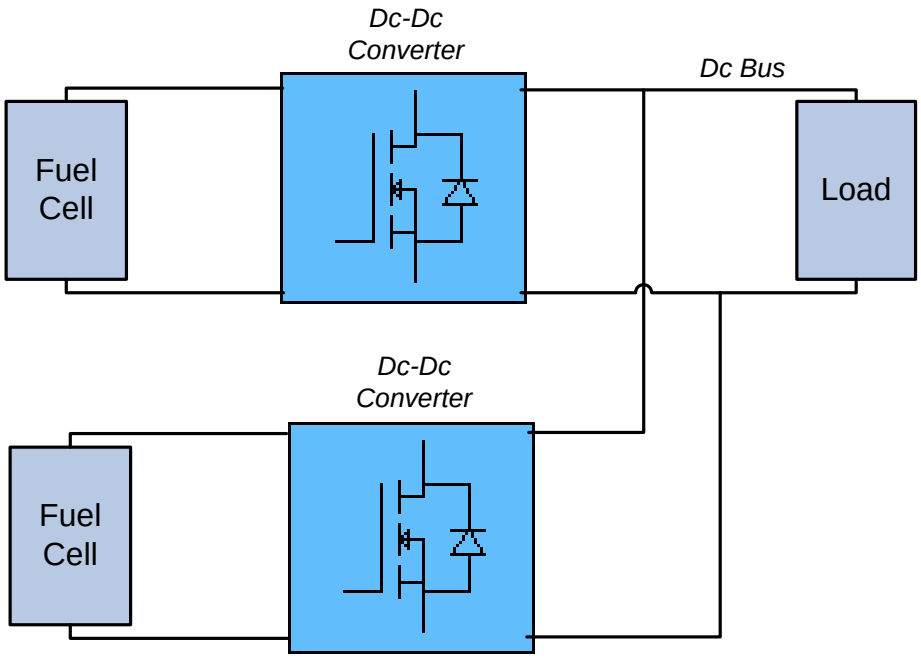

Figure 4.9: Simulated hybrid system consisting of two fuel cells.

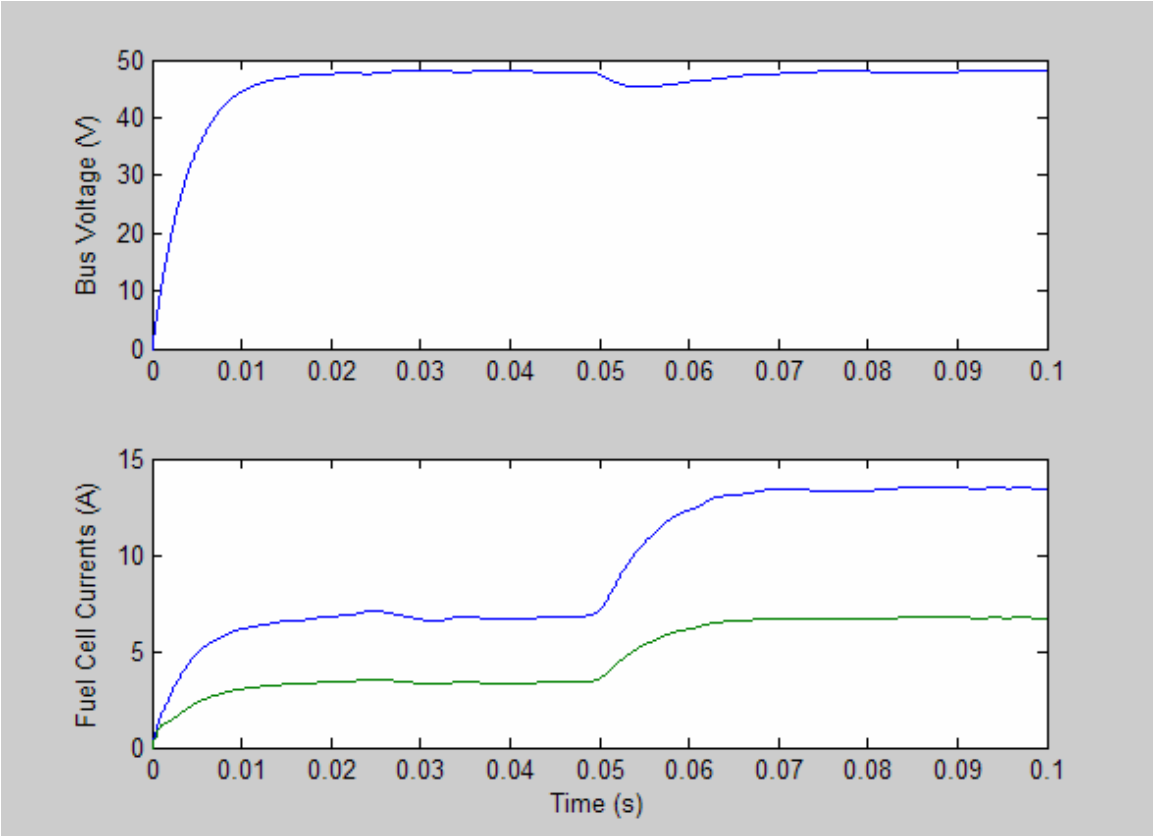

Figure 4.10: Simulated hybrid system's response to step load change: (a) bus voltage (b) fuel cell currents.

4.6 Assessment

Fuel cells are emerging as one of the more promising technologies for meeting the new energy demands, but barriers still exist before they may be widely adopted, such as their slower time constants and dynamics, which are limited by the fuel delivery system. It was deduced that hybrids combining fuel cells with fast ESS are good solutions to the fuel cell's load following problems, while also offering improved energy and power density, efficiency, reliability, start-up control, and reduced total cost, thereby producing a synergistic system where the whole is greater than the sum of its parts. Various technologies may be well suited for use in conjunction with the fuel cell, and each offers its own benefits for the application at hand. Batteries, which are technologically mature and have high energy density, were chosen due to their availability for experimental use in the laboratory.

Rather than allowing the power sharing amongst the hybrid sources to be passively determined by the components' characteristics, a dc-dc converter is placed between the fuel cell and the battery to actively regulate the power sharing. This configuration provides independent control over the sources' operating points to satisfy the load requirements, thereby greatly augmenting the peak power output, improving the bus regulation, efficiency and allowing more flexibility in the design of the system. Furthermore, it was determined that within the active hybrid configuration, placing the battery rather than the fuel cell closer to the load results in better dynamics, bus regulation, as well as offering more isolation to the fuel cell from the load and less complex converter design, while still reaping all the rewards of an active hybrid.

More complex control strategy is necessary in order to actively control the power from the different sources while ensuring efficient and robust power transfer to meet the load demand and all the benefits of a hybrid system. While the system must meet the load demand with its associated dynamics, the control strategy ensures this is performed through the most efficient and reliable means, as depicted by a list of objectives. By

connecting the battery directly to the dc bus and allowing the output current of the fuel cell to vary as a function of the bus, the CMC scheme previously devised could be directly implemented into the hybrid system to meet the objectives of the control strategy. The presented control strategy allows continuous adjustment of the output from the power sources in response to load changes and ensures the dc bus remains regulated, while avoiding the stability issues associated with the definition of operating modes in state-machine and rule-based control.

All the sources and components were modeled and the control strategy was implemented in MATLAB/Simulink. The system was simulated for different operating conditions and disturbances to analyze the dynamics and performance. The results show that the proposed system can rapidly respond to load power variations while regulating the dc bus voltage and adhering to the various operating characteristics of the sources as predetermined in the control objectives. The versatility of the control strategy was also demonstrated for the case of different hybrid sources operating in parallel. The feasibility of the control strategy in conjunction with real components will be examined in the following chapter.

Chapter 5
Experimental Results

5.1 Introduction

Experimental tests were also conducted on the fuel cell and the hybrid system to validate the results obtained throughout the dissertation. In the first section of this chapter, an overview of the experimental set-up and components will be provided, whereas the second section will present the results.

5.2 Experimental Set-up

The first stand-alone test conducted was to verify the dynamic model derived for the boost converter operating in ACMC. A function generator (Agilent 33120A) was used to superimpose sinusoidal small-signal variations in the voltage reference of the converter's control loop, and the resulting frequency response was captured using the oscilloscope (Agilent 54622A) shown in Figure 5.1. This response was then compared with the small-signal input-to-output voltage transfer function derived in the previous chapters using state-space averaging and ACMC models.

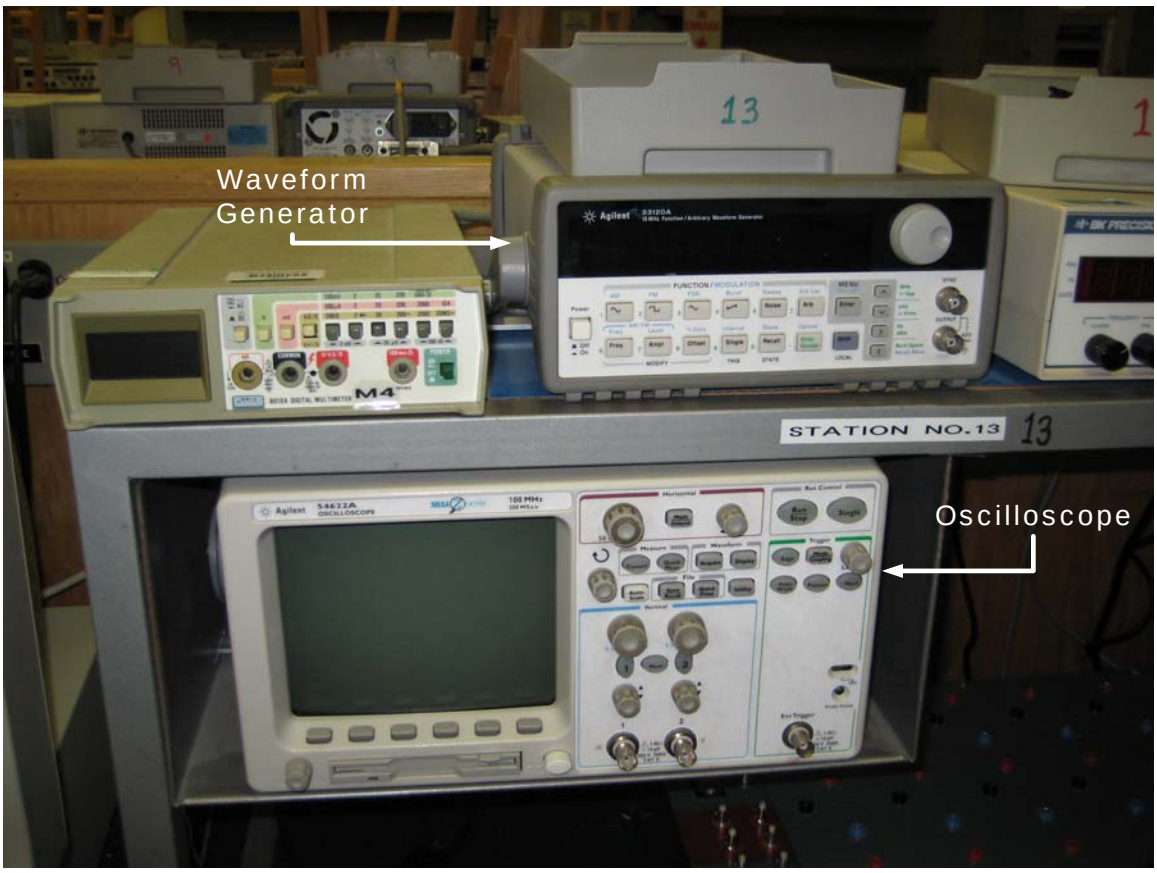

Figure 5.1: Function generator and oscilloscope.

The next tests involved exposing first the fuel cell alone and then the hybrid fuel cell and battery system to disturbances in the form of stepped loads. The former test was performed to determine the fuel cell's time-constant and thus the necessary delay to be incorporated in the design of the compensators in Chapter 3. The second test is performed to observe the dynamic response of the hybrid system and the effectiveness of the proposed control strategy. An elaborate set-up was required for these tests to control and monitor the system and ensure the necessary safety precautions due to the 'live' equipment and the presence of hydrogen to operate the fuel cell. It is therefore worthwhile to discuss in more detail the construction undertaken for this test station.

5.2.1 Hybrid Test Station

A test station was built with the objective of attaining a flexible and effective solution for assessing the research. It provides the ability to implement different control strategies and swap the various components in the hybrid system in virtually a 'plug and play' format. This 'bench' scale prototype could then be used in the development phase of the larger system by providing an efficient, safe, cost-effective and speedy design process.

- Components:

The test station included all the components for the hybrid system previously presented. A summary of the components, which have already been modeled in the thesis, is given in Table 5.1.

Table 5.1: Test station components.

Component	Manufacturer	Model	Rating	Operating range
Fuel Cell	Ballard	Nexa	1.2 kW 46 A	22 – 50 V
Dc-Dc Converter	Zahn Electronics	DC6350F-SU	1.7 kW 50 A (input) 62.5 kHz	Input: 12 – 59 V Output: 14 – 63 V
Battery Unit	Genesis	Pure lead-tin VRLA	12 V 16 Ah	11 – 13 V
Load Box	TDI Power	RBL232 50-150-800	50V 800W	-

Thus, a total of four batteries connected in series were used to attain the desired voltage rating of approximately 48 Volts for the dc bus, which in turn could deliver a constant power discharge of approximately 4 kilowatts for 5 minutes [46].

- Integration:

The physical components are shown in Figure 5.2, with their interconnection and wiring shown in Figure 5.3. Additional auxiliary electronic devices were required in order to safely operate the test station and protect the equipment, such as a blocking diode at the fuel cell's output as previously discussed, an additional diode at the converter's output to prevent reverse current being fed into the converter, contactors at the output of each source, relays, fuses, emergency stop power switches, and adequate dc bus. Hydrogen leak sensors are also installed near the test station with the necessary ventilation in place in accordance with standard laboratory practices. Finally, current sensors and a voltage divider were put in place to monitor the required signals. Basic monitoring and diagnostic features for the fuel cell were also provided via Labview software. A screen shot of this interface is shown in Figure 5.4. Due to the poor resolution offered through this interface, as can be observed, a separate data logger with better accuracy suitable for this application was also used to produce the necessary plots for the experimental tests shown below.

- Control:

The controller's communication was based on RS232 protocol. The nonconforming equipment based on RS485 protocol was converted to RS232 via adapters. The control wiring diagram is also shown in Figure 5.3.

The electronic control unit used for the test station is the MotoTron MotoHawk ECU555-80. This embedded control system met the design requirements in terms of number of inputs and outputs, and power requirement to manage the various control signals to the equipment. It also provided a simple and flexible solution to integrating the proposed control strategies by providing a suitable interface to directly compile the control algorithms designed and implemented in MATLAB/Simulink. Dual CAN 2.0B datalinks ensure interoperability with other system components.

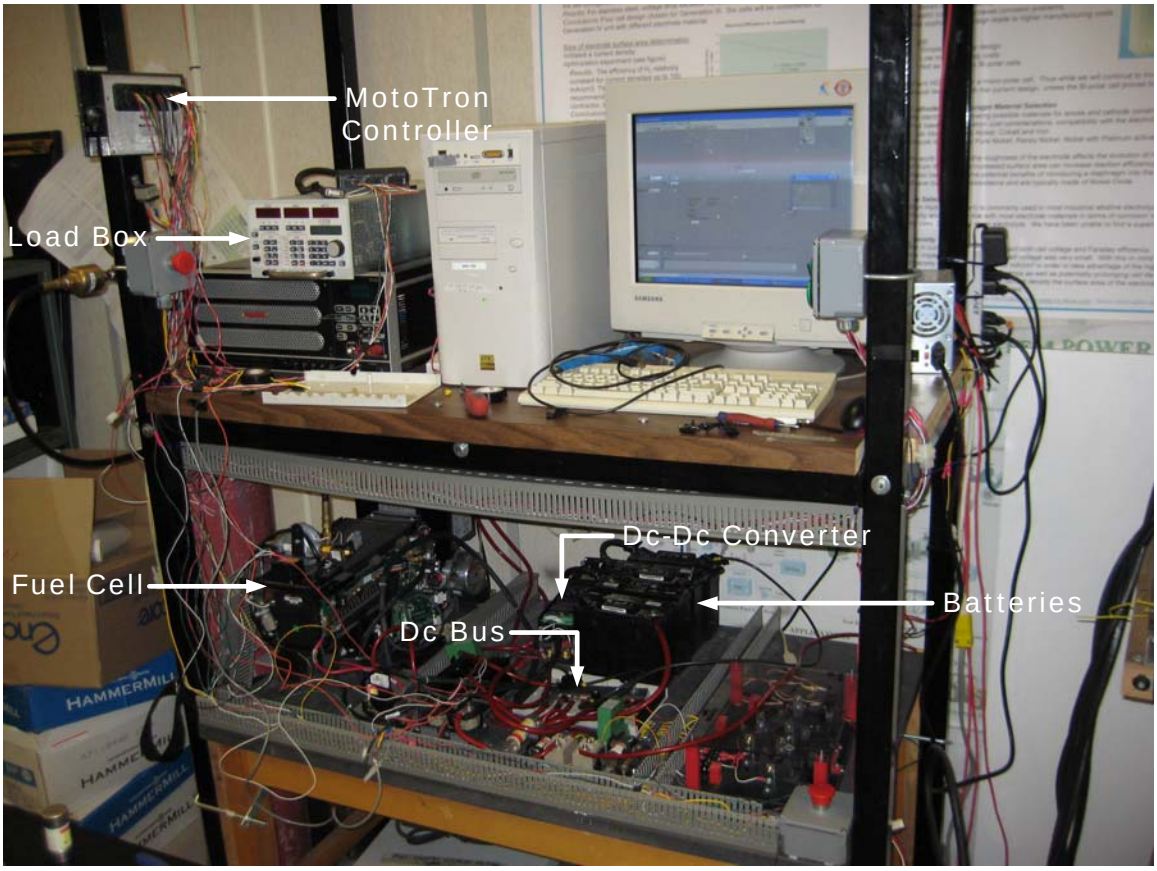

Figure 5.2: Test station.

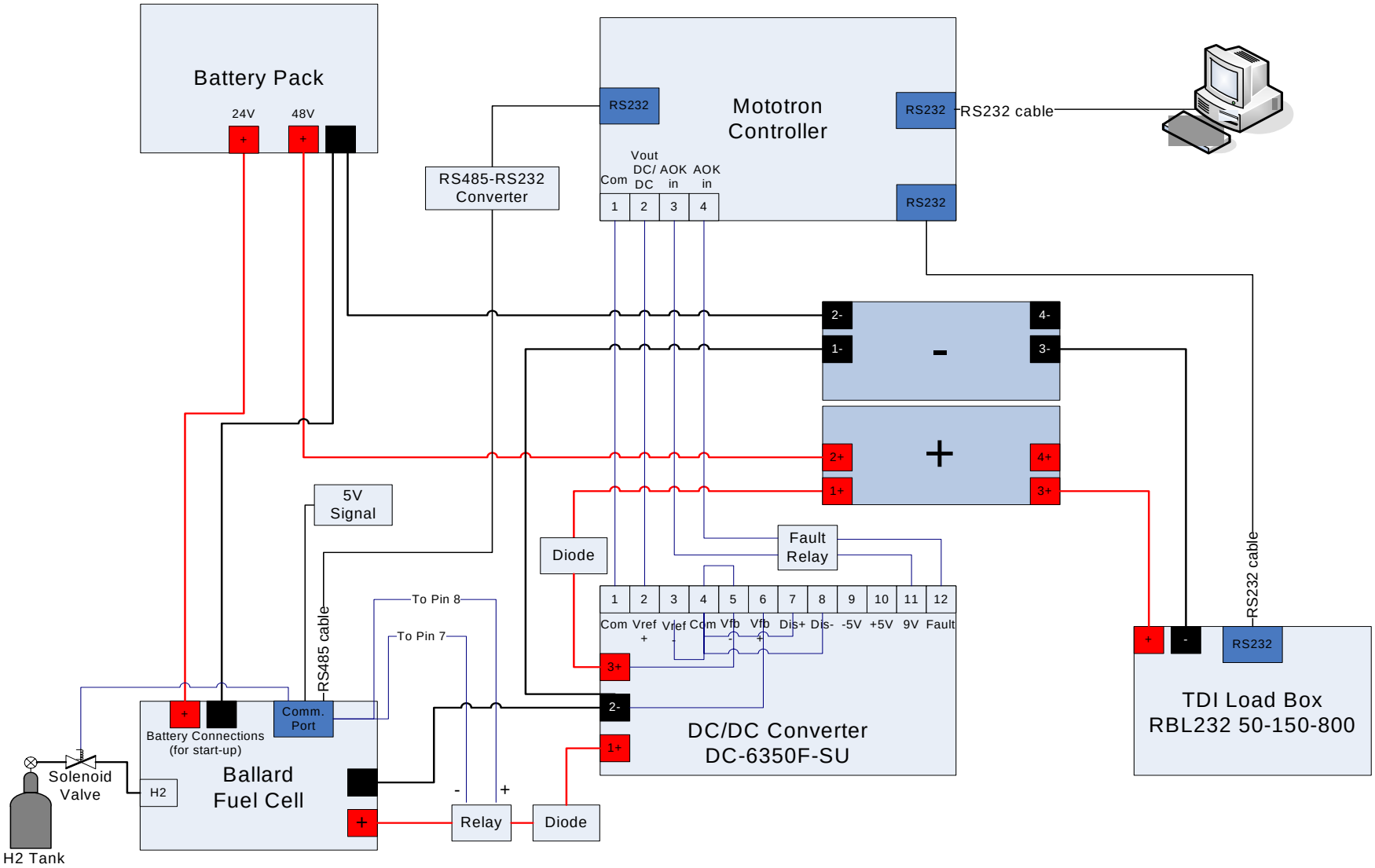

Figure 5.3: Test station wiring diagram.

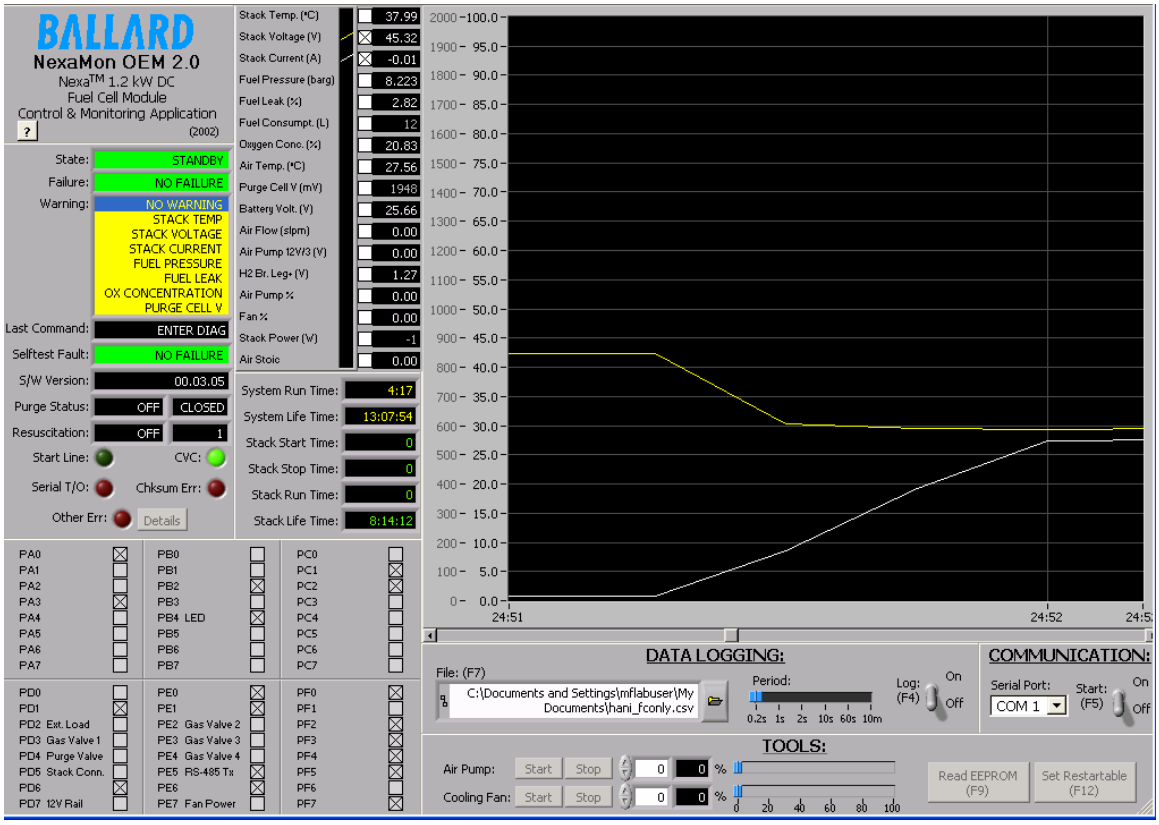

Figure 5.4: Fuel cell Labview interface.

5.3 Experimental Results

5.3.1 Converter Modeling

As previously stated, a test was first performed using only a network analyzer to obtain the small-signal input-to-output Bode plot of the experimental converter operating in ACMC. A relatively small sinusoidal signal was superimposed on a dc signal to form the voltage reference fed to the control loop (refer to Figure 3.1). The Bode plot is shown in Figure 5.5, where it is compared with the Bode plot previously obtained for the state-space averaged and ACMC dynamic model of the converter (Figure 3.11). It can be seen the derived frequency response is in close correspondence with the measured response at

low frequency. Still, one can observe the discrepancy at the filter's corner frequency, where the measured response from the actual plant appears to be more 'damped' as highlighted by the lack of a resonant peak, as well as a less abrupt phase lag transition. This is caused by the parasitics and non-ideal components, present in the experimental set-up, such as cables and connections, which are not accounted for in the theoretical derivation and slightly change the transient behavior [47,51]. The deviation from measurement is more apparent at above half of the switching frequency. This is to be expected and common to all average-based models since the theoretical model is based on some approximation, and typically accurate up to around one-third of the switching frequency [19,48]. The phase dependency is further significant above half the switching frequency due to the converter's response dependence on the phase of the disturbance, whereas this sensitivity is not picked up with an average-based linear time-invariant model [30]. Nevertheless, Figure 5.5 does not indicate the existence of the sampling effect as included in other models, which would create an additional 180° phase shift at half the switching frequency due to the double RHP zero in the sampling gain used to approximate the sampling effect [29,49].

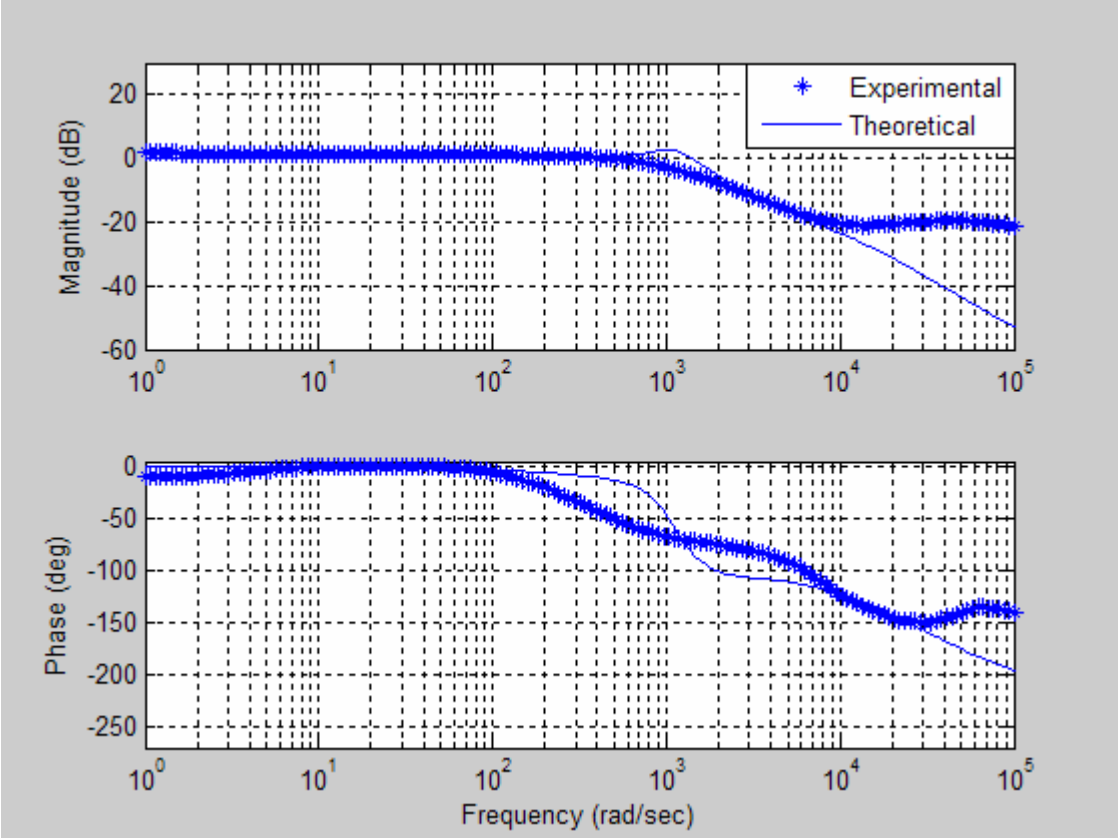

Figure 5.5: Bode plot for input-to-output voltage transfer function: experimental versus theoretical results.

5.3.2 Fuel Cell Dynamics

The fuel cell was connected directly to the electronic load unit without the converter and the battery disconnected. Step changes in the load current were then performed to study the fuel cell's dynamic response and time constant. Finally, the results from these tests were used to design the control loops in Chapter 3 and ensure sufficient delay has been incorporated to protect the fuel cell against abrupt load changes and stack lifetime degradation, whilst still providing the best possible overall dynamic response. The fuel cell's response to a step load change of 25 Amps is shown in Figure 5.6.

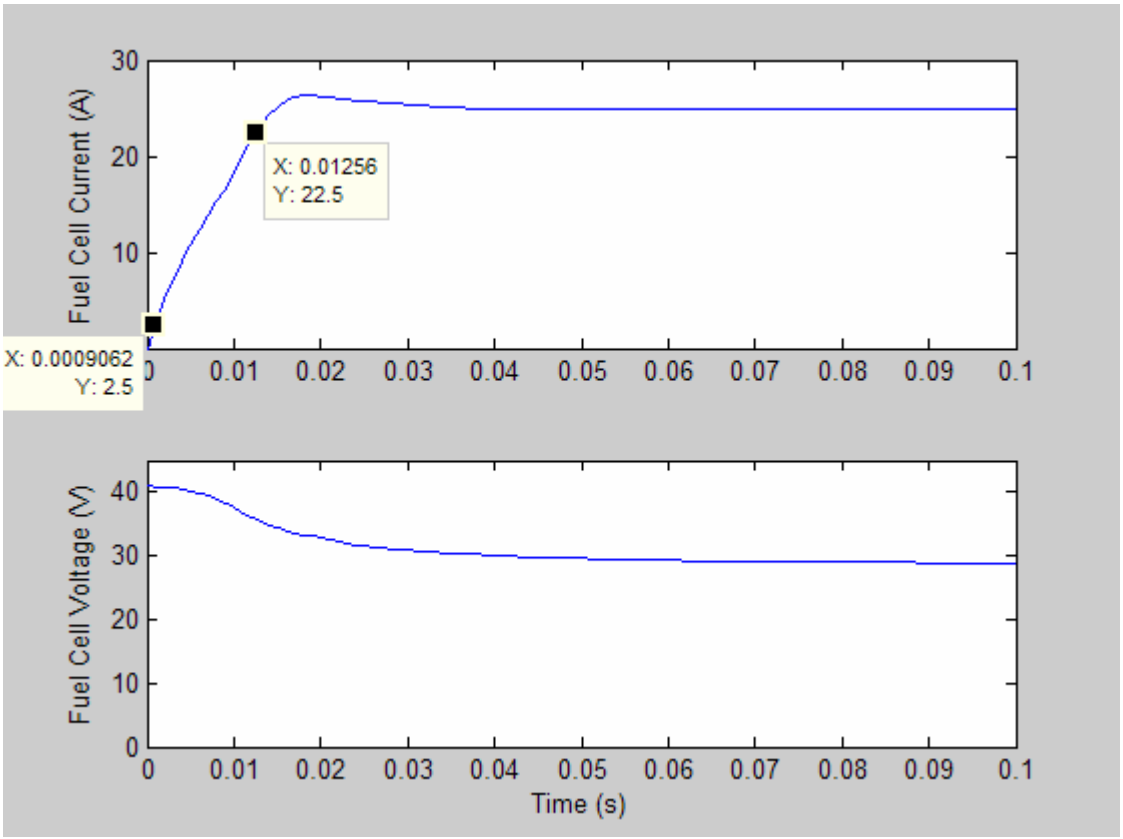

Figure 5.6: Experimental fuel cell's response to step load change.

As illustrated, the rise time is evaluated as $t_r = 0.01165$ *seconds*. Referring back to Figure 3.13, it can be seen that the rise time due to the delay introduced by the converter's control loops is $t_r = 0.01375$ *seconds*. This allowed for just enough buffer (18 percent) to protect the fuel cell and guarantee matching reactant delivery rate and usage rate, without unnecessarily slowing down the response too much. Thus, the compensators are effectively designed by incorporating the dynamics of the fuel cell. This strategy avoids the need to implement separate blocks to limit the fuel cell current slope to a maximum value, as is commonly done [50,51,52] and the implications of incorporating these blocks onto the control loops at the final stages without properly accounting for them in the design stage.

5.3.3 Hybrid Dynamics

Step disturbances were then applied to the hybrid system consisting of the fuel cell and the battery configured as previously shown for the simulation set-up in Figure 4.7. Due to certain limitations in the ratings of some components, mainly the load box as described in Table 5.1, the exact test conditions previously simulated were not replicated. First, the step load changes were limited to 10 Amps only. This is well below the capacity of both power sources, and thus does not subject them to the stress desired to demonstrate real-world applications of the devised system. This complication manifests itself in the results by causing the voltage at the batteries' terminal to marginally decrease in response to the load step and slowly reach its steady-state value as more energy is withdrawn from the batteries, as illustrated in Figure 5.7. Equally important, the converter's output voltage could not be matched exactly to that of the batteries' OCV (set to 49.6V instead of 50.2V for the OCV. Refer to Figure 4.5 for the relationship between SOC and OCV for the given batteries) due to the constraint imposed by the load box (limited to less than 50V). Finally, it can be observed in Figure 5.7 that the batteries' and fuel cell's currents are not precisely zero at no load conditon for the aforementioned reason, in addition to the non-idealities of various experimental components, including the losses in the converter.

Nevertheless, setting the output voltage of the converter to a different value than the OCV of the batteries is important to demonstrate an important aspect of the control strategy, and further highlight its flexibility. As shown in the system's response in Figure 5.7, setting the dc bus voltage lower than the OCV of the batteries causes the batteries to continue to supply average power to the load after the transient stage. This contribution can be adjusted by adjusting the dc bus voltage accordingly. This is in contrast to the response shown previously in simulations, where the dc bus voltage matched exactly the batteries' OCV, and thus caused them to only supply transient power. This relationship also serves to demonstrate the control objective in the case where the load is greater than the fuel cell's capacity, thereby causing the converter's output voltage to decline below its referenced value and in turn the battery to supply peak power demand in addition to transient power. Nevertheless, as before, the battery still supplies the transient power to

the load while the fuel cell ramps up and adjusts to the new demand, and the dc bus remains regulated and is barely disturbed.

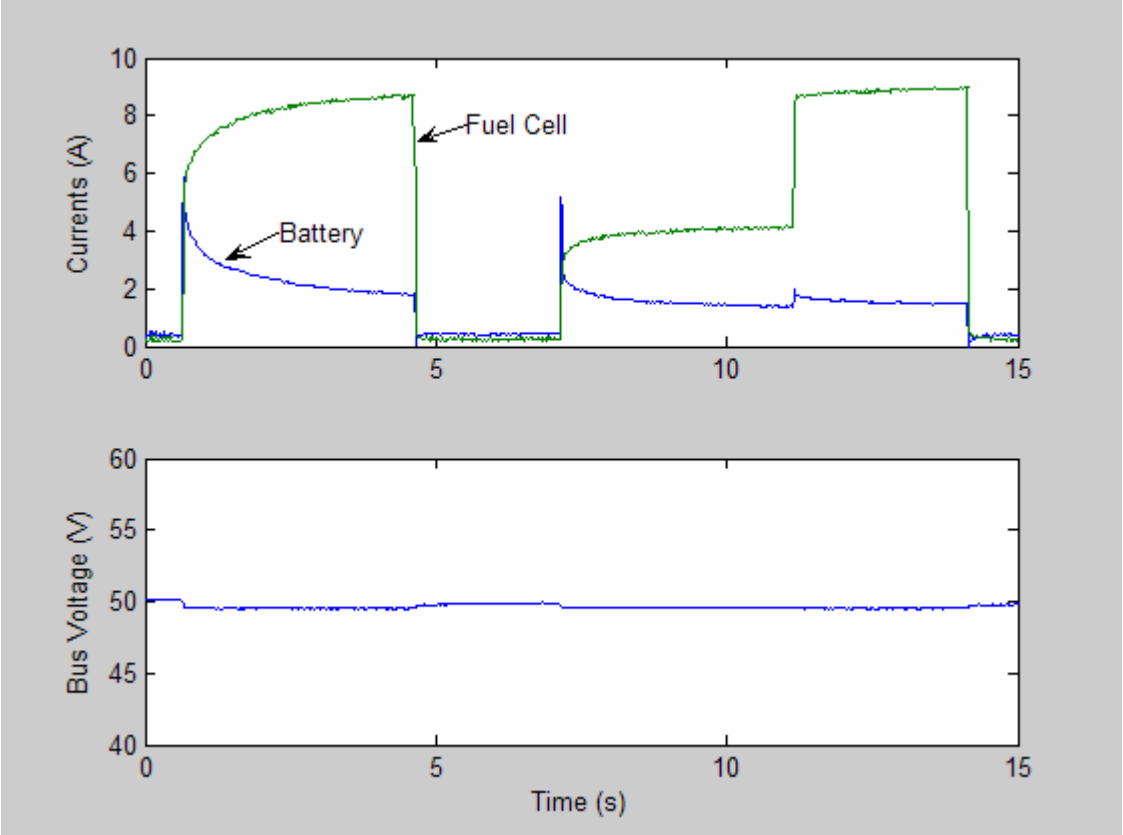

Figure 5.7: Experimental hybrid system's response to step load change.

An enlarged view of Figure 5.7 at the instant of a disturbance is shown in Figure 5.8 to better observe the dynamic response of the two sources, and thus compare with the results previously demonstrated. Despite the limitations aforementioned leading to a poor definition of the steady-state value and difficult measurement of the rise time, it can still be observed that the rise time is in close correspondence with the simulation results shown in Figure 4.8.

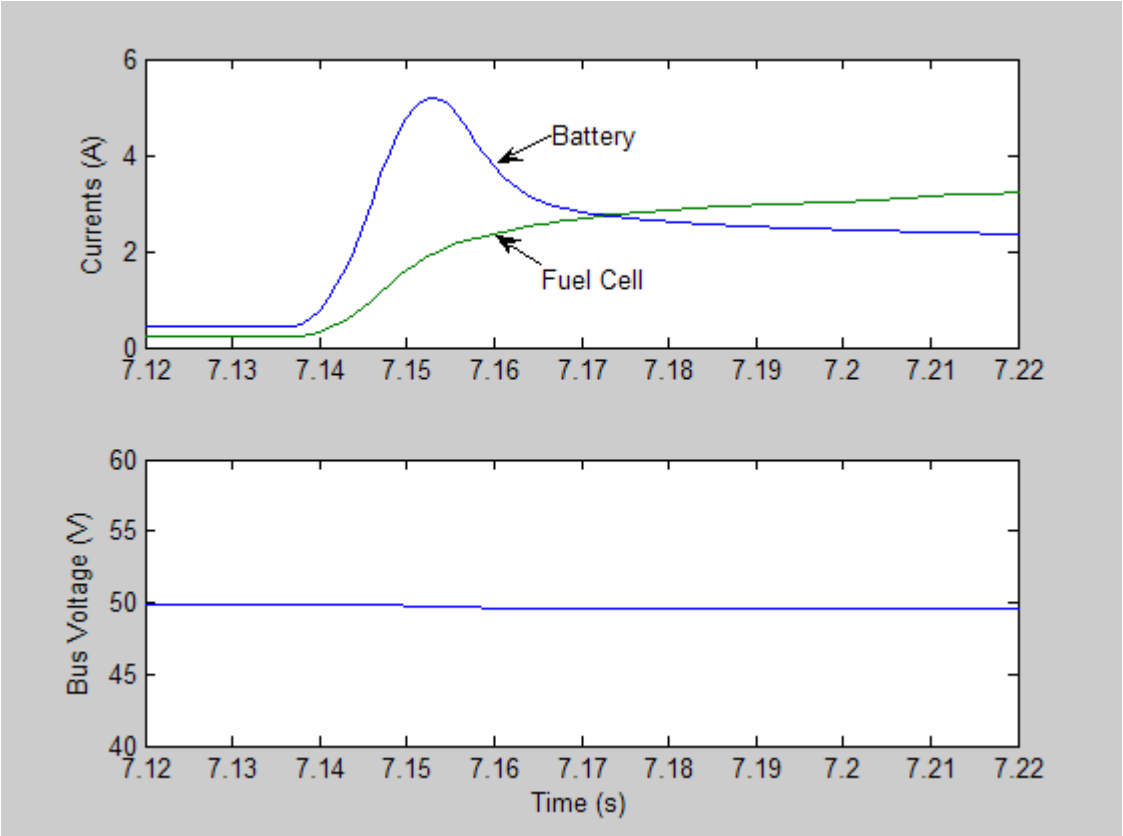

Figure 5.8: Experimental hybrid system's response to step load change: zoom in.

Thus, the results prove the effectiveness and feasibility of the devised system with real components as was desired. For completion and confirmation purposes, the hybrid system of Figure 4.7 is simulated once again with a similar disturbance to that previously shown in Figure 4.8, but with the converter's output voltage and the batteries' OCV replicated as per the above relationship for the experimental test. The results are shown in Figure B.1 in Appendix B. The batteries continue to supply average power to the load in this case, as hypothesized and shown experimentally in Figure 5.8.

5.4 Assessment

A scalable and modular test station was built in order to efficiently and effectively test the research at hand. The station was used to validate the design and simulation results brought forth in the dissertation. Tests were also conducted to confirm the models developed for the converter and control loops.

The first test assisted in validating the derived model for the boost converter operating in ACMC. The theoretical and experimental responses are in close correspondence at low frequencies. However, as expected, significant deviations were apparent above half the switching frequency due to the approximations present in the average-based model. Nevertheless, it was noted that there was no 'sampling effect' present in the model, as originally hypothesized.

The fuel cell dynamic behavior was then studied by imposing step load changes. The fuel cell's response time was then used to determine the necessary delay to be incorporated in the control loop in order to avoid fuel starvation and lifetime degradation to the stack. This avoided the need to implement external blocks in the control loops to limit the rise of the fuel cell's current, and effectively integrate its dynamics in the design of the compensators. Finally, step load changes were then applied to the fuel cell and battery hybrid system to observe the complete system's response. Despite certain limitations in the components, the experimental results further confirmed the excellent performance and feasibility of the proposed control strategy in conjunction with the hybrid system to improve the system's dynamics and meet the load demand.

Chapter 6
Conclusions

Despite the fuel cell's numerous benefits and potential to be a major player in the new era of distributed generation, it suffers from poor output voltage regulation and slower dynamics. These shortcomings must be compensated for by the PCU to improve the fuel cell's overall performance and tap into its potential.

The most critical component for the PCU is the dc-dc converter, which, being the closest to the fuel cell, is most affected by its operation while at the same time is responsible for its protection against the various disturbances in the system. The power sharing and control of the various sources at the dc level is also the best method to effectively meet the load demand and requirements. If ac loads are to be supplied, the conditioned dc power can then be inverted using a simple dc-ac inverter.

A dc-dc boost converter is utilized since designing fuel cell stacks for higher voltages is not efficient. In order to gain insight into the converter's behavior, it must be dynamically modeled. Approximations must be drawn on, which although limit the validity and accuracy of the model, are still valuable for the purpose of designing suitable compensators. Upon modeling the converter with the elements' non-idealities taken into account, it was found that the output capacitor's ESR contributes to an additional zero in the LHP. More importantly, a RHP zero also exists as a result of the boost converter's operation, which introduces delay in the system and greatly limits the system's performance as no control strategy may divest the system from this complexity. To make matters worse, its frequency varies with operating conditions.

Sophisticated control processes must therefore be developed for the application at-hand to obtain satisfactory static and dynamic performance and robustness against disturbances. It was determined that CMC is better suited than VMC due to its better

inherent dynamics. Furthermore, the use of an CEA in the ACMC scheme helps overcome many of the shortcomings with PCMC, and it also provides design flexibility to tailor the compensator for optimum performance.

In order to design suitable compensators, the poles and zeros are chosen to counteract the zeros and poles in the system's transfer functions derived from the small-signal model. In particular, in order to obtain any sort of wide bandwidth and adequate stability margin, zeros must be used to counteract the converter's second order output filter characteristics. The poles are placed at dc for zero steady-state error and at high frequency to eliminate switching noise. To avoid the instability issues associated with the RHP zero, the gain crossover frequency must be chosen well below the zero's worst-case lowest frequency to maintain adequate phase margin. Bode plots and simulations confirm the compensators' ability to meet the design objectives in conjunction with the derived models and their robustness to external disturbances.

It was determined that combining the fuel cell with an ESS brings about numerous potential advantages and synergy to the hybrid system. Nonetheless, the configuration of the various components and the control strategy is critical to reap the potential benefits while also avoiding detrimental effects to the components. Interposing the dc-dc converter between the fuel and ESS and placing the ESS closer to the load results in an 'active' hybrid configuration that provides the ability to tap into all these benefits. A robust and flexible control strategy is also implemented, which allows direct implementation of the ACMC scheme previously devised, avoids the instability issues associated with the mode definitions in rule-based control and can be easily extended to various hybrid systems. The excellent performance is demonstrated using simulation and experimental tests.

A scalable and modular test station was built such that the conducted research may be effectively verified. As expected, the derived model for the boost converter operating in ACMC compares well with the experimental response at low frequency only, and no sampling effect exists. Tests were performed on the fuel cell alone to study its dynamic

response and integrate its specific attributes in the design of the compensators, thereby avoiding the implications of inserting external control blocks not properly accounting for in the design process. Despite component limitations when performing the experimental tests on the hybrid system, the flexibility and feasibility of the control strategy with real components is further confirmed by observing the dynamic response of the system to external disturbances.

6.1 Contributions

The contributions of this thesis, as originally proposed in the list of objectives, can be summarized as follows:

1) Devised an effective topology of the PCU to enable active management of the power flow amongst the different power sources while satisfying their constraints and the load requirements
2) Devised suitable models of the PCU components to gain insight into their behavior and designed compensators based on the models that effectively overcome the limitations of the system and take into account the specific characteristics of the fuel cell
3) Devised a flexible and robust hybrid control strategy that enables accurate, efficient and reliable power sharing amongst the various power sources while regulating the bus voltage
4) Developed a modular ‘plug-and-play’ bench scale test facility to efficiently and cost-effectively test the research and prove its feasibility using real components
5) Finally, performed research critical to the success and deployment of fuel cells as a viable solution to the current energy crisis

Appendix A
State-Space Matrices for Boost Converter Dynamic Model

The state-space equations for the boost converter of Figure 2.3 are shown below. For the first interval where the bottom switch is *on*, the switched circuit model as given by Figure 2.4 (a) can be represented by:

$$\begin{aligned} \dot{x} &= A_1 x + B_1 u \qquad during \;\; d \cdot T_s \\ y &= C_1 \cdot x \end{aligned} \tag{A.1}$$

where:

$$x = \begin{bmatrix} V_{co} \\ V_{ci} \\ i_L \end{bmatrix}, \qquad u = \begin{bmatrix} I_{out} \\ V_s \end{bmatrix} \tag{A.2}$$

Taking the output voltage as the output variable, and the duty-cycle as the control variable, the system matrices used to derive the transfer function are given by:

$$A_1 = \begin{bmatrix} 0 & 0 & 0 \\ 0 & -\dfrac{1}{C_i \cdot (R_s + R_{ci})} & -\dfrac{R_s}{C_i \cdot (R_s + R_{ci})} \\ 0 & \dfrac{R_s}{L \cdot (R_s + R_{ci})} & -\dfrac{R_s \cdot R_L + R_L \cdot R_{ci} + R_{ci} \cdot R_s}{L \cdot (R_s + R_{ci})} \end{bmatrix} \tag{A.3}$$

$$B_1 = \begin{bmatrix} -\dfrac{1}{C_o} & 0 \\ 0 & \dfrac{1}{C_i \cdot (R_s + R_{ci})} \\ 0 & \dfrac{R_{ci}}{L \cdot (R_s + R_{ci})} \end{bmatrix}, \qquad C_1 = \begin{bmatrix} 1 & 0 & 0 \end{bmatrix}$$

Similarly, for the second interval where the top switch is *on,* the switched circuit model as given by Figure 2.4 (b) can be represented by:

$$\begin{aligned} \dot{x} &= A_2 x + B_2 u \qquad \textit{during} \ \ (1-d) \cdot T_s \\ y &= C_2 \cdot x \end{aligned} \tag{A.4}$$

where:

$$A_2 = \begin{bmatrix} 0 & 0 & \dfrac{1}{C_o} \\ 0 & -\dfrac{1}{C_i \cdot (R_s + R_{ci})} & -\dfrac{R_s}{C_i \cdot (R_s + R_{ci})} \\ -\dfrac{1}{L} & \dfrac{R_s}{L \cdot (R_s + R_{ci})} & -\dfrac{R_s \cdot R_L + R_L \cdot R_{ci} + R_{ci} \cdot R_s + R_s \cdot R_{co} + R_{co} \cdot R_{ci}}{L \cdot (R_s + R_{ci})} \end{bmatrix} \quad \text{(A.5)}$$

$$B_2 = \begin{bmatrix} -\dfrac{1}{C_o} & 0 \\ 0 & \dfrac{1}{C_i \cdot (R_s + R_{ci})} \\ \dfrac{R_{co}}{L} & \dfrac{R_{ci}}{L \cdot (R_s + R_{ci})} \end{bmatrix}, \qquad C_2 = \begin{bmatrix} 1 & 0 & R_{co} \end{bmatrix}$$

In the case where the inductor current is the output variable, the respective *A* and *B* matrices are still as given above, however the *C* matrices are now given by:

$$C_1 = C_2 = \begin{bmatrix} 1 & 0 & 0 \end{bmatrix} \quad \text{(A.6)}$$

Appendix B
Additional Simulations Results for Hybrid System

The hybrid system depicted in Figure 4.7 is simulated once again and the results are presented here. Whereas in Chapter 4 the converter's output voltage and the battery's OCV were both set to 48 Volts, the following test illustrates the case where a mismatch exists between the two. The battery's OCV is set to 50.2 Volts and the converter's output voltage is adjusted to 49.6 Volts to mimic the experimental hybrid test of Chapter 5, and thus form the basis for comparison.

As shown in Figure B.1, the battery's current does not drop off to zero after the transient stage as hypothesized, but instead remains at a value dictated by its characteristics (i.e., its ESR) and the voltage difference between its OCV and the converter's output voltage. As previously mentioned, these results demonstrate the control strategy's flexibility and objectives previously set forth, where the battery pack's contribution can be regulated to supplement the fuel cell in order to supply average base power or peak power in case the demand is greater than the fuel cell's capacity. These results compare well with and confirm the experimental results shown in Chapter 5.

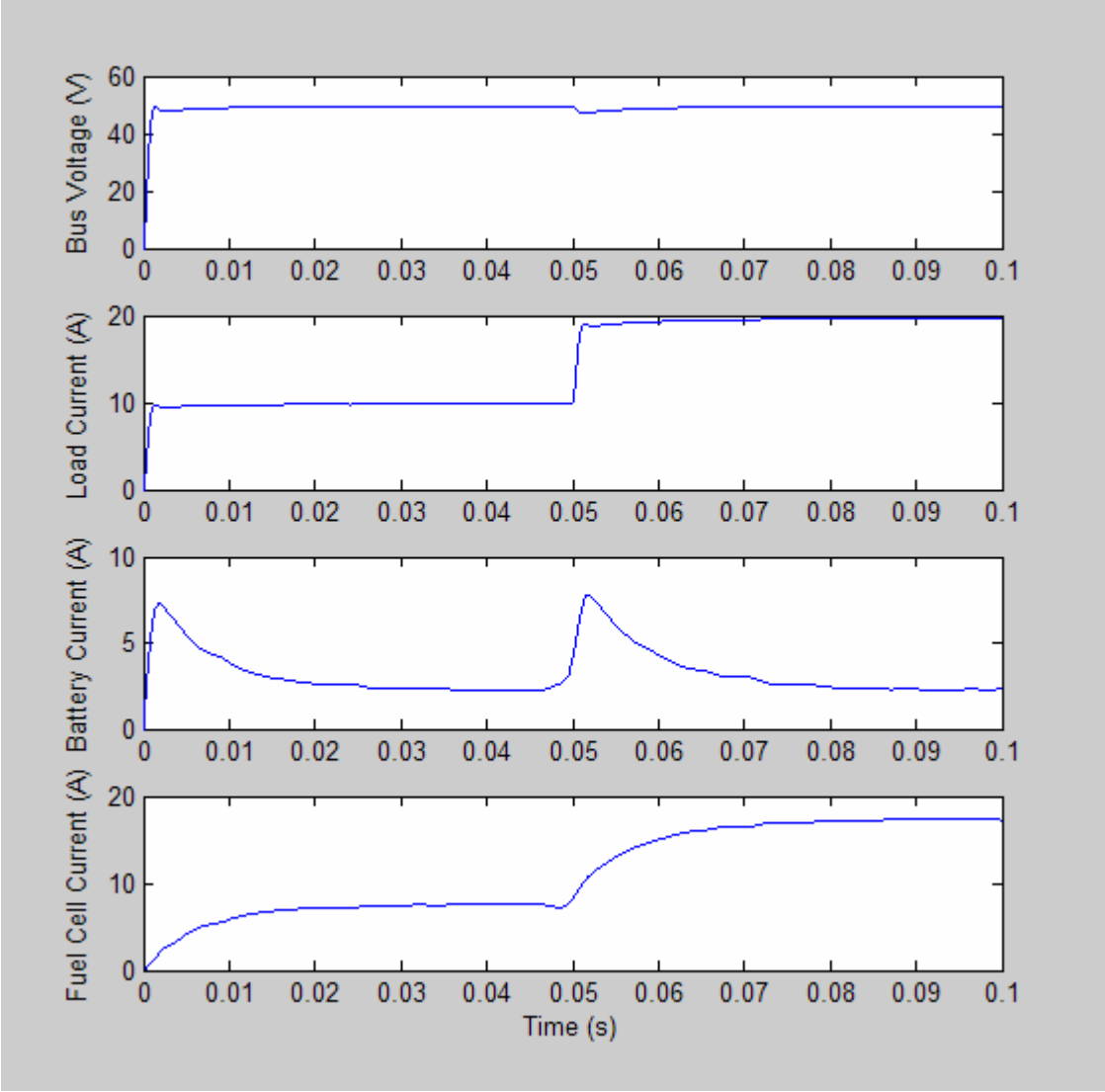

Figure B. 1: Simulated hybrid system's response to step load change with mismatch between converter's output voltage and battery's OCV: (a) bus voltage (b) load current (c) battery current (d) fuel cell current.

References

[1] M. H. Nebrir, C. Wang and S.R. Shaw, "*Fuel Cells: Promising Devices for Distributed Generation*", IEEE Power and Energy Magazine, Vol. 4(1), pp. 47-53, 2006

[2] J. Yao and D. Popovic, "*Stability of a Medium Voltage Distribution Network with Electronically Interfaced Distributed Generation*", Proceedings of the 12th IEEE Mediterranean Electrotechnical Conference, Vol. 3, pp. 975 – 978, 2004

[3] H. Xu, L. Kong and X. Wen, "*Fuel Cell Power System and High Power DC-DC Converter*", IEEE Trans. on Power Electronics, Vol. 19(5), pp. 1250-1255, 2004

[4] A. Nasiri, V.S. Rimmalapudi, A. Emadi, D.J. Chmielewski and S. Al-Hallaj, "*Active Control of a Hybrid Fuel Cell – Battery System*", 4th International Power Electronics and Motion Control Conference, Vol. 2, pp. 491 – 496, 2004

[5] J. Lee, J. Jo, S. Choi and S.B. Han, "*A 10kW SOFC Low-Voltage Battery Hybrid Power Conditioning System for Residential Use*", IEEE Transaction on Energy Conversion, Vol. 21(2), pp. 575 – 585, 2006

[6] D. Candusso, L. Valero and A. Walter, "*Modelling, Control and Simulation of a Fuel Cell Based Power Supply System with Energy Management*", IEEE 2002 28th Annual Conference of the Industrial Electronics Society, Vol. 2, pp. 1294 – 1299, 2002

[7] J. H. Hirchenhofer, D. B. Stauffer, R. R. Engleman and M. G. Klett, "*Fuel Cell Handbook*", 7th Edition, US Department of Energy, Morgantown, WV, USA, 2004

[8] M. A. Laughton and D. J. Warne, "*Electrical Engineer's Reference Book*", 16th Edition, Newnes, pp. 27/17 – 27/21, 2003

[9] K. Rajashekara, "*Propulsion System Strategies for Fuel Cell Vehicles*", SAE 2000 World Congress, Detroit, MI, 2000

[10] L.P. Jarvis, T.B. Atwater and P.J. Cygan, "*Hybrid Fuel Cell for Pulse Power Applications*", Twelfth Annual Battery Conference on Applications and Advances, pp. 37 – 41, 1997

[11] A. W. Leedy and R. M. Nelms, "*Analysis of a Capacitor-Based Hybrid Source Used for Pulsed Load Applications*", 2002 37th Intersociety Energy Conversion Engineering Conference, pp. 1 6, 2004

[12] J.P. Zheng, T.R. Jow and M.S. Ding,, "*Hybrid Power Sources for Pulsed Current Applications*", IEEE Transactions on Aerospace and Electronic Systems, Vol. 37(1), pp. 288 – 292, 2001

[13] K. Ro and S. Rahman, "*Two-Loop Controller for Maximizing Performance of a Grid-Connected Photovoltaic – Fuel Cell Hybrid Power Plant*", IEEE Transaction on Energy Conversion, Vol. 13(3), pp. 276 – 281, 1998

[14] M. Shen, S. Hodek and F.Z. Peng, "*Control of the Z-Source Inverter for FCHEV with the Battery Connected to the Motor Neutral Point*", IEEE Power Electronics Specialists Conference, pp. 1485 – 1490, 2007

[15] K. Holland, M. Shen and F.Z. Peng, "*Z-Source Inverter Control for Traction Drive of Fuel Cell - Battery Hybrid Vehicles*", Conference Record of the 2005 Industry Applications Conference, Vol. 3, pp. 1651 – 1656, 2005

[16] J. Anzicek and M. Thompson, "*DC/DC Boost Converter Design for Kettering University's GEM Fuel Cell Vehicle*", Proceedings of Electrical Insulation Conference and Electrical Manufacturing Expo, pp. 307 – 316, 2005.

[17] R. D. Middlebrook and S. Cúk, "*A General Unified Approach to Modelling Switching-Converter Power Stages*", IEEE Power Electronics Specialists Conference Record, pp. 18-34, 1976

[18] D. Czarkowski, "*Power Electronics Handbook*", Chap. 13, pp. 221, Academic Press, 2001

[19] A. J. Forsyth and S. V. Mollov, "*Modelling and Control of DC-DC Converters*", Power Engineering Journal, Vol. 12(5), pp. 229-236, 1998

[20] M. Brown, "*Practical Switching Power Supply Design*", Motorola Series in Solid State Electronics, Academic Press, Inc., pp. 141-168, 1990

[21] L.E. Gallaher, "*Current Regulator with AC and DC Feedback,*" U.S. Patent 3,350,628, 1967.

[22] Venable Industries, "*Current Mode Control*", Technical Paper #5, [Online]. Available: http://www.venable.biz/tp-05.pdf, 2006

[23] R. B. Ridley, "*A New Small-Signal Model for Current-Mode Control*", Ph.D. Dissertation, Virginia Polytechnic Institute and State University, Blacksburg, 1990

[24] Maxim Integrated Products, "*DC-DC Controllers Use Average-Current-Mode Control for Infotainment Applications*", Application Note 3939, [Online]. Available: http://www.maxim-ic.com/appnotes.cfm/an_pk/3939, 2006

[25] B. Suppanz, "*Sampling Effects and Slope Considerations*", [Online]. Available: http://www.geocities.com/CapeCanaveral/Lab/9643/samp-ef.htm, 2004

[26] L.H. Dixon, "*Average Current Mode Control of Switching Power Supplies*", Unitrode Power Supply Design Seminar handbook, pp. 5.1-5.14, 1990

[27] K.D. Purton and R.P. Lisner, "*ACMC in Power Electronic Converters: Analog versus Digital*", [Online]. Available: http://www.itee.uq.edu.au/~aupec/aupec02/Final-Papers/K-D-Purton.pdf, 2006

[28] C.C. Fang and E.H. Abed, "*Sampled-Data Modeling and Analysis of Closed-Loop PWM DC-DC Converters*", Proceedings of the 1999 IEEE International Symposium on Circuits and Systems, Vol. 5, pp. 110 – 115, 1999

[29] W. Tang, F.C. Lee, and R.B. Ridley, "*Small Signal Modeling of Average Current-Mode Control*", IEEE Trans. on Power Electronics, Vol. 8, No. 2, pp. 112-119, 1993

[30] J. Sun and R. Bass, "*Modeling and Practical Design Issues for Average Current Control*", IEEE Applied Power Electronics Conference and Exposition, pp. 980-986, 1999

[31] P. Cooke, "*Modeling Average Current Mode Control*", IEEE Applied Power Electronics Conference and Exposition, 2000, pp. 256-262, 2000

[32] Z. Jiang and R.A. Dougal, "*A Compact Digitally Controlled Fuel Cell/Battery Hybrid Power Source*", IEEE Transactions on Industrial Electronics, Vol. 53(4), pp. 1094 – 1104, 2006

[33] H. Fadali and E.F. El-Saadany, "*Improved Interface and Efficiency of Fuel Cell Inverter System*", 12th International Conference on Harmonics and Quality of Power, 2006

[34] D. Zahn, Personal Conversation, Jan. 2007

[35] Z. Jiang, L. Gao and R.A. Dougal, "*Adaptive Control Strategy for Active Power Sharing in Hybrid Fuel Cell/Battery Power Sources*", IEEE Transaction on Energy Conversion, Vol. 22(2), pp. 507 – 515, 2007

[36] M.J. Kim, H. Peng, C.C. Lin, E. Stamos and D. Tran, "*Testing, Modeling, and Control of a Fuel Cell Hybrid Vehicle*", Proceedings of the 2005 American Control Conference, Vol. 6, pp. 3859 – 3864, 2005

[37] EnerSys Power/Full Solutions, "*Genesis Selection Guide*", 4th Edition, Publication No.: US-GPL-SG-001, 2003

[38] H.Y. Cho, W. Gao and H.L. Ginn, "*A New Power Control Strategy for Hybrid Fuel Cell Vehicles*", Power Electronics in Transportation, pp. 159 – 166, 2004

[39] Y. Gao and M. Ehsani, "*Systematic Design of Fuel Cell Powered Hybrid Vehicle Drive Train*", IEEE International Electric Machines and Drives Conference, pp. 604 – 611, 2001

[40] L. Zhang, M. Pan, S. Quan, Q. Chen and Y. Shi, "*Adaptive Neural Control Based on PEMFC Hybrid Modeling*", The 6th World Congress on Intelligent Control and Automation, Vol. 2, pp. 8319 – 8323, 2006

[41] A. Vahidi, A. Stefanopoulou and H. Peng, "*Current Management in a Hybrid Fuel Cell Power System: A Model-Predictive Control Approach*", IEEE Transactions on Control Systems Technology, Vol. 14(6), pp. 1047 – 1057, 2006

[42] M.J. Kim and H. Peng, "*Combined Control/Plant Optimization of Fuel Cell Hybrid Vehicles*", American Control Conference, 2006

[43] T. Zhu, S.R. Shaw and S.B. Leeb, "*Transient Recognition Control for Hybrid Fuel Cell Systems*", IEEE Transaction on Energy Conversion, Vol. 21(1), pp. 195 – 201, 2006

[44] J. Schiffer, O. Bohlen, R.W. DeDoncker, D.U. Sauer and Y.A. Kyun, "*Optimized Energy Management for Fuel Cell-Supercap Hybrid Electric Vehicles*", IEEE Conference on Vehicle Power and Propulsion, pp. 341 – 348, 2005

[45] R. Saeks, C.J. Cox, J. Neidhoefer, P.R. Mays and J.J. Murray, "*Adaptive Control of a Hybrid Electric Vehicle*", IEEE Transactions on Intelligent Transportation Systems, Vol. 3(4), pp. 213 – 234, 2002

[46] Genesis EP PureLead, "*Range Summary*", Publication No.: US-EP-RS-001, 2006

[47] L. Guo, "*Design and Implementation of Digital Controllers for Buck and Boost Converters using Linear and Nonlinear Control Methods*", Ph.D. Dissertation, Auburn University, Alabama, 2006

[48] D. He and R.M. Nelms, "*Average Current-Mode Control for a Boost Converter using an 8-bit Microcontroller*", IEEE International Symposium on Industrial Electronics, Vol. 2, pp. 1185 – 1190, 2004

[49] A.S. Kislovski, “Small-Signal, Low Frequency Analysis of a Buck Type PWM Conductance Controller”, IEEE Power Electronics Specialists’ Conference, pp. 88-95, 1990

[50] P. Thounthong, S. Rael and B. Davat, “*Control of Fuel Cell/Supercapacitors Hybrid Power Sources*”, 31st Annual Conference of IEEE Industrial Electronics Society, 2005

[51] L. Solero, A. Lidozzi, and J.A. Pomilio, “*Design of Multiple-Input Power Converter for Hybrid Vehicles*”, IEEE Transactions on Power Electronics, Vol. 20(5), pp. 1007 – 1016, 2005

[52] Z. Jiang, “*Power Management of Hybrid Photovoltaic-Fuel Cell Power Systems*”, IEEE Power Engineering Society General Meeting, 2006